Magnonic spin transport in magnetic insulators

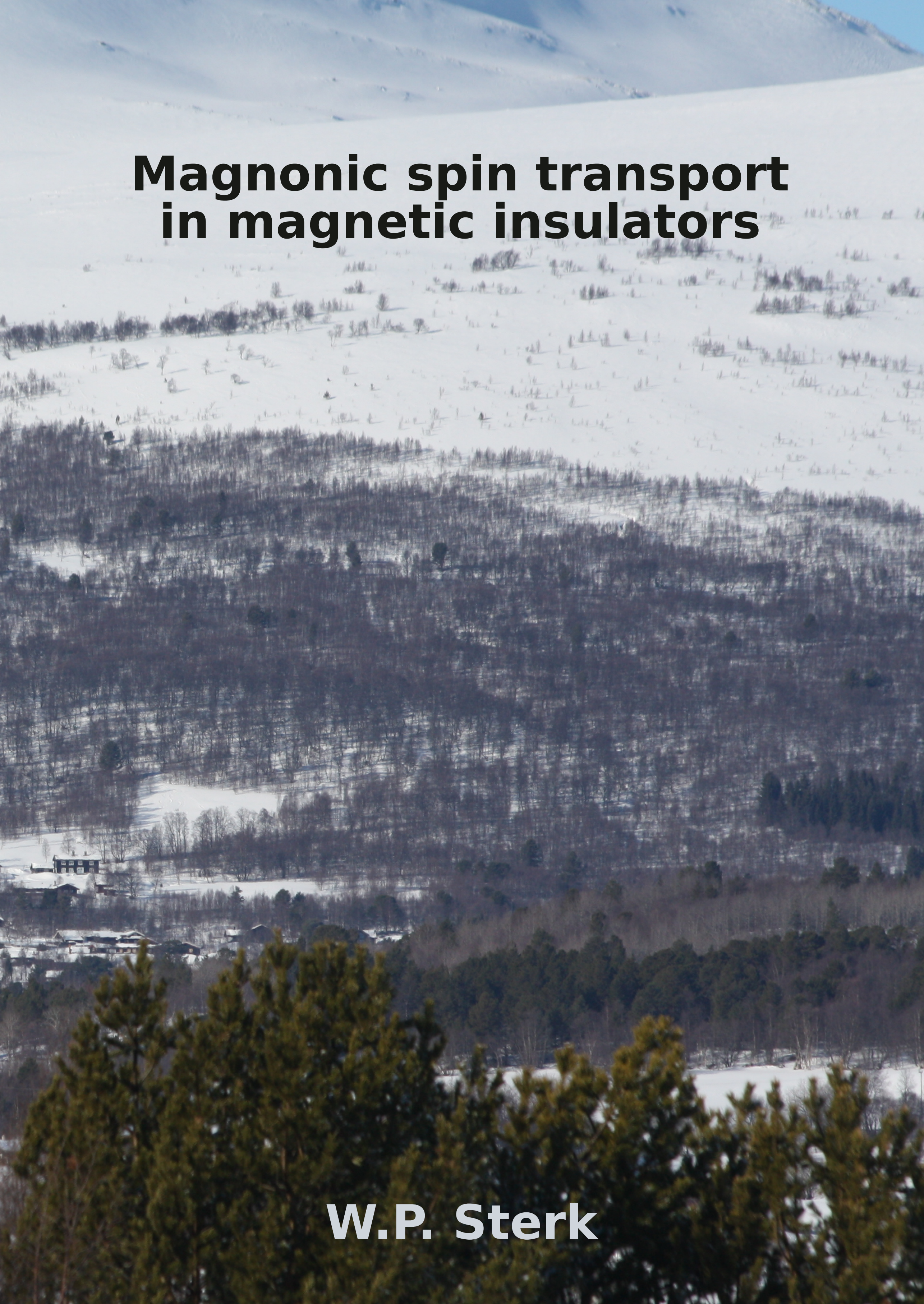

W.P. Sterk

Magnonic spin transport in magnetic insulators

W.P. Sterk

W.P. Sterk
Magnonic spin transport in magnetic insulators
Doctoral thesis
2022
Utrecht
Institute for Theoretical Physics
Utrecht University
ISBN: 978-94-6469-022-4
DOI: 10.33540/1499
Printed by: ProefschriftMaken

MAGNONIC SPIN TRANSPORT IN MAGNETIC INSULATORS

MAGNONISCH SPINTRANSPORT IN MAGNETISCHE ISOLATOREN
(met een samenvatting in het Nederlands)

Proefschrift

ter verkrijging van de graad van doctor aan de
Universiteit Utrecht
op gezag van de
rector magnificus, prof.dr. H.R.B.M. Kummeling,
ingevolge het besluit van het college voor promoties
in het openbaar te verdedigen op

maandag 31 oktober 2022 des ochtends te 10.15 uur

door

Willem Pieter Sterk

geboren op 26 februari 1990
te Goes

Promotor:
Prof. dr. R. A. Duine

Copromotor:
Dr. L. Fritz

Beoordelingscommissie:
Dr. A. Kamra
Prof. dr. J. Aarts
Prof. dr. P. van der Straten
Prof. dr. C. de Morais Smith
Prof. dr. ir. H.T.C. Stoof

Dit proefschrift werd (mede) mogelijk gemaakt met financiële steun van de European Research Council (ERC).

To my beloved mother,
the light on my darkest days

I dream of my future
Remote from time bounds
Becoming myself
In truth

– Men I Trust, “I Hope to Be Around”

LIST OF PUBLICATIONS

The main chapters of this thesis are based on the following works:

- Chapter 4: W. P. Sterk, D. Peerlings, and R. A. Duine. Magnon contribution to unidirectional spin hall magnetoresistance in ferromagnetic-insulator/heavy-metal bilayers. *Phys. Rev. B*, 99:064438, Feb 2019. doi:10.1103/PhysRevB.99.064438
- Chapter 5: W. P. Sterk, H. Y. Yuan, Andreas Rückriegel, Babak Zare Rameshti, and R. A. Duine. Green's function formalism for nonlocal elliptical magnon transport. *Phys. Rev. B*, 104:174404, Nov 2021. doi:10.1103/PhysRevB.104.174404

Additional publications not included in this thesis:

- H. Y. Yuan, W. P. Sterk, Akashdeep Kamra, and Rembert A. Duine. Pure dephasing of magnonic quantum states. *Phys. Rev. B*, 106:L100403, Sep 2022. doi:10.1103/PhysRevB.106.L100403
- H. Y. Yuan, W. P. Sterk, Akashdeep Kamra, and Rembert A. Duine. Master equation approach to magnon relaxation and dephasing. *arXiv e-prints*, art. arXiv:2209.02961, September 2022. doi:10.48550/arXiv.2209.02961

CONTENTS

List of publications **i**

1 Non-mathematical introduction **1**
1.1 This thesis 2

2 Niet-wiskundige inleiding in het Nederlands **5**
2.1 Deze scriptie 7

3 Advanced introduction **9**
3.1 Magnetic models and the Holstein-Primakoff transformation . . . 10
3.1.1 Para-unitary diagonalization 17
3.2 Anisotropies and fields 19
3.3 Spin-flip scattering and the spin Hall effect 21

4 Magnon contribution to unidirectional spin Hall magnetoresistance **27**
4.1 Introduction 27
4.2 Magnonic spin accumulation 29
4.3 Results 33
4.3.1 Equal-temperature, finite gap case 33
4.3.2 Thermal effects 35
4.3.3 Spin Hall angle 35
4.3.4 A note on the magnon spin diffusion length 36
4.3.5 Effect of the magnon gap 38
4.4 Conclusions 41
4.5 Appendix: System parameters for a Pt|YIG bilayer film. 43
4.6 Appendix: Interfacial spin current integrals 44

5 Green's function formalism for nonlocal elliptical magnon transport **45**
5.1 Introduction 45

5.2 Methods 46
5.2.1 System and Hamiltonian 47
5.2.2 Non-equilibrium Green's function formalism 50
5.2.3 Observables 54
5.3 Numerical implementation and results 59
5.3.1 Spin conductances 60
5.3.2 Correlation functions and squeezing 63
5.4 Conclusions and outlook 70
5.5 Appendix: Derivation of the steady-state spin current 71

6 Nonlocal spin transport in one-dimensional antiferromagnetic insulators 75
6.1 Introduction 75
6.2 Methods and results 76
6.2.1 System and Hamiltonian 76
6.2.2 Green's function formalism 80
6.2.3 Spin conductance 82
6.2.4 Correlation functions 85
6.3 Discussion, conclusions and outlook 88

7 Summary and outlook 91

8 Samenvatting en vooruitblik 95

Acknowledgements 99

Curriculum vitæ 101

Bibliography 103

1 Non-mathematical introduction

If one were to compile a list of humanity's greatest achievements, it would be a grave error to omit the invention of the transistor by Lilienfeld [5] in 1925 and its first physical realization in 1947 by Bardeen, Brattain and Shockley [6]. After all, it is this humble component that allowed us to miniaturize the massive World War II-era mainframes to the size of a fingernail and bring the sum total of human knowledge to the palm of anyone's hand, even in the remotest corners of the world.

By making transistors smaller and smaller, the number of components in a single integrated circuit has grown exponentially for decades—an observation (and, in part, a self-fulfilling prophecy [7]) known as Moore's law [8]. By linking more and more transistors together, the capabilities of electronic computation devices have followed the same trend. However, the limits of Moore's law are fast approaching: as transistors shrink, thermal and quantum fluctuations become more significant, and inevitably produce errors. Yet, without shrinking the transistor, increases in complexity come at the steep cost of increased power consumption and heat production, leading to impractical cooling and power supply requirements. Exotic semiconductor materials and ultra-short-wavelength lithography only provide a brief respite before the inevitable catastrophic breakdown of the exponential growth of computing power.

Even with virtually perfect materials and lithography techniques, transistor-based devices run foul of a fundamental problem, stemming from the fact that their function is to move around electrons, which invariably incurs an energy loss in the form of Joule heating. Thus, one of the best ways to push Moore's law further would be to find a way to move around information that does not involve physically moving electrons.

Enter spintronics, a field of research that seeks to use the spin of the electron as a carrier of information [9, 10], rather than its charge. Unlike its charge, which has the fixed value of $-e \overset{\text{def}}{=} -1.602\,176\,634 \times 10^{-19}\,\mathrm{C}$, an electron's spin can be either 'up' or 'down' (with respect to some quantization axis, typically the direction of a magnetic field). Instead of defining a logical 'one' ('zero') as the presence (absence) of an electron, one could keep the electrons present and motionless, and map spin-up (spin-down) to logical 'one' ('zero'). Crucially, it is not necessary to move an electron in order to flip its spin, thus leading to potentially lower energy consumption than conventional electronics.

In practice, using the spin of a single electron to represent a bit is difficult. Rather, a typical spintronic device consists of one or more ferromagnetic or antiferromagnetic materials connected to peripheral structures such as leads or waveguides, that are used to manipulate or probe the local magnetic order. The net (mesoscale) magnetic order of e.g. a single magnetic domain may then be mapped to a bit. Fortunately, changes in magnetic order tend to have very fast timescales, with switching frequencies on the order of tens of gigahertz in ferromagnets [11, 12], and hypothetically up to terahertz in antiferromagnets [13]. As this is much faster than the typical timescales in electronic systems, it allows the use of higher clock speeds than those suitable for electronics, providing another enticing benefit to spintronics.

As the field of spintronics is still in its infancy (at least in comparison to electronics), physically realized devices generally rely heavily on electronics for measurement and manipulation, rather than being 'pure spintronics'. For example, transporting spin between parts of a system often involves a spin-polarized electron current [14], which—needless to say—runs foul of the same Joule heating problems as ordinary electronics. However, an alternative does exist in the form of spin waves [14, 15]. In a classical ferromagnet, a spin wave is essentially a precession of the local electron spin around its equilibrium, that is passed between neighboring electrons to form a wave. The quantum mechanical analog is called a magnon, and carries a spin of $\hbar$ (compared to $+\frac{\hbar}{2}$ or $-\frac{\hbar}{2}$ for electrons). It has been shown [16] that it is possible to use magnons to transport spin through ferromagnetic insulators, thus avoiding the need to move electrons.

Although a few spintronic devices such as magnetic hard disks have been in commercial use for decades, serious strides can only be made with a solid theoretical understanding of the underlying physics. Accurate theoretical models of magnonic spin transport could be used, for example, to design new spintronic devices, or to optimize spin transport in spintronic circuits.

1.1 This thesis

In this thesis, I investigate the magnon transport properties of ferromagnetic and antiferromagnetic insulators in contact with heavy-metal leads. Passing an electronic current through a lead generates magnons in the magnetic material, which may either be absorbed at another lead, or allowed to accumulate. In a ferromagnet with only the injecting lead attached, the accumulation of magnons depends on the direction of the electric current, which in turn affects the resistivity of the lead itself—the magnonic contribution to a phenomenon called unidirectional spin-Hall magnetoresistance (USMR), which has previously only been described as originating from an electronic spin accumulation. When one or more leads are attached to a strongly anisotropic ferromagnet, elliptically polarized magnons are generated. Unlike 'normal' circular magnons, these do not conserve spin, which gives rise to a variety of effects, such as a new parasitic spin resistance at the lead-to-ferromagnet interface, and a phenomenon called squeezing.

The remainder of this thesis is structured as follows. Ch. 2 is a Dutch translation of this chapter. In Ch. 3, I shall give a more technical introduction to the concepts underlying this work. Basic knowledge of condensed matter theory and quantum theory is assumed, e.g. concepts such as creation and annihilation operators, Fourier transformation and the Brillouin zones. In Ch. 4, I analyse the magnonic contribution to USMR in platinum/yttrium iron garnet bilayers. In Ch 5, I develop a non-equilibrium Green's function (NEGF) formalism for the ballistic transport of elliptically polarized magnons in strongly anisotropic ferromagnetic insulators. In Ch. 6 I outline the extension of the NEGF formalism to antiferromagnets. Ch. 7 is a summary to this thesis, and an outlook into the future of theoretical magnonics. Finally, Ch. 8 is a Dutch translation of said summary and outlook.

2 NIET-WISKUNDIGE INLEIDING IN HET NEDERLANDS

Als men een lijst zou maken van de grootste prestaties van de mensheid, zou het een grove fout zijn om daarin niet de uitvinding van de transistor door Lilienfeld [5] in 1925, en de eerste fysieke implementatie daarvan in 1947 door Bardeen, Brattain en Shockley [6] te vermelden. Het is immers deze elektronische bouwsteen die het mogelijk heeft gemaakt om de gigantische mainframecomputers uit de Tweede Wereldoorlog te miniaturiseren tot de grootte van een vingernagel, en om de totale kennis van de mensheid letterlijk binnen ieders handbereik te brengen, zelfs in de meest afgezonderde uithoeken van de wereld.

Door transistoren kleiner en kleiner te maken heeft het aantal componenten in één geïntegreerd circuit decennialang exponentiële groei ondervonden—een fenomeen (en deels zelfvervullende voorspelling [7]) dat de Wet van Moore genoemd wordt [8]. Door steeds meer tranistoren met elkaar te verbinden, is de rekenkracht van computers aan een soortgelijke trend onderheven. De grenzen van deze ‘wet’ komen echter snel naderbij: naarmate transistoren kleiner worden, nemen thermische- en kwantumfluctuaties toe, tot het punt waarop deze onvermijdelijk fouten veroorzaken. Als men de transistor echter niet verder verkleint, moet grotere complexiteit duur betaald worden: het stroomverbruik en de warmteontwikkeling zullen sterk toenemen, waardoor de eisen voor voedings- en koelsystemen onpraktisch worden. Zelfs het overschakelen naar exotische halfgeleiders en lithografie met ultra-korte golflengte bieden maar voor korte tijd respijt van het catastrofale einde van de Wet van Moore.

Zelfs met bijna perfecte materialen en lithografietechnieken hebben circuits die op transistoren zijn gebaseerd een fundamenteel probleem dat veroorzaakt wordt door het feit dat ze elektronen heen en weer bewegen: hierbij is energieverlies door Ohmse verwarming onvermijdelijk. Eén van de beste manieren om de granzen van de Wet van Moore op te rekken zou dus te vinden moeten zijn in een manier om informatie te verplaatsen, waarbij men níet fysiek elektronen hoeft te verplaatsen.

Ziedaar, spintronica: een vakgebied dat probeert om de spin van het elektron als informatiedrager te gebruiken [9, 10], in plaats van de lading. In tegenstelling tot de lading, die de vaste waarde $-e \overset{\text{def}}{=} -1.602\,176\,634 \times 10^{-19}\,\mathrm{C}$ heeft, kan de spin van een elektron danwel 'up' ('omhoog'), danwel 'down' ('omlaag') zijn (ten opzichte van een gegeven kwantisatieas, meestal de richting van een magneetveld). In plaats van een binaire 'één' ('nul') te definiëren als de aanwezigheid (afwezigheid) van een elektron, kan men dan de elektronen altijd aanwezig en bewegingsloos laten, en de spin-up (spin-down) toestand vertalen naar de binaire 'één' ('nul'). Het cruciale punt is hierbij dat het niet nodig is om een elektron te verplaatsen om de spin om te klappen, waardoor het mogelijk wordt om minder energie te verbruiken dan in gewone elektronica het geval is.

In de praktijk blijkt het lastig om de spin van één elektron als een bit te gebruiken. In plaats daarvan bestaat een typisch spintronisch apparaat uit één of meer ferromagnetische of antiferromagnetische materialen in verbinding met 'randapparatuur' zoals draden of golfgeleiders, die gebruikt worden om lokaal de magnetische orde te manipuleren of meten. De netto (mesoscopische) magnetische orde van bijvoorbeeld een enkel magnetisch domein kan dan naar een bit vertaald worden. Het voordeel is dat veranderingen in magnetische orde zeer korte tijdschalen hebben, met schakelfrequenties op de orde van tientallen gigahertz in ferromagneten [11, 12], en hypothetisch tot een terahertz in antiferromagneten [13]. Aangezien dit veel sneller is dan de typische tijdschalen in elektronische systemen, kan men hogere kloksnelheden gebruiken dan in elektronica het geval is, wat spintronica dus nog een verleidelijk voordeel geeft.

Gezien spintronica als vakgebied nog in de kinderschoenen staat (in elk geval vergeleken met elektronica), hebben fysieke spintronische apparaten doorgaans nog veel elektronica nodig voor metingen en manipulatie, waardoor van 'pure spintronica' nog geen sprake is. Het transporteren van spin tussen onderdelen van een systeem gebruikt bijvoorbeeld vaak een spin-gepolariseerde elektrische stroom [14], die—het mag geen verassing zijn—nog steeds last heeft van hetzelfde Ohmse verwarmingsprobleem als gewone elektronica. Er bestaat echter een alternatief: spingolven [14, 15]. In een klassieke ferromagneet is een spingolf kortgezegd een precessie van de lokale elektronspin rond zijn evenwicht, die tussen naburige elektronen doorgegeven wordt om zo een golf te vormen. De kwantummechanische tegenhanger wordt een magnon genoemd, en draagt een spin van $\hbar$ (vergeleken met $+\frac{\hbar}{2}$ of $-\frac{\hbar}{2}$ voor elektronen). Men heeft aangetoond [16] dat het mogelijk is om via magnonen spin te transporteren door ferromagnetische isolatoren, waarbij het verplaatsen van elektronen dus vermeden wordt.

Hoewel enkele spintronische apparaten zoals harde schijven al decennia op commercieel niveau in gebruik zijn, kan men alleen echte voortgang boeken door een goed theoretisch begrip van de onderliggende fysica. Nauwkeurige theoretische modellen van magnonisch spintransport zouden bijvoorbeeld gebruikt kunnen worden om nieuwe spintronische apparaten to ontwerpen, of om spintransport in spintronische circuits te optimaliseren.

2.1 Deze scriptie

In deze scriptie onderzoek ik de transporteigenschappen van magnonen in ferromagnetische en antiferromagnetische isolatoren in contact met draden gemaakt van zware metalen. Door elektrische stroom door een draad te sturen worden in het magnetische materiaal magnonen opgewekt, die danwel door een andere draad geabsorbeerd kunnen worden, danwel opeen kunnen hopen. In een ferromagneet met alleen de ingaande draad bevestigd, hangt de opeenhoping van magnonen af van de richting van de elektrische stroom, welke op zijn beurt de soortelijke weerstand van de draad zelf beïnvloedt—de magnonische bijdrage aan een verschijnsel genaamd unidirectionele spin-Hallmagnetoresistentie (USMR), wat voorheen alleen beschreven is als voortkomende uit een opeenhoping van eletronenspin. Als één of meer draden bevestigd worden aan een sterk anisotrope ferromagneet, worden elliptisch gepolariseerde magnonen opgewekt. In tegenstelling tot 'gewone' circulaire magnonen, is spin in dit geval niet behouden, waardoor er verscheidene effecten optreden, waaronder een nieuwe parasitische spinweerstand op de interface tussen de draad en de ferromagneet, en een fenomeen dat *squeezing* wordt genoemd.

De rest van deze scriptie is alsvolgt geordend. In Hoofdstuk 3 geef ik een technischere inleiding in de concepten waarop deze scriptie is gebaseerd. Hier wordt een basiskennis aangenomen in de theorie van gecondenseerde materie en kwantumtheorie, bijvoorbeeld concepten zoals creatie- en annihilatieoperatoren, Fouriertransformatie en de Brillouinzones. In Hoofdstuk 4 analyseer ik de magnonische bijdrage aan USMR in platina/yttrium-ijzergranaatbilagen. In Hoofdstuk 5 ontwikkel ik een niet-equilibrium Greense functieformalisme (NEGF-formalisme) voor het ballistisch transport van elliptisch gepolariseerde magnonen in sterk anisotrope ferromagnetische isolatoren. In Hoofdstuk 6 leg ik een uitbreiding van het NEGF-formalisme naar antiferromagneten voor. Hoofdstuk 7 is een samenvatting van deze scriptie in het Engels en een vooruitblik in de toekomst van theoretische magnonica. Als laatste is Hoofdstuk 8 een Nederlandse vertaling van de samenvatting en vooruitblik.

3 Advanced introduction

Most elementary particles exhibit a nonzero angular momentum not associated with orbital motion. Being a purely quantum mechanical effect, this intrinsic angular momentum—called 'spin'—occurs only in half-integer (for fermions) or full-integer (for bosons) multiples of the reduced Planck constant $\hbar \overset{\text{def}}{=} \frac{1}{2\pi} \times 6.626\,070\,15 \times 10^{-34}\,\mathrm{kg\,m^2\,s^{-1}}$. Of particular interest is the spin of the electron, which may be either $+\frac{\hbar}{2}$ or $-\frac{\hbar}{2}$ ('spin-up' and 'spin-down'), and gives rise to a nonzero magnetic dipole moment.

Due to the Pauli exclusion principle, electrons in atoms inhabit fixed orbitals, forming pairs of spin-up and spin-down electrons that have zero net magnetic moment. However, in atoms with unfilled orbitals, not all electrons form pairs, and a net magnetic moment remains. When two atoms are in close proximity, as is the case in a solid, the partially filled orbitals may overlap, giving rise to an exchange interaction between the electrons. Following Hund's rules, this causes the spins to become aligned either parallel or anti-parallel to one another.

Because atoms in a solid generally have multiple close neighbors, the short-range exchange interaction may still give rise to long-range order, creating magnetic domains in which all pairs of nearest-neighbor electron spins are parallel or antiparallel. In the case of parallel alignment, the magnetic moments of the electrons in the domain add, creating a ferromagnet (FM) that exhibits a net magnetization. Conversely, if the spins are aligned anti-parallel, the moments of each participating pair subtract, creating an antiferromagnet (AFM) that does not exhibit magnetization (in the absence of an external field). FMs and AFMs exhibit second-order phase transitions, characterized by transition temperatures—the Curie temperature for FMs and Néel temperature for AFMs—below which magnetic order forms spontaneously.

The magnetic order of mesoscopic structures is one of the key properties of interest in the field of spintronics. The direction of magnetization of FMs, and the manipulation thereof, is used in well-known commercialized devices such as magnetic-core memory (a historic form of random-access memory that fell to disuse as early as the mid-1970s), magnetic tape and hard disks, and in more experimental or speculative devices such as racetrack memory, spin torque oscillators, and spin valves. Having no spontaneous magnetization, AFMs have not yet obtained widespread use, but potential applications have been envisioned, for example, in terahertz oscillators [17].

Although no introduction to spintronics should omit reference to devices utilizing the mesoscale magnetic order directly (and the reader is highly encouraged to peruse the wealth of literature available on the subject), the prime focus of this thesis is the somewhat narrower subfield of magnonics—the generation, detection and manipulation of spin waves. In magnonics, the global magnetic order is considered to be a fixed (or, rarely, dynamic) background, upon which live bosonic perturbations called magnons: quantized spin waves.

3.1 Magnetic models and the Holstein-Primakoff transformation

The majority of magnetically ordered materials are crystals with complicated unit cells, many of which are the subject of vast works that describe their magnetic, optic and thermal properties in excruciating detail [18–22]. Fortunately, one can strip away virtually all of these minutiae and still be left with a functional model of a ferromagnet or antiferromagnet. The simplest model that captures the properties necessary for theoretical magnonics is the Heisenberg (anti)ferromagnet [23, 24]. This model considers abstract spins in a regular lattice, with neighboring spins having an exchange interaction that tries to align them parallel or antiparallel to one another. It is represented by the concise Hamiltonian

$$H_0 = \mp \frac{J}{2} \sum_{\langle i,j \rangle} \hat{\boldsymbol{S}}_i \cdot \hat{\boldsymbol{S}}_j. \tag{3.1}$$

Here, $\hat{\boldsymbol{S}}_i$ is the vectorial spin operator for spin i, of which the components obey the commutation relations $[\hat{S}_i^a, \hat{S}_j^b] = \mathrm{i}\hbar \varepsilon_{abc} \delta_{ij} \hat{S}_i^c$, where a, b, c refer to any of the three Cartesian directions, ε_{abc} is the Levi-Civita symbol, and δ_{ij} is the Kronecker delta. The Hamiltonian sums over nearest-neighbor sites i and j of the lattice, and the factor of $\frac{1}{2}$ prevents double-counting. J is a positive real constant representing the exchange energy involved with the alignment of two nearest-neighbor spins, and the sign preceding it determines the nature of the magnetic material: a negative sign favors aligned spins and thus produces a ferromagnet, while a positive sign favors counter-alignment and thus produces an antiferromagnet.

Note that many works use alternative conventions regarding the prefactor: the range of J may be extended to the full real line so that the sign of J itself

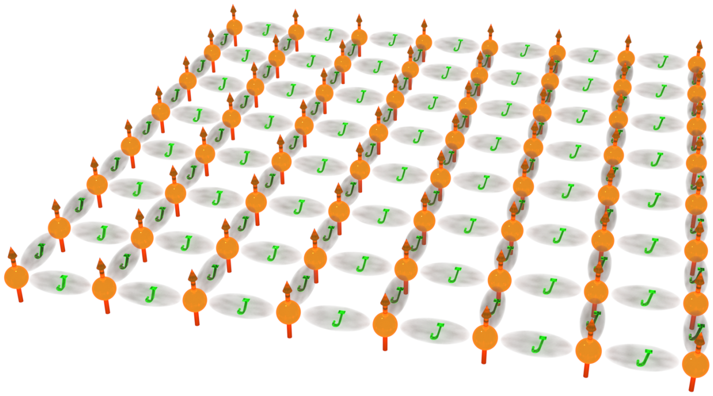

Figure 3.1: Two-dimensional square-lattice Heisenberg ferromagnet in its ground state, with all spins 'up'. Shown are the couplings J between nearest neighbors.

determines the nature of the magnetic material, and the factor of $\frac{1}{2}$ may be replaced with $-\frac{1}{2}, 1, -1, 2$ or -2 depending on the author.

In the ground state of the Heisenberg ferromagnet, all spins are mutually aligned. In absence of anisotropies or external fields, the alignment axis is arbitrary, and is conventionally considered to be the z-axis. In three- or higher-dimensional systems, mutual alignment of the spins occurs at a finite temperature, called the Curie temperature, due to spontaneous symmetry breaking. However, in one- and two-dimensional systems, the Mermin-Wagner theorem [25] forbids spontaneous alignment; in this case, anisotropies and/or magnetic fields may be used to ensure the system obtains a nonzero magnetization at finite temperatures (see Section 3.2).

Let us now consider a ferromagnet in the ground state, with all spins aligned with the z-axis (Fig. 3.1). A small perturbation of this ground state produces a spin wave (in a classical description) or magnon (in a quantum description)—however, as a quantum spin is represented by an operator rather than a simple vector, the perturbation theory that produces magnons contains some subtleties.

If the spin quantum number S of one site is large (at minimum, $S > 1$)—which is the case, for example, when a theoretical 'site' corresponds to a large physical unit cell with many free electrons, that collectively act as a single entity—we may expand the spin operator in terms of spin-1 bosonic creation and annihilation operators $\hat{a}_i^\dagger$ and $\hat{a}_i$, a process known as the Holstein-Primakoff

(HP) transformation [26, 27]. The three Cartesian spin operators are then given by

$$\hat{S}_i^x = \frac{1}{2}\left[\sqrt{2S - \hat{a}_i^\dagger \hat{a}_i}\hat{a}_i + \hat{a}_i^\dagger \sqrt{2S - \hat{a}_i^\dagger \hat{a}_i}\right], \tag{3.2a}$$

$$\hat{S}_i^y = -\frac{\mathrm{i}}{2}\left[\sqrt{2S - \hat{a}_i^\dagger \hat{a}_i}\hat{a}_i - \hat{a}_i^\dagger \sqrt{2S - \hat{a}_i^\dagger \hat{a}_i}\right], \tag{3.2b}$$

and

$$\hat{S}_i^z = S - \hat{a}_i^\dagger \hat{a}_i. \tag{3.2c}$$

(N.B.: commonly, the HP transformation is expressed in terms of the ladder operators $\hat{S}_i^\pm \equiv \hat{S}_i^x \pm \mathrm{i}\hat{S}_i^y$ and $\hat{S}_i^z$ instead of the Cartesian spin operators.) Note that HP magnons are circularly polarized and carry a spin of $\hbar$. In the presence of anisotropy, the correct low-energy excitations are *elliptically* polarized magnons, which are superpositions of HP states, and therefore carry a spin that is not exactly $\hbar$ (see Chapter 5).

As the expressions for $\hat{S}_i^x$ and $\hat{S}_i^y$ contain operators under the square root, the HP transformation is in principle a series with infinite interaction terms between HP magnons. However, in practise—and henceforth in this thesis—it is often sufficient to initially truncate all interaction terms, and validate this approach post-hoc by comparing the local magnon number density $\left\langle \hat{a}_i^\dagger \hat{a}_i \right\rangle$ (for all sites i) to the spin S: if the first is small compared to the latter, the magnons can safely be assumed to be non-interacting. The quadratic ferromagnetic magnon Hamiltonian then reads

$$\begin{aligned} H_{\mathrm{FM}}^{(2)} &= \frac{JS}{2}\sum_{\langle i,j\rangle}\left[\hat{a}_i^\dagger \hat{a}_i + \hat{a}_j^\dagger \hat{a}_j - \hat{a}_i^\dagger \hat{a}_j - \hat{a}_j^\dagger \hat{a}_i - S\right] \\ &= \frac{JS}{2}\sum_{\boldsymbol{r},\boldsymbol{\delta}}\Big[\hat{a}^\dagger(\boldsymbol{r})\hat{a}(\boldsymbol{r}) + \hat{a}^\dagger(\boldsymbol{r}+\boldsymbol{\delta})\hat{a}(\boldsymbol{r}+\boldsymbol{\delta}) \\ &\qquad - \hat{a}^\dagger(\boldsymbol{r})\hat{a}(\boldsymbol{r}+\boldsymbol{\delta}) - \hat{a}^\dagger(\boldsymbol{r}+\boldsymbol{\delta})\hat{a}(\boldsymbol{r}) - S\Big], \end{aligned} \tag{3.3}$$

where the vectors $\boldsymbol{r}$ now represent the positions of sites previously labelled i, and the vectors $\boldsymbol{\delta}$—the number of which is given by the coordination number z—represent the offsets to the z nearest neighbors of a site at the origin (a d-hypercubic lattice will have $z = 2d$ vectors $\boldsymbol{\delta}$). We assume $\boldsymbol{r}$ is expressed in the basis of lattice vectors.

In translationally invariant systems, this Hamiltonian is diagonalized by a Fourier transformation:

$$\hat{a}(\boldsymbol{r}) = \frac{1}{\sqrt{N}} \sum_{\boldsymbol{k}} \hat{a}(\boldsymbol{k}) \mathrm{e}^{\mathrm{i}\boldsymbol{r}\cdot\boldsymbol{k}}. \tag{3.4}$$

Assuming periodic boundary conditions, the component ρ of the vector $\boldsymbol{k}$ takes the values $2\pi n_\rho / N_\rho$, with N_ρ the total number of sites along the lattice vector ρ and n_ρ an item from a set of N_ρ successive integers. For simplicity, we assume N_ρ is even, and specify that $\boldsymbol{k}$ lies in the first Brillouin zone, i.e. $-N_\rho/2 \leq n_\rho < N_\rho/2$. Inserting this operator and its Hermitian conjugate into Eq. (3.3), we obtain

$$H^{(2)}_{\mathrm{FM}} = -\frac{JS^2 N z}{2} + \sum_{\boldsymbol{k}} \omega_{\mathrm{FM}}(\boldsymbol{k}) \hat{a}^\dagger(\boldsymbol{k}) \hat{a}(\boldsymbol{k}), \tag{3.5}$$

where

$$\omega_{\mathrm{FM}}(\boldsymbol{k}) = JSz - JS \sum_{\boldsymbol{\delta}} \cos\left(\boldsymbol{\delta} \cdot \boldsymbol{k}\right) \tag{3.6}$$

is the frequency of the mode with wavevector $\boldsymbol{k}$.

A similar treatment for antiferromagnets is somewhat more complicated, as they consist of sublattices whose ground-state magnetizations cancel one another (Fig. 3.2). Here, the simplest model is a d-hypercubic lattice consisting of two sublattices, typically called A and B, arranged such that every A-site has $2d$ B-type nearest neighbors, and vice-versa. The general Hamiltonian (3.1), remains unchanged, but sites subscripted with i (j) now correspond to A (B) sites.

To ensure the ground state has no magnetization, the A-sites must have spin projection $+S$ on the z-axis, while the B-sites have projection $-S$. To this end, the A-part of the HP transformation remains the same as given by Eqs. (3.2), while the B-operators become [28]

$$\hat{S}^{Bx}_j = \frac{1}{2}\left[\sqrt{2S - \hat{b}^\dagger_j \hat{b}_j}\,\hat{b}_j + \hat{b}^\dagger_j \sqrt{2S - \hat{b}^\dagger_j \hat{b}_j}\right], \tag{3.7a}$$

$$\hat{S}^{By}_j = \frac{\mathrm{i}}{2}\left[\sqrt{2S - \hat{b}^\dagger_j \hat{b}_j}\,\hat{b}_j - \hat{b}^\dagger_j \sqrt{2S - \hat{b}^\dagger_j \hat{b}_j}\right], \tag{3.7b}$$

and

$$\hat{S}^{Bz}_j = \hat{b}^\dagger_j \hat{b}_j - S. \tag{3.7c}$$

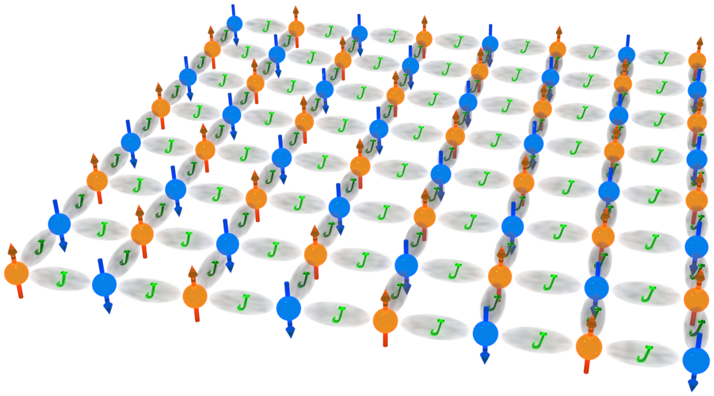

Figure 3.2: Two-dimensional square-lattice Heisenberg antiferromagnet in its ground state, with A-sublattice spins (amber) ‘up’ and B-sublattice spins (blue) ‘down’.

(In terms of the ladder operators, $\hat{S}_j^{B+}$ and $\hat{S}_j^{B-}$ have their definitions swapped compared to the A-sublattice, while $\hat{S}_j^z$ is multiplied with -1.)

Note that it is not necessary for an antiferromagnet to have a hypercubic lattice structure. However, other crystal symmetries complicate the sublattice approach: consider, for example, three antiferromagnetic spins in a triangle. Choose one spin to be ‘up’, and the other two ‘down’. Then there exist two pairs of nearest neighbors that satisfy the antiferromagnetic coupling, but one pair that does not. This principle is known as *frustration*, and makes it impossible to uniquely define two sublattices. It further leads to an extremely degenerate ground state and a complicated energy landscape. While frustrated systems are an interesting topic in their own right—to the extent that Giorgio Parisi was awarded the 2021 Nobel Prize in Physics for finding new theoretical methods to tackle them [29]—they are far outside the scope of this dissertation, and we shall therefore restrict discussion to the hypercubic lattice.

The quadratic magnon Hamiltonian may then be expressed in a separate sum for each sublattice (we assume there are $N/2$ A-spins and an equal number of

B spins):

$$\begin{aligned}
H^{(2)}_{\mathrm{AFM}} = \frac{JS}{2}\sum_{\boldsymbol{\delta}}\Bigg\{ &\sum_{\boldsymbol{r}\in A}\Big[\hat{a}^\dagger(\boldsymbol{r})\hat{a}(\boldsymbol{r}) + \hat{b}^\dagger(\boldsymbol{r}+\boldsymbol{\delta})\hat{b}(\boldsymbol{r}+\boldsymbol{\delta}) \\
&\qquad + \hat{a}(\boldsymbol{r})\hat{b}(\boldsymbol{r}+\boldsymbol{\delta}) + \hat{a}^\dagger(\boldsymbol{r})\hat{b}^\dagger(\boldsymbol{r}+\boldsymbol{\delta}) - S\Big] \\
&+ \sum_{\boldsymbol{r}\in B}\Big[\hat{a}^\dagger(\boldsymbol{r}+\boldsymbol{\delta})\hat{a}(\boldsymbol{r}+\boldsymbol{\delta}) + \hat{b}^\dagger(\boldsymbol{r})\hat{b}(\boldsymbol{r}) \\
&\qquad + \hat{a}(\boldsymbol{r}+\boldsymbol{\delta})\hat{b}(\boldsymbol{r}) + \hat{a}^\dagger(\boldsymbol{r}+\boldsymbol{\delta})\hat{b}^\dagger(\boldsymbol{r}) - S\Big]\Bigg\} \qquad (3.8) \\
= \frac{JS}{2}\sum_{\boldsymbol{\delta}}\Bigg\{ &\sum_{\boldsymbol{k}}\Big[\hat{a}^\dagger(\boldsymbol{k})\hat{a}(\boldsymbol{k}) + \hat{b}^\dagger(\boldsymbol{k})\hat{b}(\boldsymbol{k}) \\
&\qquad + \mathrm{e}^{-\mathrm{i}\boldsymbol{\delta}\cdot\boldsymbol{k}}\hat{a}(\boldsymbol{k})\hat{b}(-\boldsymbol{k}) + \mathrm{e}^{\mathrm{i}\boldsymbol{\delta}\cdot\boldsymbol{k}}\hat{a}^\dagger(\boldsymbol{k})\hat{b}^\dagger(-\boldsymbol{k}) - S\Big] \\
&+ \sum_{\boldsymbol{k}}\Big[\hat{a}^\dagger(\boldsymbol{k})\hat{a}(\boldsymbol{k}) + \hat{b}^\dagger(\boldsymbol{k})\hat{b}(\boldsymbol{k}) \\
&\qquad + \mathrm{e}^{\mathrm{i}\boldsymbol{\delta}\cdot\boldsymbol{k}}\hat{a}(\boldsymbol{k})\hat{b}(-\boldsymbol{k}) + \mathrm{e}^{-\mathrm{i}\boldsymbol{\delta}\cdot\boldsymbol{k}}\hat{a}^\dagger(\boldsymbol{k})\hat{b}^\dagger(-\boldsymbol{k}) - S\Big]\Bigg\} \\
= JSz\sum_{\boldsymbol{k}}\Big\{ &\hat{a}^\dagger(\boldsymbol{k})\hat{a}(\boldsymbol{k}) + \hat{b}^\dagger(\boldsymbol{k})\hat{b}(\boldsymbol{k}) \\
&\qquad + C(\boldsymbol{k})\Big[\hat{a}(\boldsymbol{k})\hat{b}(-\boldsymbol{k}) + \hat{a}^\dagger(\boldsymbol{k})\hat{b}^\dagger(-\boldsymbol{k})\Big] - S\Big\}, \qquad (3.9)
\end{aligned}$$

where

$$C(\boldsymbol{k}) \equiv \frac{1}{z}\sum_{\boldsymbol{\delta}}\cos(\boldsymbol{\delta}\cdot\boldsymbol{k}). \qquad (3.10)$$

Thus we see that even in translationally invariant systems, a Fourier transformation is no longer sufficient to diagonalize the AFM Hamiltonian, due to the presence of anomalous terms of the form $\hat{a}(\boldsymbol{k})\hat{b}(-\boldsymbol{k})$ (and h.c.). Instead, we must follow the Fourier transformation with a Bogoliubov transformation that mixes the sublattices:

$$\hat{a}(\boldsymbol{k}) = u(\boldsymbol{k})\hat{\alpha}(\boldsymbol{k}) + v(\boldsymbol{k})\hat{\beta}^\dagger(-\boldsymbol{k}), \qquad (3.11a)$$

$$\hat{b}(\boldsymbol{k}) = u(\boldsymbol{k})\hat{\beta}(\boldsymbol{k}) + v(\boldsymbol{k})\hat{\alpha}^\dagger(-\boldsymbol{k}), \qquad (3.11b)$$

where $u(\boldsymbol{k}) = u(-\boldsymbol{k})$ and $v(\boldsymbol{k}) = v(-\boldsymbol{k})$.

Inserting this into Eq. (3.9), we find

$$\begin{aligned} H^{(2)}_{\mathrm{AFM}} = JSz\sum_{\boldsymbol{k}} \Big\{ & \left[\hat{\alpha}^{\dagger}(\boldsymbol{k})\hat{\alpha}(\boldsymbol{k}) + \hat{\beta}^{\dagger}(\boldsymbol{k})\hat{\beta}(\boldsymbol{k})\right] \\ & \times \left[u^2(\boldsymbol{k}) + v^2(\boldsymbol{k}) + 2u(\boldsymbol{k})v(\boldsymbol{k})C(\boldsymbol{k})\right] \\ & + \left[\hat{\alpha}(\boldsymbol{k})\hat{\beta}(-\boldsymbol{k}) + \hat{\alpha}^{\dagger}(\boldsymbol{k})\hat{\beta}^{\dagger}(-\boldsymbol{k})\right] \\ & \times \left[u^2(\boldsymbol{k})C(\boldsymbol{k}) + v^2(\boldsymbol{k})C(\boldsymbol{k}) + 2u(\boldsymbol{k})v(\boldsymbol{k})\right] \\ & + \left[2v^2(\boldsymbol{k}) + 2u(\boldsymbol{k})v(\boldsymbol{k})C(\boldsymbol{k})\right] \Big\} - JS^2Nz. \end{aligned} \tag{3.12}$$

To diagonalize this Hamiltonian, we must eliminate the terms containing $\hat{\alpha}(\boldsymbol{k})\hat{\beta}(-\boldsymbol{k})$ and $\hat{\alpha}^{\dagger}(\boldsymbol{k})\hat{\beta}^{\dagger}(-\boldsymbol{k})$. Because the new operators $\hat{\alpha}(\boldsymbol{k})$ and $\hat{\beta}(\boldsymbol{k})$ must also satisfy the bosonic commutation relations, we require that $u^2(\boldsymbol{k}) - v^2(\boldsymbol{k}) = 1$, or

$$u(\boldsymbol{k}) = \cosh\left[\theta(\boldsymbol{k})\right], \tag{3.13a}$$

$$v(\boldsymbol{k}) = \sinh\left[\theta(\boldsymbol{k})\right], \tag{3.13b}$$

where $\theta(\boldsymbol{k}) = \theta(-\boldsymbol{k})$. To eliminate the anomalous terms, we then require

$$\cosh^2\left[\theta(\boldsymbol{k})\right] + \sinh^2\left[\theta(\boldsymbol{k})\right] = -\frac{\sinh\left[2\theta(\boldsymbol{k})\right]}{C(\boldsymbol{k})}, \tag{3.14}$$

which is satisfied if

$$\theta(\boldsymbol{k}) = \frac{\operatorname{arctanh}\left[-C(\boldsymbol{k})\right]}{2}. \tag{3.15}$$

The Hamiltonian then reads

$$H^{(2)}_{\mathrm{AFM}} = \Omega_{0,\mathrm{AFM}} + \sum_{\boldsymbol{k}} \omega_{\mathrm{AFM}}(\boldsymbol{k}) \left[\hat{\alpha}^{\dagger}(\boldsymbol{k})\hat{\alpha}(\boldsymbol{k}) + \hat{\beta}^{\dagger}(\boldsymbol{k})\hat{\beta}(\boldsymbol{k})\right], \tag{3.16}$$

where

$$\Omega_{0,\mathrm{AFM}} = -JS(1+S)Nz + \sum_{\boldsymbol{k}} \omega_{\mathrm{AFM}}(\boldsymbol{k}) \tag{3.17}$$

and

$$\omega_{\mathrm{AFM}}(\boldsymbol{k}) = JSNz\sqrt{1 - C^2(\boldsymbol{k})}. \tag{3.18}$$

3.1.1 Para-unitary diagonalization

The previous discussion pertains only to translationally invariant systems, where periodic boundary conditions may be applied in order to perform the Fourier transformation. When this is not the case, discrete FM and AFM Hamiltonians are diagonalized by a para-unitary transformation [30], which may be viewed as a combination of a pseudo-Fourier transformation and a Bogoliubov transformation. Consider a Hamiltonian that can be described by the matrix structure

$$H = \begin{pmatrix} \hat{a}^\dagger & \hat{a} \end{pmatrix} \begin{pmatrix} h_1 & h_2 \\ h_2^\dagger & h_3 \end{pmatrix} \begin{pmatrix} \hat{a} \\ \hat{a}^\dagger \end{pmatrix} \equiv \phi^\dagger h \phi. \tag{3.19}$$

Here, we define the operator $\phi \equiv (\hat{a}, \hat{a}^\dagger)^\mathrm{T}$, where $\hat{a}$ is a vector operator of dimension N (with each component $\hat{a}_i$ an operator acting on site i), h_1 and h_3 are Hermitian $N \times N$ matrices, and h_2 is a general complex $N \times N$ matrix. The $2N \times 2N$ matrix h is required to be positive definite. The components of the operator $\hat{a}$ obey bosonic commutation relations:

$$[\hat{a}_i, \hat{a}_j^\dagger] = \delta_{ij} \tag{3.20}$$

$$[\hat{a}_i, \hat{a}_j] = [\hat{a}_i^\dagger, \hat{a}_j^\dagger] = 0. \tag{3.21}$$

The goal is to find a matrix $\mathcal{T}$, such that

$$\phi^\dagger h \phi = \Psi^\dagger D \Psi \equiv \phi^\dagger \mathcal{T}^\dagger D \mathcal{T} \phi, \tag{3.22}$$

where D is a diagonal matrix, and we define the vector operators $\Psi \equiv \mathcal{T}\phi \equiv (\hat{\psi}, \hat{\psi}^\dagger)^\mathrm{T}$. The matrix $\mathcal{T}$ must be chosen such that $\hat{\psi}$ preserves the commutation relations of $\hat{a}$:

$$[\hat{\psi}_i, \hat{\psi}_j^\dagger] = \delta_{ij} \tag{3.23}$$

$$[\hat{\psi}_i, \hat{\psi}_j] = [\hat{\psi}_i^\dagger, \hat{\psi}_j^\dagger] = 0. \tag{3.24}$$

To satisfy this condition, the matrix $\mathcal{T}$ must be para-unitary, i.e., it must obey the relation

$$\sigma_3 \mathcal{T}^\dagger = \mathcal{T}^{-1} \sigma_3, \tag{3.25}$$

where

$$\sigma_3 = \begin{pmatrix} \mathbb{I}_N & 0 \\ 0 & -\mathbb{I}_N \end{pmatrix} \tag{3.26}$$

is the $2N \times 2N$ analog of the third Pauli matrix, and $\mathbb{I}_N$ is the $N \times N$ identity matrix.

The procedure of constructing the inverse transformation $\mathcal{T}^{-1}$ is similar to that of constructing an ordinary unitary transformation: first, one solves the characteristic equation to find the paravalues (cf. eigenvalues), and using these one solves for the paranormalized paravectors (cf. normalized eigenvectors), which then make up the columns of the inverse transformation matrix. The para-unitary characteristic equation is given by

$$|h - \lambda_\mu \sigma_3| = 0, \tag{3.27}$$

and produces $2N$ paravalues λ_μ (possibly degenerate). All λ_μ are positive if and only if h is positive-definite [30], and each paravalue gives rise to a paravector

$$p_\mu \equiv \begin{pmatrix} u_\mu \\ v_\mu \end{pmatrix}, \tag{3.28}$$

where u_μ and v_μ are N-vectors. Next, one must compute the paranorm of the vectors p_μ, which is defined as

$$(p_\mu)^\dagger \sigma_3 p_\mu = (u_\mu)^\dagger u_\mu - (v_\mu)^\dagger v_\mu. \tag{3.29}$$

Upon dividing by the square root of the absolute value of their paranorm, the vectors p_μ are said to be paranormalized. The inverse transformation matrix $\mathcal{T}^{-1}$ then has as its first N columns the paravectors with paranorm 1, and as its last N columns the paravectors with paranorm -1.

Note further that the para-unitary diagonalization of h is equivalent to the unitary diagonalization of the matrix $\sigma_3 h$, which yields N positive and N negative eigenvalues, and has the vectors p_μ as its eigenvectors.

Up to a constant, the ferromagnetic magnon Hamiltonian (3.3) may be cast into the form of Eq. (3.19) using the bosonic commutation relations. While the bare Heisenberg Hamiltonian can be unitarily diagonalized, the introduction of anisotropy terms (see Section 3.2) produces nonzero h_2-submatrices, making the para-unitary treatment a requirement. The constant that remains does not change the spacing between energy levels, and can often be ignored.

The para-unitary approach is likewise necessary to diagonalize the antiferromagnetic Hamiltonian (3.8). Observant readers will note that this Hamiltonian contains $\hat{a}$ and $\hat{b}$ operators, whereas the operator $\hat{\phi}$ is defined only in terms of the $\hat{a}$ operator. However, as terms combining $\hat{a}^\dagger$ with $\hat{b}$ or $\hat{a}$ with $\hat{b}^\dagger$ (i.e., terms that convert a B-magnon into an A-magnon or vice-versa) are absent from the quadratic Hamiltonian, the overall Bogoliubov structure remains, so that one may redefine ϕ as $(\hat{a}, \hat{b}^\dagger)^{\mathrm{T}}$ and proceed as before.

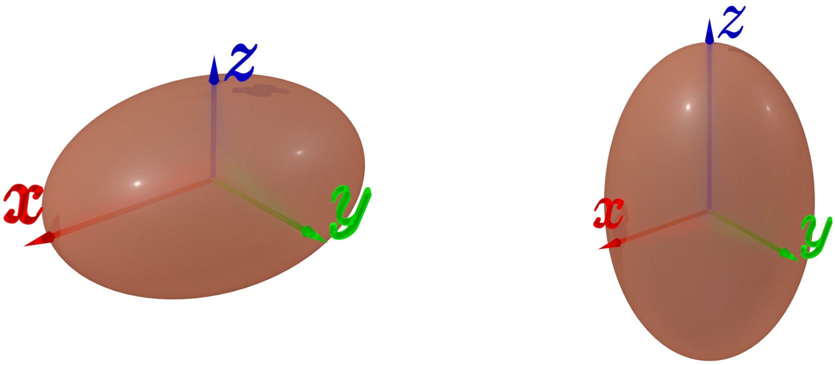

(a) (b)

Figure 3.3: Visualization of the three-component anisotropy model as an axis-aligned ellipsoid. The full anisotropy tensor is a rotated form of this object. (a): easy-z-axis anisotropy, where the z axis is shorter than the x and y axes. (b): easy-xy-plane anisotropy, where the x and y axes are equal and shorter than the z axis.

3.2 Anisotropies and fields

While the Heisenberg Hamiltonian (3.1) produces the basic phenomenology of (anti)ferromagnetism, real magnetic materials invariably include a certain amount of anisotropy. Various sources may be distinguished, such as the crystalline nature of the material, the shape of mesoscopic structures, and applied strain. The latter may in turn be 'built in' during the crystal grows process, or originate from externally applied bending, shearing, etcetera. These anisotropies act to create preferred directions for the magnetization or Néel vector (the difference between the magnetization vectors of the two sublattices), and may further be position-dependent, for example, in the presence of crystal defects or across the boundary of a grain.

At the lowest relevant order, the combined effect of these anisotropies can be captured by a Hamiltonian term of the form

$$H_{\mathrm{ani}} = \sum_i \hat{\boldsymbol{S}}_{\boldsymbol{i}}^{\mathrm{T}} \mathcal{K}_i \hat{\boldsymbol{S}}_{\boldsymbol{i}}, \tag{3.30}$$

where $\mathcal{K}$ is a Hermitian 3×3 matrix. Restricting to the case where $\mathcal{K}$ is real, this anisotropy matrix may be decomposed into the form $R_i^{\mathrm{T}} \operatorname{diag}(K_i^x, K_i^y, K_i^z) R_i$, where R_i is a rotation (orthogonal matrix).

Roughly speaking, one can view the diagonal anisotropy matrix $\mathrm{diag}(K_i^x, K_i^y, K_i^z)$ as forming an axis-aligned ellipsoid, acting to align the equilibrium spin with its shortest axis, i.e. the one corresponding to the smallest K^ν. If there is one distinct smallest anisotropy constant, the Hamiltonian describes an easy-axis magnet (Fig. 3.3a); conversely, if the ellipsoid is a prolate spheroid, such that two anisotropy constants are equal and the third is larger, the Hamiltonian describes an easy-plane magnet (Fig. 3.3b). Note that because only the square of the spin operators appears in Eq. (3.30), terms of this form leave the system invariant under reversal of the (sublattice) magnetization.

Upon Holstein-Primakoff transformation (to second order in the magnon operators) and, if necessary, completing the square (i.e. transforming $\hat{a}_i \to \hat{a}_i' = \hat{a}_i + \lambda_i$ and choosing the complex constant λ such that the Hamiltonian coefficient of the single-operator terms $\hat{a}'$ and $\hat{a}^{\dagger\prime}$ vanishes), Eq. (3.30) may always be brought into the form

$$H_{\mathrm{ani}}^{(2)} = S \sum_i \left[\mathcal{A}_i \hat{a}_i^\dagger \hat{a}_i + \mathcal{B}_i \hat{a}_i \hat{a}_i + \mathcal{B}_i^* \hat{a}_i^\dagger \hat{a}_i^\dagger + \mathcal{C}_i \right], \tag{3.31}$$

and similar for the B-sublattice of an AFM. Here, $\mathcal{A}_i$ and $\mathcal{C}_i$ are real constants, and $\mathcal{B}_i$ is a complex constant. $\mathcal{B}_i$ vanishes only when the projection of the anisotropy ellipsoid on the xy plane (i.e. the plane perpendicular to the quantization axis) is circular. In all other cases, the Hamiltonian will have non-vanishing anomalous terms of the form $\hat{a}\hat{a}$ and $\hat{a}^\dagger \hat{a}^\dagger$, so that a Bogoliubov or para-unitary transformation is needed to diagonalize it.

Another key ingredient that is present in virtually every treatment (be it theoretical or experimental) is an external magnetic field. In the context of theoretical magnonics, this may be used, for example, to break ground state degeneracy, fix natural a spin quantization axis, and tune the magnon energy gap. Furthermore, the processes typically present in spintronic systems have varying dependence on both the direction and magnitude of the external field, making it an indispensable tool for discerning concurrent effects in experimental research.

The magnetic field is a vector that couples linearly to the spin:

$$H_{\mathrm{mag}} = \sum_i \boldsymbol{h}_i \cdot \hat{\boldsymbol{S}}_i. \tag{3.32}$$

In the context of magnonics, one typically uses the magnetic field to fix the direction of the magnetization or Néel vector in the ground state before performing the Holstein-Primakoff transformation. For position-independent fields ($\boldsymbol{h}_i = \boldsymbol{h}$), it is then a natural choice to define one's coordinate system such that $\boldsymbol{h}$ lies along the z-axis.

In AFMs, spins from both sublattices try to align parallel to the magnetic field. However, this implies A-type spins are parallel to B-type spins, which is carries an energy penalty due to the exchange interaction. As a result, the actual ground state configuration of an isotropic AFM in a magnetic field has its spins aligned *perpendicular* to the field, and mutually antiparallel; this is known as the spin-flop phase. Within the plane to which the magnetic field is normal, this ground state exhibits rotational symmetry, which is undesirable in light of the Holstein-Primakoff transformation. For this reason, one typically introduces an easy-axis anisotropy term into the AFM Hamiltonian, parallel to the magnetic field, so that mutually antiparallel alignment of all spins, collinear to the external field becomes the unique ground state.

3.3 Spin-flip scattering and the spin Hall effect

To use magnons as an information carrier, one must be able to inject magnons into a magnetically ordered material. Although various means exist to do so (e.g. optical or thermal methods), for the purpose of this work, we shall consider only electronic spin flip scattering.

In this process, a conductor is interfaced with a magnetic material (MM – this can be either an FM or an AFM). When a spin-up ($+\frac{\hbar}{2}$) electron moving through the conductor hits the interface, it can flip its spin (to $-\frac{\hbar}{2}$), transferring the angular momentum to the MM by creating a magnon of spin $\hbar$. Conversely, when a magnon moving through the MM reaches the interface, it can flip the spin of a spin-down electron, annihilating the magnon in the process. The operator forms of these processes—the Feynman diagrams of which can be found in Figure 3.4—are easily derived from the exchange coupling between electrons at the interface and spins in the MM.

Consider an itinerant electron at position $\boldsymbol{r}$ in a lead, and a nearby spin in the MM at position $\boldsymbol{r'}$. The Hamiltonian term corresponding to the exchange interaction between the lead electron and MM spin is given by

$$H_{\text{ex}}(\boldsymbol{r},\boldsymbol{r'}) = J(\boldsymbol{r},\boldsymbol{r'})\hat{\boldsymbol{S}}^{\text{lead}}(\boldsymbol{r}) \cdot \hat{\boldsymbol{S}}^{\text{MM}}(\boldsymbol{r'}). \tag{3.33}$$

The Cartesian components $\nu \in \{x, y, z\}$ of the lead electron's spin operator $\hat{\boldsymbol{S}}^{\text{lead}}$ can be expressed in terms of the Pauli matrices σ_ν and spin-up (-down) fermionic creation and annihilation operators $\hat{c}^\dagger_{\uparrow(\downarrow)}$ and $\hat{c}_{\uparrow(\downarrow)}$ as [31]

$$\hat{S}^{\text{lead}}_\nu(\boldsymbol{r}) = \begin{pmatrix} \hat{c}^\dagger_\uparrow(\boldsymbol{r}) & \hat{c}^\dagger_\downarrow(\boldsymbol{r}) \end{pmatrix} \sigma_\nu \begin{pmatrix} \hat{c}_\uparrow(\boldsymbol{r}) \\ \hat{c}_\downarrow(\boldsymbol{r}) \end{pmatrix}, \tag{3.34}$$

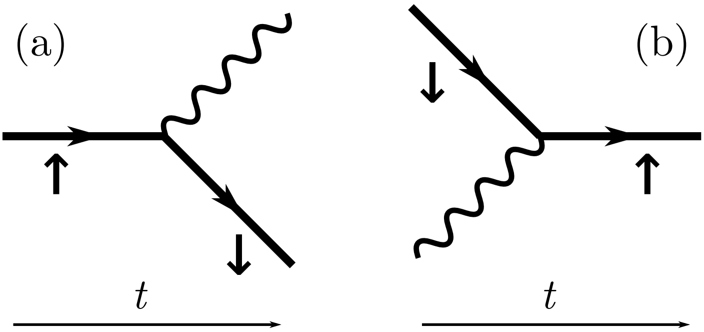

Figure 3.4: Feynman diagrams for spin-flip scattering processes, whereby an electron (thick straight lines) creates (a) or annihilates (b) a magnon (wavy lines). Arrows represent the electron spin. The horizontal direction represents time t.

or, in Cartesian vector notation,

$$\hat{\boldsymbol{S}}^{\text{lead}}(\boldsymbol{r}) = \begin{pmatrix} \hat{c}^\dagger_\downarrow(\boldsymbol{r})\hat{c}_\uparrow(\boldsymbol{r}) + \hat{c}^\dagger_\uparrow(\boldsymbol{r})\hat{c}_\downarrow(\boldsymbol{r}) \\ -\mathrm{i}\hat{c}^\dagger_\downarrow(\boldsymbol{r})\hat{c}_\uparrow(\boldsymbol{r}) + \mathrm{i}\hat{c}^\dagger_\uparrow(\boldsymbol{r})\hat{c}_\downarrow(\boldsymbol{r}) \\ \hat{c}^\dagger_\uparrow(\boldsymbol{r})\hat{c}_\uparrow(\boldsymbol{r}) - \hat{c}^\dagger_\downarrow(\boldsymbol{r})\hat{c}_\downarrow(\boldsymbol{r}) \end{pmatrix}. \tag{3.35}$$

The MM spin operator is expressed in bosonic operators using the Holstein-Primakoff transformation (3.2), so that we obtain (to quadratic order, for an FM or A-sublattice spin in an AFM)

$$\begin{aligned} H_{\text{ex}}(\boldsymbol{r}, \boldsymbol{r'}) = \sqrt{2S}J(\boldsymbol{r}, \boldsymbol{r'}) \left[\hat{c}^\dagger_\downarrow(\boldsymbol{r})\hat{c}_\uparrow(\boldsymbol{r})\hat{a}^\dagger(\boldsymbol{r'}) + \hat{c}^\dagger_\uparrow(\boldsymbol{r})\hat{c}_\downarrow(\boldsymbol{r})\hat{a}(\boldsymbol{r'})\right] \\ + J(\boldsymbol{r}, \boldsymbol{r'}) \left[\hat{c}^\dagger_\downarrow(\boldsymbol{r})\hat{c}_\downarrow(\boldsymbol{r}) - \hat{c}^\dagger_\uparrow(\boldsymbol{r})\hat{c}_\uparrow(\boldsymbol{r})\right] \left[S - \hat{a}^\dagger(\boldsymbol{r'})\hat{a}(\boldsymbol{r'})\right]. \end{aligned} \tag{3.36}$$

Here, the first line describes the spin-flip scattering processes: a spin-up electron is annihilated to produce a spin-down electron and a magnon, or conversely, a spin-down electron and a magnon are annihilated to create a spin-up electron. The terms on the second line produce an overall energy shift that depends on the spin accumulation and magnon density, but leave the magnon number invariant (and are therefore irrelevant to the present discussion).

Normally, the magnon creation and annihilation contributions to the spin-flip scattering process are (on average over large scales) exactly balanced, so that there is no net magnon injection or extraction. The balance is broken when one electron spin species is more prevalent at the interface inside the conductor, e.g. when the current passed through it is spin-polarized. However, rather than deferring the generation of spin imbalance to the current source, a more direct means exists in the form of the spin Hall effect (SHE) [32], which allows the required spin imbalance to be created from a spin-unpolarized electron current in a metallic contact to the magnonic device.

The SHE occurs when an electric current is passed through a conductor which exhibits strong spin-orbit coupling, and is essentially a solid-state version of a spin-dependent electron scattering effect proposed by Mott [33] in 1929. Per Gay and Dunning [34], Mott scattering, and by extension the spin Hall effect, is best explained in terms of classical physics.

Consider a heavy atom of atomic number Z, such that the electrical charge of its nucleus is eZ. At a separation $\boldsymbol{r}$ from the nucleus, an electron experiences a magnetic field

$$\boldsymbol{B} = \frac{eZ}{cm_\mathrm{e}|\boldsymbol{r}|^3}\boldsymbol{L} = \frac{eZ}{c|\boldsymbol{r}|^3}\boldsymbol{r} \times \boldsymbol{v} \tag{3.37}$$

originating from the charge of the nucleus. Here, c is the speed of light, m_e is the electron's mass, $\boldsymbol{L} = m_\mathrm{e}\boldsymbol{r} \times \boldsymbol{v}$ is the orbital angular momentum, and $\boldsymbol{v}$ is the electron's velocity. The magnetic field in turn couples to the electron's intrinsic (spin) magnetic moment $\boldsymbol{\mu}_\mathbf{s}$, giving rise to a potential term

$$V_\mathrm{so} = -\boldsymbol{\mu}_\mathbf{s} \cdot \boldsymbol{B}, \tag{3.38}$$

which causes the electron to deflect in the direction normal to the plane spanned by its motion and its magnetic moment. As the motion of electrons in a metal is proportional to the electric current $\boldsymbol{j}_\mathbf{e}$, electrons with their magnetic moment aligned to some given axis $\hat{\boldsymbol{n}}$ produce a transverse spin current $\boldsymbol{j}_\mathbf{s} \propto \boldsymbol{j}_\mathbf{e} \times \hat{\boldsymbol{n}}$; see Figure 3.5a.

More generally, if the direction of the electrons' spin is not specified, one may describe a spin current by a tensor j^s_{ij}, where the index i describes the direction of motion and the index j describes the spin orientation. In an isotropic heavy metal (HM), spin-orbit coupling introduces an interdependence between the charge current j^e_i and the spin current j^s_{ij} [35]:

$$j^\mathrm{e}_i = j^{\mathrm{e}(0)}_i + \gamma\epsilon_{ijk}j^\mathrm{s}_{jk}, \tag{3.39}$$

$$j^\mathrm{s}_{ij} = j^{\mathrm{s}(0)}_{ij} - \gamma\epsilon_{ijk}j^\mathrm{e}_k, \tag{3.40}$$

where γ is a small scalar parameter, ϵ_{ijk} is the Levi-Civita symbol, and $j^{\mathrm{e}(0)}_i$ and $j^{\mathrm{s}(0)}_{ij}$ are, respectively, the charge and spin currents in absence of spin-orbit coupling.

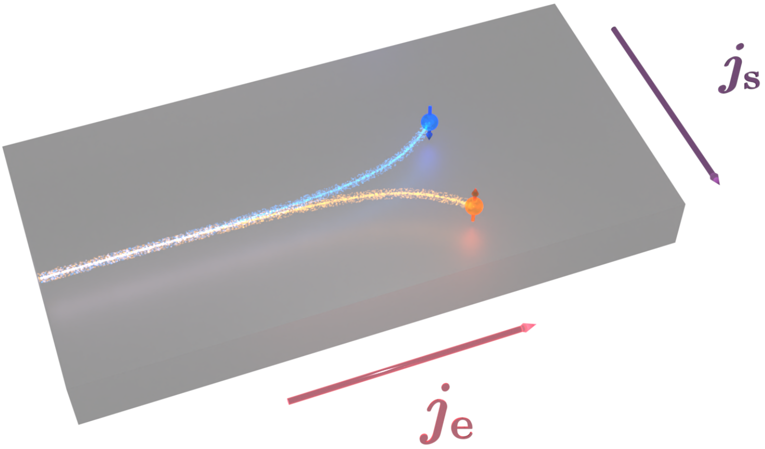

(a)

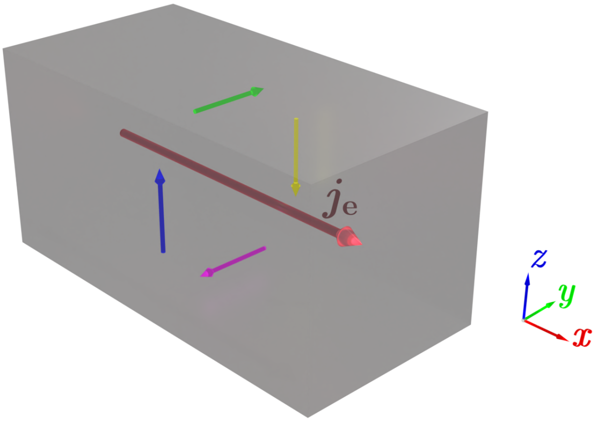

(b)

Figure 3.5: Graphical depictions of the spin Hall effect. (a) Spin deflection of electrons with a given spin orientation. In a heavy metal, spin species deflect in the plane normal to the electric current $\boldsymbol{j}_\mathbf{e}$, producing a spin current $\boldsymbol{j}_\mathbf{s}$. (b) Spin accumulation profile arising from an electric current. The large red arrow represents the electron current $\boldsymbol{j}_\mathbf{e}$, flowing in the positive x-direction. The four tangential arrows represent the direction of the current-induced spin accumulation at the conductor's edges.

Analogous to the ordinary Hall effect, in which the transverse electric current causes a voltage to build up, the spin Hall effect produces a spin accumulation at opposite sides of the spin Hall device perpendicular to the charge current (see Figure 3.5b). By interfacing the HM with an FM or AFM [36–38], the SHE directly produces the spin imbalance necessary to inject magnons through spin-flip scattering.

By the principle of Onsager reciprocity, there also exists an inverse spin Hall effect (ISHE): a pure spin current leads to a transverse charge current. As a result, a heavy-metal lead may be used to detect the presence of magnonic spin in a ferromagnet. In 2015, Cornelissen *et al.* [16] used the ISHE to measure magnonic spin transport through a ferromagnetic insulator (yttrium iron garnet; YIG), injected using the SHE several micrometres away from the detector.

4 MAGNON CONTRIBUTION TO UNIDIRECTIONAL SPIN HALL MAGNETORESISTANCE

...IN FERROMAGNETIC-INSULATOR/HEAVY-METAL BILAYERS

We develop a model for the magnonic contribution to the unidirectional spin Hall magnetoresistance (USMR) of heavy metal/ferromagnetic insulator bilayer films. We show that diffusive transport of Holstein-Primakoff magnons leads to an accumulation of spin near the bilayer interface, giving rise to a magnoresistance which is not invariant under inversion of the current direction. Unlike the electronic contribution described by Zhang and Vignale [Phys. Rev. B **94**, 140411 (2016)], which requires an electrically conductive ferromagnet, the magnonic contribution can occur in ferromagnetic insulators such as yttrium iron garnet. We show that the magnonic USMR is, to leading order, cubic in the spin Hall angle of the heavy metal, as opposed to the linear relation found for the electronic contribution. We estimate that the maximal magnonic USMR in Pt|YIG bilayers is on the order of 10^{-8}, but may reach values of up to 10^{-5} if the magnon gap is suppressed, and can thus become comparable to the electronic contribution in e.g. Pt|Co. We show that the magnonic USMR at a finite magnon gap may be enhanced by an order of magnitude if the magnon diffusion length is decreased to a specific optimal value that depends on various system parameters.

4.1 Introduction

The total magnetoresistance of metal/ferromagnet heterostructures is known to comprise several independent contributions, including but not limited to anisotropic magnetoresistance (AMR) [39], giant magnetoresistance (GMR, in stacked magnetic multilayers) [40] and spin Hall magnetoresistance (SMR) [41]. A common characteristic of these effects is that they are linear; in particular, this means the measured magnetoresistance is invariant under reversal of the polarity of the current.

In 2015, however, Avci *et al.* [42] measured a small but distinct asymmetry in the magnetoresistance of Ta|Pt and Co|Pt bilayer films. Due to its striking similarity to the current-in-plane spin Hall effect (SHE) and GMR, save for its nonlinear resistance/current characteristic, this effect was dubbed unidirectional spin Hall magnetoresistance (USMR).

In the years following its discovery, USMR has been detected in bilayers consisting of magnetic and nonmagnetic topological insulators [43], and the dependence of the USMR on layer thickness has been investigated experimentally for Co|Pt bilayers [44]. Additionally, Avci *et al.* [45] have shown that USMR may be used to distinguish between the four distinct magnetic states of a ferromagnet|normal metal|ferromagnet trilayer stack, highlighting its potential application in multibit electrically controlled memory cells.

Although USMR is ostensibly caused by spin accumulation at the ferromagnet|metal interface, a complete theoretical understanding of this effect is lacking. In bilayer films consisting of ferromagnetic metal (FM) and heavy metal (HM) layers, electronic spin accumulation in the ferromagnet caused by spin-dependent electron mobility provides a close match to the observed results [46]. It remains unknown, however, whether this is the full story; indeed, this model's underestimation of the USMR by a factor of two lends plausibility to the idea that there may be additional, as-yet unknown contributions providing the same experimental signature. Additionally, the electronic spin accumulation model cannot be applied to bilayers consisting of a ferromagnetic insulator (FI) and a HM, as there will be no electric current in the ferromagnet to drive accumulation of spin.

Kim *et al.* [47] have measured the USMR of Py|Pt (where Py denotes for permalloy) bilayer and claim, using qualitative arguments, that a *magnonic* process is involved. Likewise, for Co|Pt and CoCr|Pt, more recent results by Avci *et al.* [48] argue in favor of the presence of a magnon-scattering contribution consisting of terms linear and cubic in the applied current, and having a magnitude comparable to the electronic contribution of Zhang and Vignale [46]. Although these experimental results provide a great deal of insight into the underlying processes, a theoretical framework against which they can be tested is presently lacking. In this work, we aim to take first steps to developing such a framework, by considering an accumulation of magnonic spin near the FI|HM bilayer interface, which we describe by means of a drift-diffusion model.

The remainder of this article is structured as follows: in Sec. 4.2, we present our analytical model as generically as possible. In Sec. 4.3 we analyze the behavior of our model using parameters corresponding to a Pt|YIG (YIG being yttrium iron garnet) bilayer as a basis. In particular, in Sec. 4.3.1 we give quantitative predictions of the magnonic USMR in terms of the applied current and layer thicknesses, and in Sec. 4.3.2 we take into account the effect of Joule heating. In the remainder of Sec. 4.3, we investigate the influence of various material parameters. Finally, in Sec. 4.4 we summarize our key results and present some open questions.

4.2 Magnonic spin accumulation

To develop a model of the magnonic contribution to the USMR, we focus on the simplest FI|HM heterostructure: a homogeneous bilayer. We treat the transport of magnonic and electronic spin as diffusive, and solve the resulting diffusion equations subject to a quadratic boundary condition at the interface. In this approach, valid in the opaque interface limit, current-dependent spin accumulations—electronic in the HM and magnonic in the FI—form near the interface. In particular, the use of a nonlinear boundary condition breaks the invariance of the SMR under reversal of the current direction, i.e. it produces USMR.

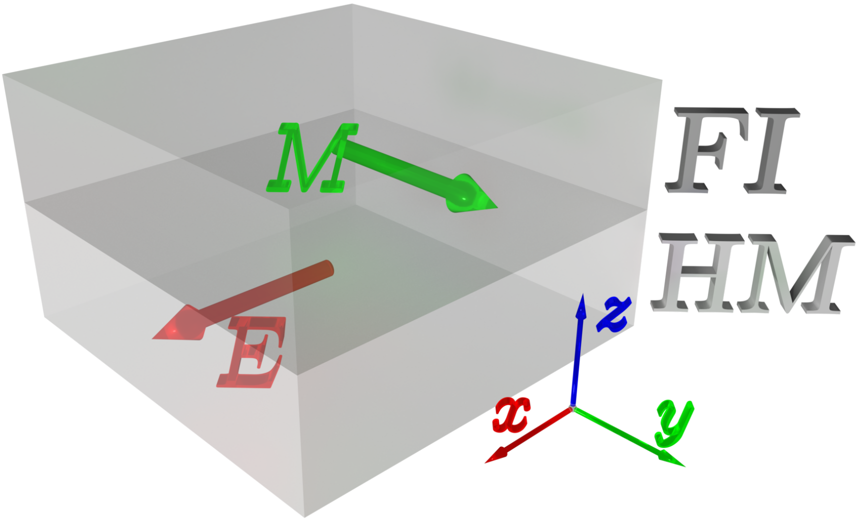

Figure 4.1: Schematic depiction of our system. The magnetization M of the FI layer lies in the $+y$ direction, an electric field of magnitude E is applied to the heavy metal layer (HM) in the $\pm x$ direction, and the interface between the layers lies in the xy plane.

We consider a sample consisting of a FI layer of thickness L_{FI} directly contacting a HM layer of thickness L_{HM}. We take the interface to be the xy plane, such that the FI layer extends from $z = 0$ to L_{FI} and the HM layer from $z = -L_{\mathrm{HM}}$ to 0. The magnetisation is chosen to lie in the positive y-direction, and an electric field $\boldsymbol{E} = \pm E\hat{\mathbf{x}}$ is applied in the x-direction. The set-up is shown in Fig. 4.1.

The extents of the system parallel to the interface are taken to be infinite, and the individual layers completely homogeneous. This allows us to treat the system as quasi-one-dimensional, in the sense that we will only consider spin currents that flow in the z-direction. We account for magnetic anisotropy only indirectly through the existence of a magnon gap. We further assume that our system is adequately described by the Drude model (suitably extended to include spin effects[49]), and that the interface between layers is not fully transparent to spin current, i.e., has a finite spin-mixing conductance [50]. For simplicity, we assume electronic spin and charge transport may be neglected in the ferromagnet, as is the case for ferromagnetic insulators.

We describe the transfer of spin across the interface microscopically by the continuum-limit interaction Hamiltonian

$$H_{\mathrm{int}} = -\int \mathrm{d}^3\boldsymbol{r}\mathrm{d}^3\boldsymbol{r'}\, J(\boldsymbol{r},\boldsymbol{r'})\Big[b^\dagger(\boldsymbol{r'})c^\dagger_\downarrow(\boldsymbol{r})c_\uparrow(\boldsymbol{r}) + b(\boldsymbol{r'})c^\dagger_\uparrow(\boldsymbol{r})c_\downarrow(\boldsymbol{r})\Big], \tag{4.1}$$

where $c^\dagger_\alpha(\boldsymbol{r})$ $[c_\alpha(\boldsymbol{r})]$ are fermionic creation [annihilation] operators of electrons with spin $\alpha \in \{\uparrow,\downarrow\}$ at position $\boldsymbol{r}$ in the HM, and $b^\dagger(\boldsymbol{r'})$ $[b(\boldsymbol{r'})]$ is the bosonic creation [annihilation] operator of a circularly polarized Holstein-Primakoff magnon [26] at position $\boldsymbol{r'}$ inside the ferromagnet. We leave $J(\boldsymbol{r},\boldsymbol{r'})$ to be some unknown coupling between the electrons and magnons, which is ultimately fixed by taking the classical limit [51, 52].

Transforming to momentum space and using Fermi's golden rule, we obtain the interfacial spin current $j_{\mathrm{s}}^{\mathrm{int}}$, which can be expressed in terms of the real part of the spin mixing conductance per unit area $g_{\mathrm{r}}^{\uparrow\downarrow}$ as [51, 53]

$$j_{\mathrm{s}}^{\mathrm{int}} = \frac{g_{\mathrm{r}}^{\uparrow\downarrow}}{\pi s}\int \mathrm{d}\varepsilon\, g(\varepsilon)(\varepsilon - \Delta\mu) \times \left[n_{\mathrm{B}}\left(\frac{\varepsilon-\Delta\mu}{k_{\mathrm{B}}T_{\mathrm{e}}}\right) - n_{\mathrm{B}}\left(\frac{\varepsilon-\mu_{\mathrm{m}}}{k_{\mathrm{B}}T_{\mathrm{m}}}\right)\right]. \tag{4.2}$$

(Similar expressions were derived by Takahashi *et al.* [54] and Zhang and Zhang [55], although these are not given in terms of the spin-mixing conductance.)

Here, s is the saturated spin density in the FI layer, $g(\varepsilon)$ is the magnon density of states, $n_{\mathrm{B}}(x) = [\mathrm{e}^x - 1]^{-1}$ is the Bose-Einstein distribution function, k_{B}

is Boltzmann's constant, and T_m and T_e are the temperatures of the magnon and electron distributions, respectively, which we do not assume *a priori* to be equal (although the equal-temperature special case will be our primary interest). Of crucial importance in Eq. (4.2) are the magnon effective chemical potential μ_m—which we shall henceforth primarily refer to as the magnon spin accumulation—and the electron spin accumulation $\Delta\mu \equiv \mu^\uparrow - \mu^\downarrow$, which we define as the difference in chemical potentials for the spin-up and spin-down electrons. (In both cases, a positive accumulation means the majority of spin magnetic moments point in the $+y$ direction.)

We employ the magnon density of states

$$g(\varepsilon) = \frac{\sqrt{\varepsilon - \Delta}}{4\pi^2 J_\mathrm{s}^{\frac{3}{2}}} \Theta(\varepsilon - \Delta). \tag{4.3}$$

Here, J_s is the spin wave stiffness constant, $\Theta(x)$ is the Heaviside step function, and Δ is the magnon gap, caused by a combination of external magnetic fields and internal anisotropy fields in ferromagnetic materials [56]. In our primary analysis of a Pt|YIG bilayer, we take $\Delta \equiv \mu_\mathrm{B} \times 1\,\mathrm{T} \approx k_\mathrm{B} \times 0.67\,\mathrm{K}$ with μ_B the Bohr magneton, in good agreement with e.g. Cherepanov *et al.* [18], and in Sec. 4.3.5 we specifically consider the limit of a vanishing magnon gap.

To treat the accumulations on equal footing, we now redefine $\mu_\mathrm{m} \to \delta\mu_\mathrm{m}$ and $\Delta\mu \to \delta\Delta\mu$, expand Eq. (4.2) to second order in δ, and set $\delta = 1$ to obtain

$$\begin{aligned} j_\mathrm{s}^\mathrm{int} \simeq -\Bigg[& k_\mathrm{B} T_\mathrm{m} I_0 + I_\mathrm{e} \Delta\mu + I_\mathrm{m} \mu_\mathrm{m} + \frac{I_\mathrm{ee}}{k_\mathrm{B} T_\mathrm{e}} (\Delta\mu)^2 \\ & + \frac{I_\mathrm{mm}}{k_\mathrm{B} T_\mathrm{m}} \mu_\mathrm{m}^2 + \frac{I_\mathrm{me}}{k_\mathrm{B} T_\mathrm{m}} \mu_\mathrm{m} \Delta\mu \Bigg] \frac{g_\mathrm{r}^{\uparrow\downarrow} (k_\mathrm{B} T_\mathrm{m})^{\frac{3}{2}}}{4\pi^3 J_\mathrm{s}^{\frac{3}{2}} s}. \end{aligned} \tag{4.4}$$

Here, the I_i are dimensionless integrals given by Eqs. (4.15) in the Appendix. All I_i are functions of T_m and Δ, and I_0, I_e and I_ee additionally depend on T_e. In the special case where $T_\mathrm{m} = T_\mathrm{e}$, I_0 vanishes, $I_\mathrm{m} = -I_\mathrm{e}$, and $I_\mathrm{ee} = -(I_\mathrm{mm} + I_\mathrm{me})$.

In addition to $j_\mathrm{s}^\mathrm{int}$, the spin accumulations and the electric driving field E give rise to the following spin currents in the z direction:

$$j_\mathrm{s}^\mathrm{e} = \frac{\hbar}{2e} \left(-\frac{\sigma}{2e} \frac{\partial \Delta\mu}{\partial z} - \sigma \theta_\mathrm{SH} E \right), \tag{4.5a}$$

$$j_\mathrm{s}^\mathrm{m} = -\frac{\sigma_\mathrm{m}}{\hbar} \frac{\partial \mu_\mathrm{m}}{\partial z}. \tag{4.5b}$$

Here j_s^e and j_s^m are the electron and magnon spin currents, respectively. σ is the electrical conductivity in the HM, σ_m is the magnon conductivity in the ferromagnet, e is the elementary charge, and θ_SH is the spin Hall angle.

In line with Cornelissen *et al.* [57] and Zhang and Zhang [58], we assume the spin accumulations μ_m and $\Delta\mu$ obey diffusion equations along the z-axis:

$$\frac{\mathrm{d}^2\mu_\mathrm{m}}{\mathrm{d}z^2} = \frac{\mu_\mathrm{m}}{l_\mathrm{m}^2}, \qquad \frac{\mathrm{d}^2\Delta\mu}{\mathrm{d}z^2} = \frac{\Delta\mu}{l_\mathrm{e}^2}, \tag{4.6}$$

where l_m and l_e are the magnon and electron diffusion lengths, respectively. We solve these equations analytically subject to boundary conditions that demand continuity of the spin current across the interface and confinement of the currents to the sample:

$$j_\mathrm{s}^\mathrm{m}(0) = j_\mathrm{s}^\mathrm{e}(0) = j_\mathrm{s}^\mathrm{int}(0), \tag{4.7}$$

$$j_\mathrm{s}^\mathrm{m}(L_\mathrm{FI}) = j_\mathrm{s}^\mathrm{e}(-L_\mathrm{HM}) = 0. \tag{4.8}$$

This system of equations now fully specifies the magnonic and electronic spin accumulations μ_m and $\Delta\mu$, the latter of which enters the charge current j_c via the spin Hall effect:

$$j_\mathrm{c}(z) = \sigma E + \frac{\sigma\theta_\mathrm{SH}}{2e}\frac{\partial\Delta\mu(z)}{\partial z}. \tag{4.9}$$

The measured resistivity at some electric field strength E is then given by the ratio of the electric field and the averaged charge current:

$$\rho(E) = \frac{E}{\frac{1}{L_\mathrm{HM}}\int_{-L_\mathrm{HM}}^{0} \mathrm{d}z\, j_\mathrm{c}(z)}. \tag{4.10}$$

Finally, we define the USMR $\mathcal{U}$ as the fractional difference in resistivity on inverting the electric field:

$$\mathcal{U} \equiv \left|\frac{\rho(E)-\rho(-E)}{\rho(E)}\right| = \left|1 + \frac{\int_{-L_\mathrm{HM}}^{0}\mathrm{d}z\, j_\mathrm{c}(z;E)}{\int_{-L_\mathrm{HM}}^{0}\mathrm{d}z\, j_\mathrm{c}(z;-E)}\right|. \tag{4.11}$$

It should be noted that the even-ordered terms in the expansion of the interface current are vital to the appearance of unidrectional SMR. Suppose our system has equal magnon and electron temperature, such that the interfacial spin Seebeck term I_0 vanishes (see Section 4.3.2), and we ignore the quadratic terms in Eq. (4.4). Then because the only term in the spin current equations (4.5) that is independent of the accumulations is $-\frac{\hbar\sigma\theta_\mathrm{SH}}{2e}E$ in Eq. (4.5a), we have that $\Delta\mu \propto \mu_\mathrm{m} \propto E$. Then by Eqs. (4.9) and (4.10), $j_\mathrm{c} \propto E$ and $\rho(E) \propto \frac{E}{E}$, such that $\mathcal{U} = 0$. Conversely, with quadratic terms in the interfacial spin current, $\rho(E) \sim \frac{E}{E+E^2}$, and likewise if I_0 does not vanish, $\rho(E) \sim \frac{E}{1+E}$. Both cases give nonvanishing USMR. Physically, one can say that the spin-dependent electron and magnon populations couple together in a nonlinear fashion (namely, through the Bose-Einstein distributions in Eq. (4.2)), leading to a nonlinear dependence on the electric field.

4.3 Results

4.3.1 Equal-temperature, finite gap case

Although our model can be solved analytically (up to evaluation of the integrals I_i), the full expression of $\mathcal{U}$ is unwieldy and therefore hardly insightful. To get an idea of the behavior of a real system, we use a set of parameters—listed in Table 4.1—corresponding to a Pt|YIG bilayer as a starting point. (Unless otherwise specified, all parameters used henceforth are to be taken from this table.)

Fig. 4.2 shows the magnonic USMR of a Pt|YIG bilayer versus applied driving current (σE) when $T_\mathrm{m} = T_\mathrm{e} = T$, at the temperature of liquid nitrogen (77 K, blue), room temperature (293 K, green) and the Curie temperature of YIG (560 K [18], red). FI and HM layer thicknesses used are 90 nm and 3 nm, respectively, in line with experimental measurements by Avci *et al.* [59].

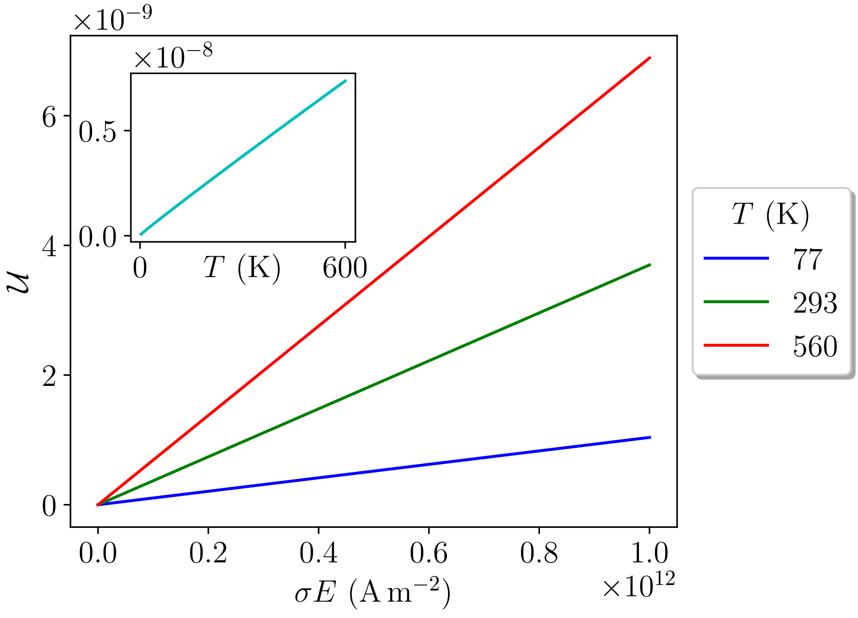

Figure 4.2: USMR $\mathcal{U}$ versus driving current σE for a Pt|YIG bilayer at liquid nitrogen temperature (77 K, blue), room temperature (293 K, green) and the YIG Curie temperature (560 K, red). Inset: USMR versus system temperature T at fixed current $\sigma E = 1 \times 10^{12}\,\mathrm{A\,m^{-2}}$.

In all cases the magnonic USMR is proportional to the applied electric current—that is, the cubic term found by Avci *et al.* [48] is absent—and at room temperature has a value on the order of 10^{-9} at typical measurement currents [42]. This is roughly four orders of magnitude weaker than the USMR obtained—both experimentally and theoretically—for FM|HM hybrids [42, 44, 46, 59], and is consistent with the experimental null results obtained for this system by Avci *et al.* [59]. Note, however, that the thickness of the FI layer used by these authors is significantly lower than the magnon spin diffusion length $l_\mathrm{m} = 326\,\mathrm{nm}$, which results in a suppressed USMR.

Furthermore, it can be seen in the inset of Fig. 4.2 that the magnonic USMR is, to good approximation, linear in the system temperature, in agreement with observations by Kim *et al.* [47] and Avci *et al.* [48].

In Fig. 4.3 we compute the USMR at $\sigma E = 1 \times 10^{12}\,\mathrm{A\,m^{-2}}$ as a function of both L_FI and L_HM. A maximum is reached around $L_\mathrm{HM} \approx 4.5\,\mathrm{nm}$, while in terms of L_FI, a plateau is approached within a few spin diffusion lengths. By varying the layer thicknesses, a maximal USMR of 4.2×10^{-8} can be achieved, an improvement of one order of magnitude compared to the thicknesses used by Avci *et al.* [59].

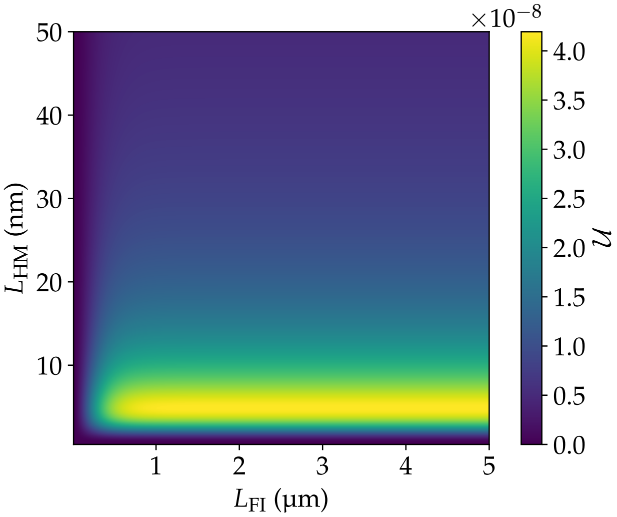

Figure 4.3: Pt|YIG USMR $\mathcal{U}$ at $T_\mathrm{m} = T_\mathrm{e} = 293\,\mathrm{K}$ versus FI layer thickness L_FI and HM layer thickness L_HM. A driving current $\sigma E = 1\times10^{12}\,\mathrm{A\,m^{-2}}$ is used. A maximal USMR of 4.2×10^{-8} is reached at $L_\mathrm{HM} = 4.5\,\mathrm{nm}$, $L_\mathrm{FI} = 5\,\mathrm{\mu m}$.

4.3.2 Thermal effects

We take into account a difference between the electron and magnon temperatures T_{e} and T_{m} by assuming these parameters are equal to the temperatures of the HM and FI layers, respectively, which we take to be homogeneous. We assume that the HM undergoes ohmic heating and dissipates this heat into the ferromagnet, which we take to be an infinite heat bath at temperature T_{m}. We only take into account the interfacial (Kapitza) thermal resistance R_{th} between the HM and FI layers, leading to a simple expression for the HM temperature T_{e}:

$$T_{\mathrm{e}} = T_{\mathrm{m}} + R_{\mathrm{th}}\sigma E^2 L_{\mathrm{HM}}. \tag{4.12}$$

Using this model, we still find a linear dependence in the electric field, $\mathcal{U} \simeq u_E(T_{\mathrm{m}})\sigma E$, but the coefficient $u_E(T_{\mathrm{m}})$ increases by three orders of magnitude compared to the case where the electron and magnon temperatures are set to be equal. The overwhelming majority of this increase can be attributed to an interfacial spin Seebeck effect (SSE) [57, 60]: it is caused by the accumulation-independent contribution I_0 (Eq. (4.15a)) in the interface current. When I_0 is artificially set to 0, $u_E(T_{\mathrm{m}})$ changes less than 1% from its equal-temperature value.

Furthermore, the overall magnitude of the interfacial SSE in our system can be attributed to the fact that we have a conductor|insulator interface: the current runs through the HM only, resulting in inhomogeneous Joule heating of the sample and a large temperature discontinuity across the interface.

4.3.3 Spin Hall angle

The electronic spin accumulation $\Delta\mu$ at the interface in the standard spin Hall effect is linear in the electric field E and spin Hall angle θ_{SH} [41]. From the linearity in E, we may conclude that the terms in Eq. (4.4) that are linear in $\Delta\mu$ have a suppressed contribution to the USMR. Thus, the contribution of the interface current is of order θ_{SH}^2. Furthermore, $\Delta\mu$ enters the charge current (Eq. (4.9)) with a prefactor θ_{SH}, leaving the magnonic USMR predominantly cubic in the spin Hall angle. Indeed, in the special case $T_{\mathrm{m}} = T_{\mathrm{e}}$, expanding the full expression for $\mathcal{U}$ (which spans several pages and is therefore not reproduced within this work) in θ_{SH} reveals that the first nonzero coefficient is that of θ_{SH}^3. This suggests a small change in θ_{SH} potentially has a large effect on the USMR.

In Fig. 4.4 we plot the USMR for a Pt|YIG bilayer—once again using $T_{\mathrm{m}} = T_{\mathrm{e}} = 293\,\mathrm{K}$—consisting of 4.5 nm of Pt and 5 µm of YIG, in which we sweep the spin Hall angle. Included is a cubic fit $\mathcal{U} = u_\theta\theta_{\mathrm{SH}}^3$, where we find $u_\theta \simeq$

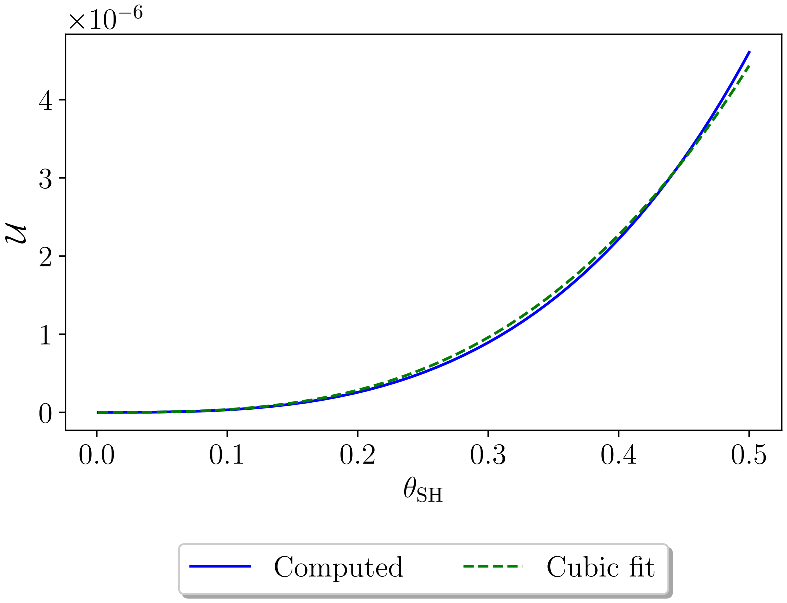

Figure 4.4: USMR $\mathcal{U}$ at $T_{\mathrm{m}} = T_{\mathrm{e}} = 293\,\mathrm{K}$ versus spin Hall angle θ_{SH}. A driving current $\sigma E = 1 \times 10^{12}\,\mathrm{A\,m^{-2}}$ and FI and HM layer thicknesses $L_{\mathrm{FI}} = 5\,\mu\mathrm{m}$ and $L_{\mathrm{HM}} = 4.5\,\mathrm{nm}$ are used. Blue curve: computed value. Dashed green curve: fit of the form $\mathcal{U} = u_\theta \theta_{\mathrm{SH}}^3$, with $u_\theta \simeq 3.1 \times 10^{-4}$.

3.1×10^{-4}. Here it can be seen that the magnonic USMR in HM|FI bilayers can, as expected, potentially acquire magnitudes roughly comparable to those in HM|FM systems, provided one can find or engineer a metal with a spin Hall angle several times greater than that of Pt. This suggests that very strong spin-orbit coupling (SOC) is liable to produce significant magnon-mediated USMR in FI|HM heterostructures, although we expect our model to break down in this regime.

4.3.4 A note on the magnon spin diffusion length

Although we use the analytic expression for the magnon spin diffusion length[55, 57, 58],

$$l_{\mathrm{m}} = v_{\mathrm{th}} \sqrt{\frac{2}{3} \tau \tau_{\mathrm{mr}}} \tag{4.13}$$

—where v_{th} is the magnon thermal velocity, τ is the combined relaxation time, and τ_{mr} is the magnonic relaxation time (see Table 4.1)—this is known to correspond poorly to reality, being at least an order of magnitude too low in the case of YIG [57]. Artificially setting the magnon spin-diffusion length to the experimental value of 10 µm (while otherwise continuing to use the parameters from Table 4.1) results in a drop in USMR of some 4 orders of magnitude.

It follows directly that there exists some optimal value of l_{m} (which we shall label $l_{\mathrm{m,opt}}$) that maximizes the USMR, which we plot as a function of the FI layer thickness L_{FI} in Fig. 4.5, at $L_{\mathrm{HM}} = 4.5\,\mathrm{nm}$ and $\sigma E = 1 \times 10^{12}\,\mathrm{A\,m^{-2}}$, and for various values of the magnon-phonon relaxation time τ_{mp}, which is the shortest and therefore most important timescale we take into account. For the physically realistic value of $\tau_{\mathrm{mp}} = 1\,\mathrm{ps}$ (blue curve), the optimal magnon spin diffusion length is just 24 nm. Although $l_{\mathrm{m,opt}}$ itself depends on τ_{mp}, the condition $l_{\mathrm{m}} = l_{\mathrm{m,opt}}$ acts to cancel the dependence of the USMR on the magnon-phonon relaxation time. Curiously, the USMR additionally loses its dependence on L_{FI}, reaching a fixed value of 4.14×10^{-7} for our parameters.

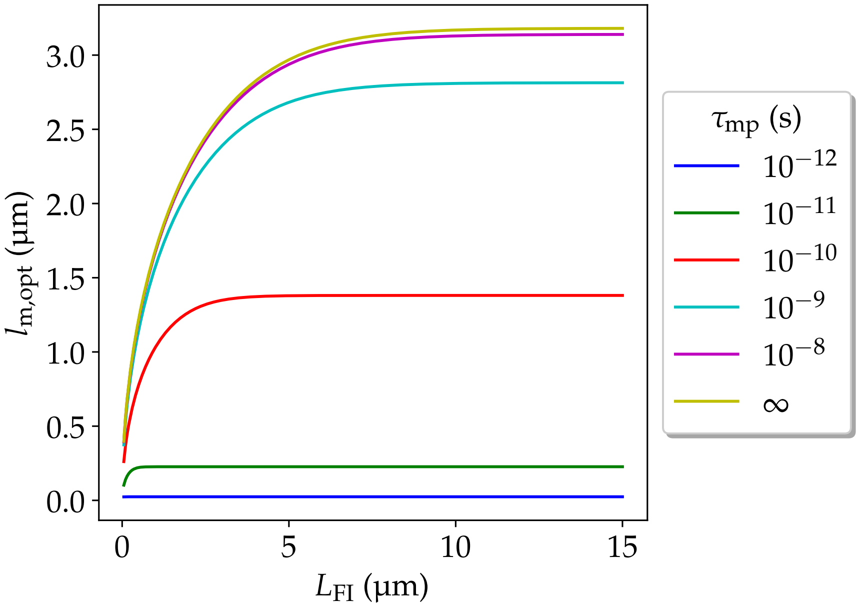

Figure 4.5: Value of the magnon spin diffusion length l_{m} that maximizes the USMR, as a function of FI layer thickness L_{FI}, at various values of the magnon-phonon relaxation time τ_{mp}.

We further find that $l_{\mathrm{m,opt}}$ is independent of the spin Hall angle and driving current, and shows a weak decrease with increasing temperature provided the magnon-phonon scattering time is sufficiently short. A significant increase in the optimal spin diffusion length is only found at low temperatures and large τ_{mp}. Similarly, a weak dependence on the Gilbert damping constant α is found, becoming more significant at large τ_{mp}, with lower values of α corresponding to larger $l_{\mathrm{m,opt}}$. When α is swept, again the USMR at $l_{\mathrm{m}} = l_{\mathrm{m,opt}}$ acquires a universal value of 4.14×10^{-7} for our system parameters.

4.3.5 Effect of the magnon gap

We have thus far utilised a fixed magnon gap with a value of $\Delta/\mu_{\mathrm{B}} = 1\,\mathrm{T}$ for YIG. Although this is reasonable for typical systems, it is possible to significantly reduce the gap size by minimizing the anisotropy fields within the sample, e.g. using a combination of external fields [61], optimized sample shapes [56, 62] and temperature [63, 64]. This leads us to consider the effect a decreased or even vanishing gap may have on our results.

Fig. 4.6 shows the USMR $\mathcal{U}$ for a Pt|YIG system (4.5 nm of Pt and 5 µm of YIG) at room temperature, plotted against the driving current σE, now for different values of the magnon gap Δ. Here it can be seen that while $\mathcal{U}$ is linear in E for large gap sizes and realistic currents, it shows limiting behavior at smaller gaps, becoming independent of the electric current above some threshold (provided one neglects the effect of Joule heating). At low current and intermediate magnon gap, the current dependence is nonlinear at $\mathcal{O}(I^2)$ as opposed to the $\mathcal{O}(I^3)$ behavior found by Avci *et al.* [48].

Note also that the saturation value of the USMR is two to three orders of magnitude greater than the values found previously in our work, and of the same magnitude as the electronic contribution found by Zhang and Vignale [46].

The maximal value of the USMR that can be achieved may be found by considering the full analytic expression for $\mathcal{U}$ in terms of the generic coefficients I_i representing the dimensionless integrals given by Eqs. (4.15) in the Appendix. In the gapless limit $\Delta \to 0$ and at equal magnon and electron temperature ($T_{\mathrm{m}} = T_{\mathrm{e}}$), the second-order coefficients I_{mm} and I_{me} diverge, while their sum takes the constant value $\lambda \equiv I_{\mathrm{mm}} + I_{\mathrm{me}} \simeq 0.323551$ at room temperature. I_{ee} does not diverge, and obtains the value $-\lambda$.

Now working in the thick-ferromagnet limit ($L_{\mathrm{FI}} \to \infty$), we substitute $I_{\mathrm{me}} \to -I_{\mathrm{mm}} + \lambda$ and take the limits $E \to \infty$ and $I_{\mathrm{mm}} \to -\infty$. By application of l'Hôpital's rule in the latter, all coefficients I_i drop out of the expression for $\mathcal{U}$.

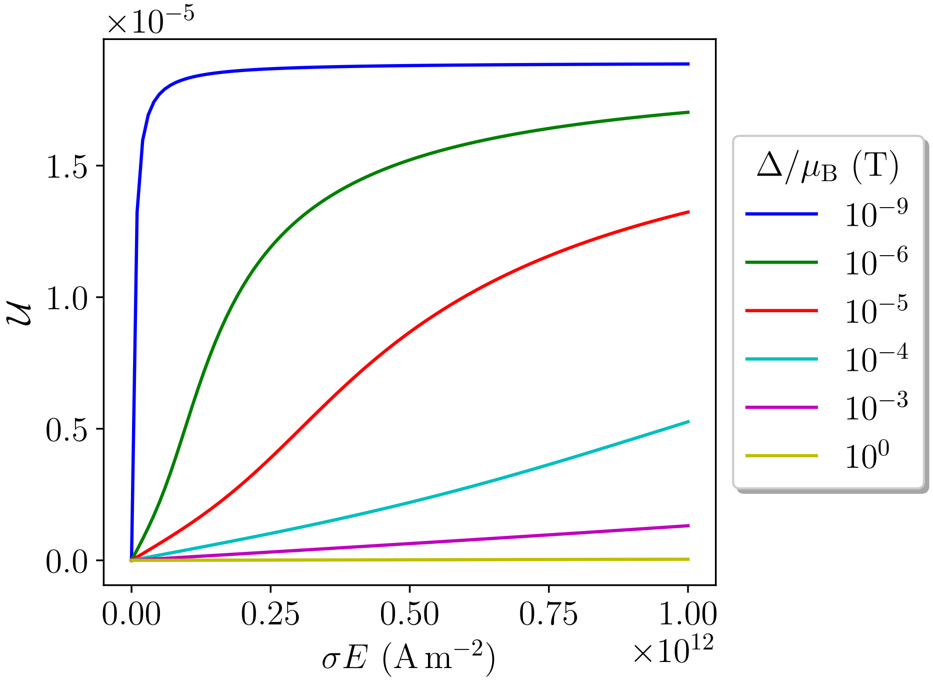

Figure 4.6: USMR $\mathcal{U}$ of a Pt(4.5 nm)|YIG(5 µm) bilayer at room temperature versus applied current σE at various values of the magnon gap Δ. For large gaps, linear behavior is recovered at realistic currents, while for smaller gap sizes, the USMR saturates as the current is increased.

This leaves only the asymptotic value, which, after expanding in θ_{SH}, reads

$$\mathcal{U}_{\max} = \frac{4e^2 l_s^2 \theta_{\mathrm{SH}}^2 \sigma_{\mathrm{m}} \tanh^2\left(\frac{L_{\mathrm{HM}}}{2l_s}\right)}{\hbar^2 l_{\mathrm{m}} L_{\mathrm{HM}} \sigma + 4 l_s e^2 L_{\mathrm{HM}} \sigma_{\mathrm{m}} \coth\left(\frac{L_{\mathrm{HM}}}{l_s}\right)} + \mathcal{O}(\theta_{\mathrm{SH}}^4). \tag{4.14}$$

Whereas the linear-in-E regime of the magnonic USMR grows as θ_{SH}^3, we thus find that the leading-order behavior of the *asymptotic* value is only θ_{SH}^2, and the third-order term vanishes completely. Physically, this can be explained by the fact that the asymptotic magnonic USMR is purely a bulk effect: all details about the interface vanish, while parameters originating from the bulk spin- and charge currents remain. The appearance of l_{m} in the denominator and its absence in the numerator of Eq. (4.14) once again highlights that a large magnon spin diffusion length acts to *suppress* the USMR.

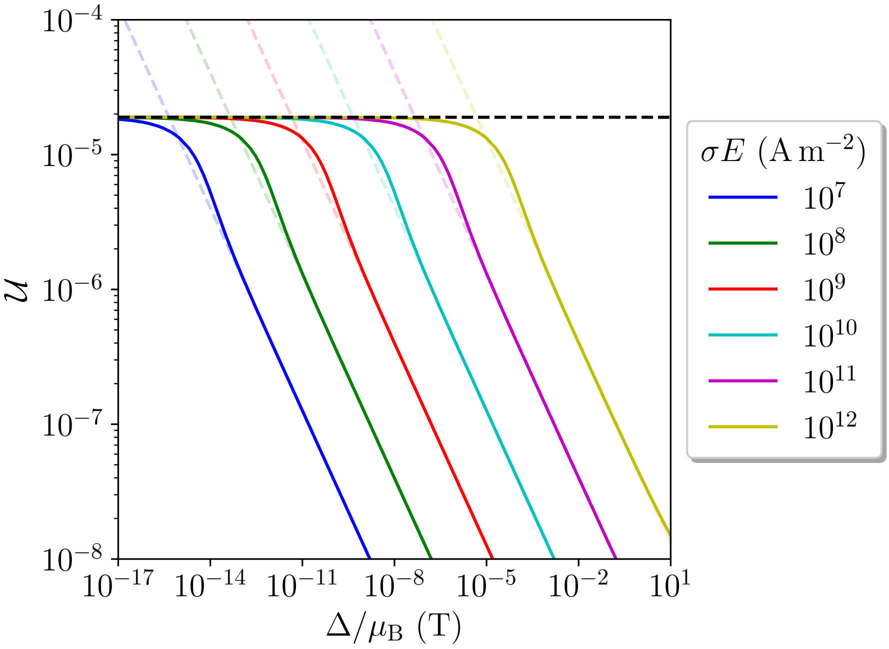

Figure 4.7: USMR $\mathcal{U}$ of a Pt(4.5 nm)|YIG(5 µm) bilayer at room temperature as function of the magnon gap size Δ, for various values of the base charge current σE. Note the log-log scaling. Solid colored lines: computed USMR. Dashed colored lines: continuations of the high-gap tails of the corresponding curves according to the one-parameter fit $\mathcal{U} = u_0/\sqrt{\Delta}$. Dashed black line: asymptotic value of the USMR as given by Eq. (4.14).

Fig. 4.7 is a log-log plot of the USMR versus gap size Δ at various values of the driving current σE. Here the value $\mathcal{U}_{\max}$ is shown as a dashed black line, indicating that this is indeed the value to which $\mathcal{U}$ converges in the gapless limit or at high current. Moreover, it shows that for given σE, one can find a turning point at which the USMR switches relatively abruptly from being nearly constant to decreasing as $1/\sqrt{\Delta}$.

A (backwards) continuation of the decreasing tails is included in Fig. 4.7 as dashed lines following the one-parameter fit $\mathcal{U} = u_0/\sqrt{\Delta}$, and we define the threshold gap Δ_{th} as the value of Δ where this continuation intersects $\mathcal{U}_{\max}$. We then find that Δ_{th} scales as E^2, or conversely, that the driving current required to saturate the USMR scales as the square root of the magnon gap.

We note that although the small-gap regime is mathematically valid (even in the limit $\Delta \to 0$, as Δ may be brought arbitrarily close to 0 in a continuous manner), it does not necessarily correspond to a physical situation: when the anisotropy vanishes, the magnetization of the FI layer may be reoriented freely, which will break our initial assumptions. Nevertheless, in taking the gapless limit, we are able to predict an upper limit on the magnonic USMR.

4.4 Conclusions

Using a simple drift-diffusion model, we have shown that magnonic spin accumulation near the interface between a ferromagnetic insulator and a heavy metal leads to a small but nonvanishing contribution to the unidirectional spin Hall magnetoresistance of FI|HM heterostructures. Central to our model is an interfacial spin current originating from a spin-flip scattering process whereby electrons in the heavy metal create or annihilate magnons in the ferromagnet. This current is markedly nonlinear in the electronic and magnonic spin accumulations at the interface, and it is exactly this nonlinearity which gives rise to the magnonic USMR.

For Pt|YIG bilayers, we predict that the magnonic USMR $\mathcal{U}$ is at most on the order of 10^{-8}, roughly three orders of magnitude weaker than the measured USMR in FM|HM hybrids (where electronic spin accumulation is thought to form the largest contribution). This is fully consistent with experiments that fail to detect USMR in Pt|YIG systems, as the tiny signal is drowned out by the interfacial spin Seebeck effect, which has a similar experimental signature and is enhanced compared to the FM|HM case due to inhomogeneous Joule heating.

We have shown that the magnon-mediated USMR is approximately cubic in the spin Hall angle of the metal, suggesting that metals with extremely large spin Hall angles may provide a significantly larger USMR than Pt. It is therefore plausible that a large magnonic USMR can exist in systems with very strong spin-orbit coupling, even though our model would break down in this regime.

The magnonic USMR depends strongly on the magnon spin diffusion length l_{m} in the ferromagnet. Motivated by a large discrepancy between experimental values and theoretical predictions of l_{m}, we have shown that a significant increase in USMR can be realized if a method is found to engineer this parameter to specific, optimal values that, for realistic values of the magnon-phonon relaxation time τ_{mp} (on the order of 1 ps for YIG), are significantly shorter than those measured experimentally or computed theoretically. We further find that when the magnon spin diffusion length has its optimal value, the USMR becomes independent of the ferromagnet's thickness and Gilbert damping constant.

Although in physically reasonable regimes, the magnonic USMR is to very good approximation linear in the applied driving current σE, it saturates to a fixed value given extremely large currents or a strongly reduced magnon gap Δ. The transition from linear to constant behavior in the driving current is heralded by a turning point which is proportional to the square root of the magnon gap. The asymptotic behavior of the USMR beyond the turning point is governed by the bulk spin- and charge currents, and is completely independent of the details of the interface.

While a vast reduction in Δ is required to bring the saturation current of a Pt|YIG bilayer within experimentally reasonable regimes, the magnonic USMR scales as $1/\sqrt{\Delta}$ at currents below the turning point, suggesting that highly isotropic FI|HM samples are most likely to produce a measurable magnonic USMR. The increase in magnonic USMR at low gaps (and large currents) is in good qualitative agreement with the recent experimental work of Avci *et al.* [48], as is the linear dependence on system temperature.

A notable disagreement with the experimental data of Avci *et al.* [48] is found in the scaling of the current dependence, which in our results lacks an $\mathcal{O}(I^3)$ term at large magnon gaps and contains an $\mathcal{O}(I^2)$ term at intermediate gaps. It is still unclear whether this discrepancy can be explained by system differences, such as the finite electrical resistance of Co or the presence of Joule heating.

Finally, we note that while our results apply to ferromagnetic insulators, it is reasonable to assume a magnonic contribution also exists in HM|FM heterostructures, although the possibility of coupled transport of magnons and electrons makes such systems more difficult to model. Additionally, various extensions of our model may be considered, such as the incorporation of spin-momentum locking [43], ellipticity of magnons, heat transport and nonuniform temperature profiles [57], directional dependence of the magnetization, etc.

4.5 Appendix: System parameters for a Pt|YIG bilayer film.

Description	Symbol	Expression	Value at $T = 293\,\mathrm{K}$	Ref.
YIG spin-wave stiffness constant	J_s		$8.458 \times 10^{-40}\,\mathrm{J\,m^2}$	[57]
YIG spin quantum number per unit cell	S		10	[57]
YIG lattice constant	a		$1.2376\,\mathrm{nm}$	[57]
YIG Gilbert damping constant	α		1×10^{-4}	[57]
YIG spin number density	s	Sa^{-3}	$5.2754 \times 10^{27}\,\mathrm{m^{-3}}$	[57]
YIG magnon gap	Δ		$9.3 \times 10^{-24}\,\mathrm{J}$	[18]
YIG magnon-phonon scattering time	τ_mp		$1\,\mathrm{ps}$	[57]
YIG magnon relaxation time	τ_mr	$\frac{\hbar}{2\alpha k_\mathrm{B} T_\mathrm{m}}$	$130\,\mathrm{ps}$	[57]
Combined magnon relaxation time	τ	$\left(\frac{1}{\tau_\mathrm{mr}} + \frac{1}{\tau_\mathrm{mp}}\right)^{-1}$	$1\,\mathrm{ps}$	[57]
Magnon thermal de Broglie wavelength	Λ	$\sqrt{\frac{4\pi J_\mathrm{s}}{k_\mathrm{B} T_\mathrm{m}}}$	$1.62\,\mathrm{nm}$	[57]
Magnon thermal velocity	v_th	$\frac{2\sqrt{J_\mathrm{s} k_\mathrm{B} T}}{\hbar}$	$35.1\,\mathrm{km\,s^{-1}}$	[57]
Magnon spin diffusion length	l_m	$v_\mathrm{th}\sqrt{\frac{2}{3}\tau\tau_\mathrm{mr}}$	$326\,\mathrm{nm}$	[57]
Magnon spin conductivity	σ_m	$\zeta\left(\frac{3}{2}\right)^2 \frac{J_\mathrm{s}}{\Lambda^3}\tau$	$1.35 \times 10^{-24}\,\mathrm{J\,s\,m^{-1}}$	[57]
Real part of spin-mixing conductance	$g_\mathrm{r}^{\uparrow\downarrow}$		$5 \times 10^{18}\,\mathrm{m^{-2}}$	[53]
Pt electrical conductivity	σ		$1 \times 10^{7}\,\mathrm{S\,m^{-1}}$	[65][1]
Pt spin Hall angle	θ_SH		0.11	[57]
Pt electron diffusion length	l_s		$1.5\,\mathrm{nm}$	[57]
Pt|YIG Kapitza resistance	R_th		$3.58 \times 10^{-9}\,\mathrm{m^2\,K\,W^{-1}}$	[60]

Table 4.1: System parameters for a Pt|YIG bilayer film.

---

[1] The conductivity of Pt is approximately inverse-linear in temperature over the regime we are considering. However, as we are not interested in detailed thermodynamic behavior, we use the fixed value $\sigma = 1 \times 10^{7}\,\mathrm{S\,m^{-1}}$ throughout this work.

4.6 Appendix: Interfacial spin current integrals

The following dimensionless integrals appear in the second-order expansion of the interfacial spin current to the spin accumulations, Eq. (4.4):

$$I_0 = \int_{\frac{\Delta}{k_B T_m}}^{\infty} \mathrm{d}x \sqrt{x - \frac{\Delta}{k_B T_m}} x \left(n_B(x) - n_B\left(\frac{T_m}{T_e}x\right)\right), \tag{4.15a}$$

$$\begin{aligned} I_e = \int_{\frac{\Delta}{k_B T_m}}^{\infty} \mathrm{d}x \sqrt{x - \frac{\Delta}{k_B T_m}} \Bigg(& n_B\left(\frac{T_m}{T_e}x\right) - n_B(x) \\ & - \frac{T_m}{T_e} x \mathrm{e}^{\frac{T_m}{T_e}x} \left[n_B\left(\frac{T_m}{T_e}x\right)\right]^2 \Bigg), \end{aligned} \tag{4.15b}$$

$$I_m = \int_{\frac{\Delta}{k_B T_m}}^{\infty} \mathrm{d}x \sqrt{x - \frac{\Delta}{k_B T_m}} x \mathrm{e}^{x} \left[n_B(x)\right]^2, \tag{4.15c}$$

$$\begin{aligned} I_{ee} = \int_{\frac{\Delta}{k_B T_m}}^{\infty} \mathrm{d}x \sqrt{x - \frac{\Delta}{k_B T_m}} \Bigg(& \mathrm{e}^{\frac{T_m}{T_e}x} \left[n_B\left(\frac{T_m}{T_e}x\right)\right]^3 \\ & \times \left[\mathrm{e}^{\frac{T_m}{T_e}x} - 1 - \frac{T_m x}{2T_e}\left(\mathrm{e}^{\frac{T_m}{T_e}x} + 1\right)\right] \Bigg), \end{aligned} \tag{4.15d}$$

$$I_{mm} = \int_{\frac{\Delta}{k_B T_m}}^{\infty} \mathrm{d}x \sqrt{x - \frac{\Delta}{k_B T_m}} \frac{x}{2} \mathrm{e}^{x} \left[\mathrm{e}^{x} + 1\right] \left[n_B(x)\right]^3, \tag{4.15e}$$

$$I_{me} = -\int_{\frac{\Delta}{k_B T_m}}^{\infty} \mathrm{d}x \sqrt{x - \frac{\Delta}{k_B T_m}} \mathrm{e}^{x} \left[n_B(x)\right]^2. \tag{4.15f}$$

5 GREEN'S FUNCTION FORMALISM FOR NONLOCAL ELLIPTICAL MAGNON TRANSPORT

We develop a non-equilibrium Green's function formalism to study magnonic spin transport through a strongly anisotropic ferromagnetic insulator contacted by metallic leads. We model the ferromagnetic insulator as a finite-sized one-dimensional spin chain, with metallic contacts at the first and last sites that inject and detect spin in the form of magnons. In the presence of anisotropy, these ferromagnetic magnons become elliptically polarized, and spin conservation is broken. We show that this gives rise to a novel parasitic spin conductance, which becomes dominant at high anisotropy. Moreover, the spin state of the ferromagnet becomes squeezed in the high-anisotropy regime. We show that the squeezing may be globally reduced by the application of a local spin bias.

5.1 Introduction

The controllable transport of spin through magnetic materials has recently attracted much attention, as it has the potential to augment or supplant modern electronics with high-frequency and low-dissipation computational elements [66]. Various strategies have been envisioned to achieve this goal, generally using either magnetic textures such as skyrmions [67, 68] or domain walls [69, 70] as the carriers of information, or using spin waves or magnons to transport spin angular momentum directly. The latter forms a broad field of research known as magnonics [71]. In recent years, significant milestones, both experimental and theoretical, have been achieved in the field of magnonics, with non-local transport of spin through ferromagnetic insulators [16, 72–76] now commonly realized and fairly well described using theoretical frameworks that range from drift-diffusion models to non-equilibrium Green's function formalism [57, 77–79].

At the core of these theoretical models is the Holstein-Primakoff (HP) magnon [26], a bosonic quasiparticle that forms a natural approximation to low-energy excitations of the Heisenberg (anti)ferromagnet [80]. The simplest variants of the Heisenberg ferromagnet do not include any form of anisotropy, or have at most a 'natural' quantization axis, generally taken to be the z axis, set by an external magnetic field. This results in a circularly polarized magnon, which appears to offer a sufficient approximation to adequately describe the broad behavior of magnon transport [53], for example in materials such as yttrium iron garnet [81].

In this work, however, we explicitly consider the effects of potentially large anisotropies, which break spin conservation and generate elliptically polarized magnons. The breaking of spin conservation is known to give rise to phenomena such as magnon tunneling between weakly coupled ferromagnetic insulators [82], which is prohibited when spin is conserved, and super-Poissonian shot noise [81]. Such phenomena are expected to arise whenever the ferromagnet under consideration has sufficiently strong anisotropy, e.g. in iron thin films [81] or exotic quantum magnets [83].

We develop a non-equilibrium Green's function (NEGF) formalism, also known as Keldysh formalism [84, 85], to study the anomalous or off-diagonal correlations that are generated by the anisotropy terms, and as a proof of concept, apply it to determine whether magnon ellipticity gives rise to observable effects in local- and nonlocal transport experiments.

We find that, given sufficiently strong anisotropy, at least two potentially observable effects are produced: a novel parasitic spin resistance, and phase-space squeezing of magnons. The parasitic spin resistance may provide experimental insight into the anisotropy of the ferromagnet, provided a way can be found to measure it directly. Squeezed magnons are predicted to yield reduced shot noise in ferromagnet/conductor hybrids [86], analogous to the application of squeezed light to reduce quantum noise in optical lasers [87, 88]. This effect may also hypothetically find an application in the recently proposed magnon laser [89].

The outline of this work is as follows: in Section 5.2, we recast the continuum field theory briefly outlined by Rückriegel and Duine [90] into a discrete, N-spin form using a bottom-up approach (similar work has been done in contexts such as the Bose-Hubbard model [91]), and in Section 5.3, show the results we obtain from a numerical implementation of the framework. In Section 5.4 we provide some concluding remarks and outline some potential further applications of the formalism developed in this work.

5.2 Methods

In this section, we give a description of our model system and the implementation of the NEGF we use to investigate its dynamics.

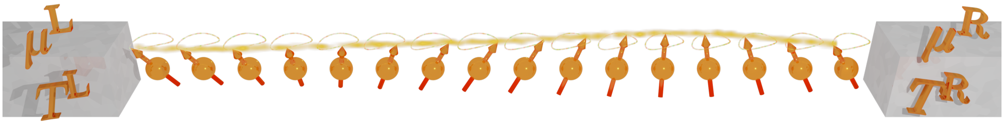

Figure 5.1: Cartoon representation of the system under consideration. A one-dimensional chain of spins is terminated at either end by heavy-metal leads, the left (right) lead having an electronic spin accumulation $\mu^{\mathrm{L(R)}}$ parallel to the magnetization axis, and temperature $T^{\mathrm{L(R)}}$. Spins precess elliptically due to the presence of high anisotropy, and can transport angular momentum in the form of an elliptical magnon or spin wave (yellow swirl).

5.2.1 System and Hamiltonian

We aim to consider systems typically used in long-distance transport experiments akin to Cornelissen *et al.* [16]: a ferromagnetic insulator with two heavy-metal leads, one of which serves to inject magnons, and one acting as a magnon detector. The system is biased by a constant electronic spin accumulation in the leads, aligned parallel to the magnetization so that there is no torque acting on the magnetization. We assume spin transport in the ferromagnetic insulator is quasi-one-dimensional, i.e., that magnons travel in a straight line from emitter to detector, and the bulk of the ferromagnet effectively consists of macroscopically many non-interacting parallel copies of the spin chain making up the transport channel for a single magnon. This allows us to treat the ferromagnetic bulk as a one-dimensional (1D) spin chain. A cartoon representation of this system is shown in Fig. 5.1. Extension to a two- or three-dimensional cubic bulk is mathematically simple (and tractable in the continuum limit), but computationally challenging for finite-sized systems due to the vast increase in lattice sites that must be taken into account.

We thus model our system using the 1D, N-particle Heisenberg [80] ferromagnetic insulator in the presence of quadratic anisotropy terms. It is described by the Hamiltonian

$$H = H_{\mathrm{H}} + H_{\mathrm{ani}}, \tag{5.1}$$

where

$$H_{\mathrm{H}} = -\frac{\tilde{J}}{2}\sum_{i=1}^{N-1} \hat{\boldsymbol{S}}_i \cdot \hat{\boldsymbol{S}}_{i+1} - h_{\mathrm{mag}} \sum_{i=1}^{N} \hat{S}_i^z \tag{5.2}$$

is the ordinary 1D Heisenberg Hamiltonian [80], and

$$H_{\mathrm{ani}} = \sum_{\nu \in \{x,y,z\}} \sum_{i=1}^{N} K_\nu (\hat{S}_i^\nu)^2 \tag{5.3}$$

is the anisotropy Hamiltonian. Here $\tilde{J} > 0$ is the exchange constant, the K_ν are the anisotropy energies in the three Cartesian directions, $\hat{\boldsymbol{S}}_i = (\hat{S}_i^x, \hat{S}_i^y, \hat{S}_i^z)^{\mathrm{T}}$ is the spin operator at site i, and h_{mag} is an externally applied magnetic field.

As we are only interested in the behavior of the ferromagnet, we have omitted Hamiltonian terms originating from coupling to the leads, and instead opt to directly write down the relevant self-energy terms when we develop our Green's function formalism later on.

The second-order, spin-S Holstein-Primakoff transformation [26]

$$\hat{S}_i^x = \sqrt{\frac{S}{2}} \left(b_i + b_i^\dagger \right), \tag{5.4a}$$

$$\hat{S}_i^y = -\mathrm{i}\sqrt{\frac{S}{2}} \left(b_i - b_i^\dagger \right), \tag{5.4b}$$

$$\hat{S}_i^z = S - b_i^\dagger b_i \tag{5.4c}$$

is used to express the Hamiltonian 5.1 in terms of magnon creation (annihilation) operators $b_i^\dagger$ (b_i) acting at site i, that obey the bosonic commutation relations $[b_i, b_j] = [b_i^\dagger, b_j^\dagger] = 0$ and $[b_i, b_j^\dagger] = \delta_{ij}$. We additionally define the vector operator

$$\phi_i \equiv \begin{pmatrix} b_i \\ b_i^\dagger \end{pmatrix} \tag{5.5}$$

and its conjugate transpose $\phi_i^\dagger$.

Note that the Holstein-Primakoff transformation is an expansion around the ground state in which all spins are aligned in the z-direction. In the absence of an external field, this puts constraints on the relative signs and strengths of the anisotropy terms K_ν, however a sufficiently strong field $h_{\mathrm{mag}} > 0$ may always be used to guarantee alignment to the z-axis.

The Hamiltion of Eq. (5.1) may be simplified somewhat if one defines the constants $\Delta \equiv S(K_x + K_y - 2K_z + \tilde{J}) + h_{\mathrm{mag}}$, $J \equiv \frac{\tilde{J}S}{2}$ and $K \equiv \frac{S}{4}(K_x - K_y)$. Then, dropping unimportant constant energy shifts, along with the additional boundary terms $-J(b_1^\dagger b_1 + b_N^\dagger b_N)$ that originate from the fact that we consider a finite-sized system (which we expect to be negligible for sufficiently large systems), the Hamiltonian (5.1) may be rewritten as

$$H = \frac{1}{2} \sum_{ij} \phi_i^\dagger h_{ij} \phi_j, \tag{5.6}$$

with the $2N \times 2N$ matrix

$$h_{ij} = \begin{pmatrix} h^{\mathrm{i}}_{ij} & K\delta_{ij} \\ K\delta_{ij} & h^{\mathrm{i}}_{ij} \end{pmatrix}. \tag{5.7}$$

Here δ_{ij} is the $N \times N$ identity matrix, and

$$h^{\mathrm{i}}_{ij} = \Delta\delta_{ij} - J\left[\delta_{i,j+1} + \delta_{i+1,j}\right] \tag{5.8}$$

is the isotropic Hamiltonian submatrix. We thus see that Δ is an on-site potential for the magnons. The rescaled exchange energy J is a hopping parameter, governing the probability for a magnon to hop from one site to the next.

The off-diagonal submatrices $K\delta_{ij}$ govern the ellipticity of the magnons, and we shall henceforth use the term "the anisotropy" interchangeably with "the scalar constant K" (alternatively, and equivalently, K could be called the "squeezing factor" or "spin nonconservation factor"). Note, however, that K is proportional to the *difference* in anisotropy energies in the x and y directions, i.e. the principal directions perpendicular to the spin quantization axis.

The presence of nonzero K breaks conservation of spin by introducing terms of the form $K\left[b_i b_i + b_i^\dagger b_i^\dagger\right]$. The Hamiltonian of Eq. (5.7) therefore cannot be unitarily diagonalized (in a physically meaningful way), and its eigenstates do not have a well-defined spin. Rather, Eq. (5.7) describes a Hamiltonian of the *Bogoliubov form*, which may be diagonalized using a para-unitary transformation [30], i.e. a transformation matrix $\mathcal{T}_{ij}$ obeying

$$\sum_i (\sigma_3)_{ij} \mathcal{T}^\dagger_{jk} = \sum_i \mathcal{T}^{-1}_{ij} (\sigma_3)_{jk}, \tag{5.9}$$

where

$$(\sigma_3)_{ij} \equiv \begin{pmatrix} \delta_{ij} & 0 \\ 0 & -\delta_{ij} \end{pmatrix} \tag{5.10}$$

is the $2N \times 2N$ analog of the third Pauli matrix (referred to as the para-identity matrix by Colpa [30]). The Hamiltonian (5.7) allows us to choose $\mathcal{T}_{ij}$ to be real, such that it takes the simple block structure

$$\mathcal{T}_{ij} = \begin{pmatrix} \mathcal{T}^{(1)}_{ij} & \mathcal{T}^{(2)}_{ij} \\ \mathcal{T}^{(2)}_{ij} & \mathcal{T}^{(1)}_{ij} \end{pmatrix}, \tag{5.11}$$

where the individual $N \times N$ blocks $\mathcal{T}_{ij}^{(1)}$ and $\mathcal{T}_{ij}^{(2)}$ are *not* symmetric.

The para-unitary diagonalization of h_{ij} is performed analytically for arbitrary $N \geq 2$ by leveraging the recurrent structure of the characteristic equation $\det\{h_{ij} - (\sigma_3)_{ij}\varepsilon\} = 0$, whereby the N-level equation can be expressed terms of the $(N-1)$- and $(N-2)$-level equations. The characteristic polynomial of the recurrence relation contains only terms of degree $N+1$, and is therefore easily solved analytically. The quasiparticles are elliptical magnons with the dispersion relation

$$\varepsilon_n = \sqrt{\left[\Delta - 2J\cos\left(\frac{n\pi}{N+1}\right)\right]^2 - K^2}, \qquad 1 \leq n \leq N. \tag{5.12}$$

Here, the natural number n is the quantum number, and ε_n monotonically increases with n. The corresponding eigenstates are plane waves [1], with the quantum number n corresponding to the wavenumber $k = \frac{n\pi}{L} = \frac{n\pi}{Na}$ for a spin chain of physical length $L = Na$, with a the lattice constant.

5.2.2 Non-equilibrium Green's function formalism

As stated in the previous subsection, diagonalization of our anisotropic ferromagnetic insulator Hamiltonian may be done analytically and results in free elliptical magnon modes. We now seek to investigate the finite-temperature steady-state behavior of such a system in the presence of two effects: (1) coupling to one or more metallic leads and (2) bulk dissipation of elliptical magnons in the form of Gilbert-like damping.

To this end, we develop a non-equilibrium Green's function framework [92], also known as Keldysh formalism [84, 85]. In what follows, we set $\hbar = 1$. The spectral properties of the magnons are encoded in the single-particle retarded Green's function

$$g_{ij}(t,t') = -\mathrm{i}\theta(t-t')\left\langle\left[\phi_i(t), \phi_j^\dagger(t')\right]\right\rangle \tag{5.13}$$

and advanced Green's function

$$g_{ij}^\dagger(t,t') = \mathrm{i}\theta(t'-t)\left\langle\left[\phi_i(t), \phi_j^\dagger(t')\right]\right\rangle, \tag{5.14}$$

where $\theta(t-t')$ is the Heaviside step function and $[\bullet,\bullet]$ is the commutator. The Keldysh Green's function

$$g_{ij}^{\mathrm{K}}(t,t') = -\mathrm{i}\left\langle\left\{\phi_i(t), \phi_j^\dagger(t')\right\}\right\rangle \tag{5.15}$$

---

[1] Specifically, the components of the paravector with quantum number n corresponding to site i are simply $\sin\left(\frac{in\pi}{N+1}\right)$, up to paranormalization.

encodes information about the occupation of the single-particle states. Here, $\{\bullet, \bullet\}$ is the anticommutator. Using these Green's functions, one may construct the lesser Green's function

$$g^{<}_{ij}(t,t') = -\mathrm{i}\left\langle \phi^{\dagger}_{i}(t)\phi_{j}(t')\right\rangle, \tag{5.16}$$

which, at equal times $t = t'$, contains the off-diagonal correlations (for $i \neq j$) and quasiparticle number density (for $i = j$), up to a prefactor of $-\mathrm{i}$. Together with the greater Green's function

$$g^{>}_{ij}(t,t') = -\mathrm{i}\left\langle \phi_{i}(t)\phi^{\dagger}_{j}(t')\right\rangle, \tag{5.17}$$

one obtains the relations [85]

$$g_{ij}(t,t') = \theta(t-t')\left[g^{>}_{ij}(t,t') - g^{<}_{ij}(t,t')\right], \tag{5.18}$$

$$g^{\dagger}_{ij}(t,t') = -\theta(t'-t)\left[g^{>}_{ij}(t,t') - g^{<}_{ij}(t,t')\right], \tag{5.19}$$

$$g^{\mathrm{K}}_{ij}(t,t') = g^{>}_{ij}(t,t') + g^{<}_{ij}(t,t'), \tag{5.20}$$

and

$$g_{ij}(t,t') - g^{\dagger}_{ij}(t,t') = g^{>}_{ij}(t,t') - g^{<}_{ij}(t,t'). \tag{5.21}$$

For simplicity, we shall henceforth drop the subscripts $i, j, \ldots$ on all matrices, as well as the explicit summations in matrix products seen in Section 5.2.1, and work in the space of 2×2 matrices, of which the four components are themselves $N \times N$ matrices. The presence of the $N \times N$ or $2N \times 2N$ identity matrix is implied when doing so does not lead to ambiguity.

For the remainder of this work, we shall only consider a system in the steady state, i.e. $g(t,t') = g(t-t')$ (and similar for the other Green's functions), and work with Fourier-transformed Green's functions. In particular, the retarded Green's function $g(\omega)$ satisfies the Dyson equation

$$g(\omega) = [\omega\sigma_3 - h - \Sigma(\omega)]^{-1}, \tag{5.22}$$

where $\Sigma(\omega)$ is the retarded self-energy, and is easily obtained by numerical matrix inversion.

Here, we opt to stay in the HP basis (i.e., the basis of the *circular* magnons defined by the operators ϕ and $\phi^{\dagger}$) instead of transforming to the elliptical basis, and thus h in Eq. (5.22) is simply given by Eq. (5.7). Lead coupling and Gilbert-like damping are to be incorporated into the (retarded) self-energy Σ.

The reason we choose to compute observables in the circular basis is twofold: (1) it provides a simple form for the lead self-energies, which will be explained shortly, and (2) experimental measurement of observables is generally done electrically (through the spin Hall effect and its inverse) [16, 93], so that electron spin is the natural measurement basis (see below).

In line with Zheng *et al.* [77], we take the self-energy component arising from lead X to have the form

$$\Sigma^X(\omega) = -\mathrm{i}\eta^X(\omega - \mu^X\sigma_3)\delta_{i,i^X}\delta_{j,i^X}, \tag{5.23}$$

where $\delta_{i,i^X}\delta_{j,i^X}$ indicates that the self-energy is zero everywhere except for its diagonal components corresponding to site i^X[2], i.e. the index where lead X is attached. The positive dimensionless real constant η^X determines the strength of the lead's coupling to the system, and μ^X is the spin accumulation—i.e. the difference in chemical potential between spin-up and spin-down electrons—in the lead, generated, for example, by the spin Hall effect. In this work, we attach at most two leads: the left lead ($X = \mathrm{L}$) at $i^\mathrm{L} = 1$ and optionally the right lead ($X = \mathrm{R}$) at $i^\mathrm{R} = N$. We choose the coupling for positive and negative modes to be equal-but-opposite [indicated by $\mu^X\sigma_3$ in Eq. (5.23)], such that our system reduces to the one considered by Zheng *et al.* [77] in the limit $K \to 0$ (up to the splitting into positive and negative modes itself, which, at $K = 0$, becomes a purely notational operation). At the level of the approximations used by Zheng *et al.* [77], the lead self-energy for this geometry is determined only by the electrons in the metal and the interfacial interaction, and is independent of the magnons and their particle-hole structure, making the form of Eq. (5.23) a natural choice for our model.

The form of the lead self-energy given by Eq. (5.23) is only valid when one assumes the spin basis is the natural basis for the lead Hamiltonians, i.e., that the leads inject a well-defined amount of spin into the ferromagnet. This is the case provided the electron spin in the leads is polarized in the z-direction and a spin-flip scattering process at the interface is the source of magnons: here a spin-$\frac{1}{2}$ excitation in the leads is flipped to $-\frac{1}{2}$, injecting a (spin-1) HP magnon into the ferromagnet. In the presence of anisotropy, the circular HP magnon is a superposition of elliptical magnons.

To find an expression for the Gilbert-like damping self-energy, it is important to carefully consider what one would expect the state of the system to be in thermal equilibrium. Given that the lead contributions are local, acting on only one or two sites of a much larger bulk, we assume our system ultimately thermalizes to states close to the eigenstates of the free anisotropic ferromagnet, i.e. the elliptical quasiparticles. Thus, what is linearly damped in our system is the density of elliptical magnons, which does not necessarily correspond to the classical magnetization—hence our use of the term ‘Gilbert-*like* damping’, as opposed to just ‘Gilbert damping’: the latter, in the strict sense, refers to damping of the classical magnetization only [94].

---

[2] Thus the full $2N \times 2N$ matrix has nonzero components at indices (i^X, i^X) and $(i^X + N, i^X + N)$.

By this rationale, we employ a simple linear damping self-energy *in the elliptical basis*:

$$\Sigma^{\mathrm{B,ell}} = -\mathrm{i}\alpha\omega. \tag{5.24}$$

Here B stands for ‘bulk’ (as this is the only bulk self-energy we take into account), and α is the Gilbert-like damping parameter.

Transforming to the spin basis, we find

$$\Sigma^{\mathrm{B}}(\omega) = -\mathrm{i}\alpha\omega\mathcal{T}^{\dagger}\mathcal{T}, \tag{5.25}$$

where $\mathcal{T}^{\dagger}\mathcal{T}$ becomes the identity matrix in the limit $K \to 0$. In this limit, the bulk self-energy reduces to standard Gilbert damping, which has been addressed by Zheng *et al.* [77].

The total (retarded) self-energy in our model is then simply the sum of the lead- and bulk self-energies in the spin basis:

$$\Sigma(\omega) = \Sigma^{\mathrm{B}}(\omega) + \Sigma^{\mathrm{L}}(\omega) + \Sigma^{\mathrm{R}}(\omega). \tag{5.26}$$

Under the assumption that the lead and bulk thermal baths are sufficiently large to be undisturbed by coupling to the spins, we may use the fluctuation-dissipation theorem [85] to find the associated Keldysh self-energy:

$$\begin{aligned}\Sigma^{\mathrm{K}}(\omega) = 2\Sigma^{\mathrm{B}}(\omega)\mathcal{T}^{-1}F^{\mathrm{B}}(\omega)\mathcal{T}& \\ + 2\Sigma^{\mathrm{L}}(\omega)F^{\mathrm{L}}(\omega) + 2\Sigma^{\mathrm{R}}(\omega)F^{\mathrm{R}}(\omega).&\end{aligned} \tag{5.27}$$

Here, we define the statistical matrix

$$\begin{aligned}F^{X}(\omega) \equiv \mathrm{diag}\Bigg\{ \coth\left(\frac{\omega-\mu^{X}}{2k_{\mathrm{B}}T^{X}}\right),& \\ -\coth\left(\frac{-\omega-\mu^{X}}{2k_{\mathrm{B}}T^{X}}\right)\Bigg\},&\end{aligned} \tag{5.28}$$

with $X \in \{\mathrm{B},\mathrm{L},\mathrm{R}\}$, k_{B} the Boltzmann constant, and T^{X} the temperature of the subsystem X. We will further assume the magnon chemical potential vanishes

($\mu^{\mathrm{B}}=0$), such that $\mathcal{T}^{-1}F^{\mathrm{B}}(\omega)\mathcal{T}=\coth\left(\frac{\omega}{2k_{\mathrm{B}}T^{\mathrm{B}}}\right)$ is a real number multiplying the identity matrix.

Finally, from the Keldysh self-energy, we compute the Keldysh Green's function [84, 95]

$$g^{\mathrm{K}}(\omega)=g(\omega)\Sigma^{\mathrm{K}}(\omega)g^{\dagger}(\omega). \tag{5.29}$$

Note that $g^{\mathrm{K}}(\omega)$ is symmetric and anti-hermitian, and therefore pure-imaginary.

5.2.3 Observables

Using the elements outlined in Section 5.2.2, we may compute any physical observable of our system. As we are primarily interested in steady-state behavior, the most obvious objects to consider are the equal-time two-point functions of the creation and annihilation operators of HP magnons. In the presence of anisotropy, we expect to obtain nonzero anomalous correlations, e.g. $\left\langle b_i b_j\right\rangle$, because the states in the system are a superposition of HP magnon states (leading to nonconservation of spin). The normal and anomalous correlation functions are conveniently collected in a single matrix through the vector operator ϕ, e.g.

$$\begin{aligned}\mathrm{i}g^{>}_{ij}(t)=\left\langle\phi_i(t)\phi_j^{\dagger}(t)\right\rangle&=\left\langle\begin{pmatrix}b_i(t)\\ b_i^{\dagger}(t)\end{pmatrix}\otimes\begin{pmatrix}b_j^{\dagger}(t) & b_j(t)\end{pmatrix}\right\rangle\\ &=\begin{pmatrix}\left\langle b_i(t)b_j^{\dagger}(t)\right\rangle & \left\langle b_i(t)b_j(t)\right\rangle\\ \left\langle b_i^{\dagger}(t)b_j^{\dagger}(t)\right\rangle & \left\langle b_i^{\dagger}(t)b_j(t)\right\rangle\end{pmatrix}.\end{aligned} \tag{5.30}$$

Conversely, we may compute two-point functions of the elliptical magnons $\Psi\equiv\mathcal{T}\phi\equiv\begin{pmatrix}\psi, & \psi^{\dagger}\end{pmatrix}$, e.g.

$$\left\langle\Psi^{\dagger}(t)\Psi(t)\right\rangle=\mathcal{T}^{*}\left\langle\phi^{\dagger}(t)\phi(t)\right\rangle\mathcal{T}^{\mathrm{T}}. \tag{5.31}$$

Here, we expect the anomalous blocks to be nonzero only when lead coupling and anisotropy are simultaneously present: if only anisotropy is present, there are no damping terms that try to push the system away from the native elliptical magnon eigenstates (spin is not conserved, but there are no explicit sources and sinks of spin). Conversely, if lead coupling is present but anisotropy is absent, the elliptical magnons are identical to the HP ones, there is no breaking of spin conservation, and the system reduces to the case investigated by Zheng *et al.* [77].

As stated in Section 5.2.2, the matrix $\rho_{\mu\nu}=\left\langle\phi_{\mu}^{\dagger}\phi_{\nu}\right\rangle$ (at some arbitrary time in the steady state, and with the indices μ and ν in the range $[1,2N]$) containing number densities and off-diagonal correlations may be computed through the lesser Green's function $g^<$:

$$\begin{aligned}\rho = \mathrm{i}g^< = \mathrm{i}\int \frac{\mathrm{d}\omega}{2\pi}\, g^<(\omega) \\ = \frac{\mathrm{i}}{2}\int \frac{\mathrm{d}\omega}{2\pi}\, \left(g^{\mathrm{K}}(\omega) - g(\omega) + g^\dagger(\omega)\right).\end{aligned} \tag{5.32}$$

For the sake of brevity, we shall refer to ρ as the density matrix, although the off-diagonal components are in fact off-diagonal correlations. Note also that by the symmetry of g and g^{K}, and anti-hermiticity of the Keldysh Green's function, the lesser Green's function is itself symmetric, anti-hermitian and pure-imaginary. One may alternatively work directly with the Keldysh Green's function, of which the corresponding observable is the semiclassical (SC) HP magnon density matrix

$$\begin{aligned}\rho^{\mathrm{SC}} = \frac{\mathrm{i}}{2}g^{\mathrm{K}} - \frac{1}{2} = \frac{1}{2}\left\langle\left\{\phi^\dagger, \phi\right\}\right\rangle - \frac{1}{2} \\ = \frac{\mathrm{i}}{2}\int \frac{\mathrm{d}\omega}{2\pi}\, g^{\mathrm{K}}(\omega) - \frac{1}{2}.\end{aligned} \tag{5.33}$$

In equilibrium, the top-left and off-diagonal blocks correspond directly to those of the true density matrix of Eq. (5.32).

From the density matrix ρ, we may compute the uncertainty operators $\Delta\bar{S}^x$ and $\Delta\bar{S}^y$ for the corresponding normalized spin operators $\bar{S}^x$ and $\bar{S}^y$, which allow us to determine whether the elliptical magnons are squeezed in phase space [87]. From the normalized spin operators

$$\bar{S}_i^x = \frac{1}{\sqrt{2}}\left(b_i + b_i^\dagger\right), \tag{5.34a}$$

$$\bar{S}_i^y = \frac{-\mathrm{i}}{\sqrt{2}}\left(b_i - b_i^\dagger\right), \tag{5.34b}$$

and

$$\bar{S}_i^z = 1 - b_i^\dagger b_i, \tag{5.34c}$$

[i.e. the HP transformation with S set to 1, and applied in reverse with respect to Eqs. (5.4)], we immediately find the uncertainty operators

$$\begin{aligned}\Delta\bar{S}_i^x \equiv \sqrt{\langle(\bar{S}_i^x)^2\rangle - \langle\bar{S}_i^x\rangle^2} \\ = \sqrt{\frac{1}{2}\left[\langle b_i b_i^\dagger\rangle + \langle b_i^\dagger b_i\rangle + \langle b_i b_i\rangle + \langle b_i^\dagger b_i^\dagger\rangle\right]} \\ = \sqrt{\frac{1}{2}\left[I_+ \rho I_+^{\mathrm{T}}\right]_{ii}}\end{aligned} \tag{5.35a}$$

and

$$\begin{aligned}\Delta\bar{S}_i^y &\equiv \sqrt{\left\langle(\bar{S}_i^y)^2\right\rangle - \left\langle\bar{S}_i^y\right\rangle^2} \\ &= \sqrt{\frac{1}{2}\left[\left\langle b_i b_i^\dagger\right\rangle + \left\langle b_i^\dagger b_i\right\rangle - \left\langle b_i b_i\right\rangle - \left\langle b_i^\dagger b_i^\dagger\right\rangle\right]} \\ &= \sqrt{\frac{1}{2}\left[I_-\rho I_-^{\mathrm{T}}\right]_{ii}},\end{aligned} \tag{5.35b}$$

where $I_\pm$ are the $N \times 2N$ matrices

$$I_\pm \equiv \delta_{ij}(1, \pm 1). \tag{5.35c}$$

Here, the one-point functions $\left\langle\bar{S}_i^x\right\rangle$ and $\left\langle\bar{S}_i^y\right\rangle$ vanish, because we do not explicitly couple to a pumping field and are not considering Bose-Einstein condensates [53]. The Robertson uncertainty principle [96] then states that $\Delta\bar{S}_i^x\Delta\bar{S}_i^y \geq \frac{1}{2}$. If either $\Delta\bar{S}_i^x < \frac{1}{\sqrt{2}}$ or $\Delta\bar{S}_i^y < \frac{1}{\sqrt{2}}$, the state is squeezed [87], and the pattern of quantum fluctuations of the spin around the z-axis takes the form of an ellipse, rather than a circle [81]. As noted by Kamra *et al.* [81], the purely quantum mechanical squeezing should not be confused with the magnetization trajectory of a classical elliptical spin wave: the latter concerns coherent excited states, whereas squeezing persists even in the ground state and affects properties such as entanglement.

In addition to the magnon density and the related observables, we may compute the spin currents in our system. These follows from the continuity equation of the magnetization; a brief outline of the derivation is given in Appendix 5.5. The total spin current $j_{\mathrm{s,tot}}^{\mathrm{L}}$ flowing out of the left lead comprises three Landauer-Büttiker-type [97] terms:

$$j_{\mathrm{s,tot}}^{\mathrm{L}}(t) = j_{\mathrm{s}}^{\mathrm{R}\to\mathrm{L}} + j_{\mathrm{s}}^{\mathrm{B}\to\mathrm{L}} + j_{\mathrm{s}}^{\mathrm{L}} \tag{5.36}$$

where

$$j_{\mathrm{s}}^X = -\operatorname{Re}\operatorname{Tr}\int\frac{\mathrm{d}\omega}{2\pi}\iota^X(\omega). \tag{5.37}$$

Here the integrands ι^X are the tunneling term

$$\begin{aligned}\iota^{\mathrm{R}\to\mathrm{L}}(\omega) = g^\dagger(\omega)\sigma_3\Sigma^{\mathrm{L}}(\omega)g(\omega)\Sigma^{\mathrm{R}}(\omega)& \\ \times\left[F^{\mathrm{R}}(\omega) - F^{\mathrm{L}}(\omega)\right]&,\end{aligned} \tag{5.38a}$$

the bulk term

$$\begin{aligned}\iota^{\mathrm{B}\to\mathrm{L}}(\omega) = g^\dagger(\omega)\sigma_3\Sigma^{\mathrm{L}}(\omega)g(\omega)\Sigma^{\mathrm{B}}(\omega)& \\ \times\left[\mathcal{T}^{-1}F^{\mathrm{B}}(\omega)\mathcal{T} - F^{\mathrm{L}}(\omega)\right]&,\end{aligned} \tag{5.38b}$$

and the lead-local term

$$\iota^{\mathrm{L}}(\omega) = g^{\dagger}(\omega)\sigma_3\Sigma^{\mathrm{L}}(\omega)g(\omega)h \\ \times \left[F^{\mathrm{L}}(\omega)\big|_{\mu^{\mathrm{L}}=0} - F^{\mathrm{L}}(\omega) \right]. \tag{5.38c}$$

Conversely, the spin current out of the right lead consists of the same expressions but with L and R swapped.

Note that the terms in $j^{\mathrm{L}}_{\mathrm{s,tot}}$ contain the statistical matrices $F^{X}(\omega)$ in place of the scalar Bose-Einstein functions one would normally find in Landauer-Büttiker equations. One may exploit various symmetries of the components of the integrals to recover the more familiar form (in the circular limit identical to the expressions given by Zheng *et al.* [77]), though this requires the transmission functions to be written in terms of the individual $N \times N$ blocks of the component $2N \times 2N$ matrices, as has been done by e.g. Rückriegel and Duine [90].

To interpret the three spin current contributions, it is useful to consider the system as a spin resistor network, shown in Fig. 5.2a. Here each node in the circuit represents a spin in our chain, and each resistor represents a coupling either between spins (tunneling resistors $\tilde{R}^{\mathrm{T}}$) or to a damping element (Gilbert-like damping for the bulk resistors $\tilde{R}^{\mathrm{B}}$, and lead damping for $R^{\mathrm{L/R}}$). The system is biased at either lead with a spin accumulation (voltage) $\mu^{\mathrm{L/R}}$. In this resistor network analogy, one may 'integrate out' the bulk spins by repeated application of the $\Delta-Y$ transform [98] to obtain Fig. 5.2b. At equal temperature ($T^{\mathrm{L}} = T^{\mathrm{R}} = T^{\mathrm{B}} = T$), the spin currents j^{X} may then be interpreted as follows:

The tunneling term $j^{\mathrm{R}\to\mathrm{L}}$ is the current flowing from right to left through the resistor R^{T} in Fig. 5.2b, and corresponds to the spin current flowing out of the left lead when a spin accumulation is applied at the right lead. Physically, it is the term corresponding to magnon-mediated non-local transport, and roughly corresponds to the current measured experimentally in a ferromagnetic insulator by Cornelissen *et al.* [16], although our work considers the ballistic regime ($\mu^{\mathrm{B}} = 0$) rather than the diffusive regime.

The bulk term $j^{\mathrm{B}\to\mathrm{L}}$ corresponds to the current flowing out of the left lead as a result of Gilbert-like damping in the bulk. It is negative when a positive spin accumulation is applied to the left lead, indicating spin current flows from the lead into the bulk, where it is dissipated into the lattice. In Fig. 5.2b, $-j^{\mathrm{B}\to\mathrm{L(R)}}$ is the current flowing to ground through the left (right) resistor R^{B}.

The lead-local term j^{L}, corresponding to the current flowing from ground upwards through R^{L} in Fig. 5.2b, is unique to systems that exhibit the Bogoliubov structure described at the start of this section. It is linear in K to lowest nonvanishing order, and, at nonzero K, vanishes unless the system is driven by the application of an electronic spin accumulation in the lead. We may therefore conclude that it arises due to the mismatch between the lead states, where spin is a good quantum number, and the elliptical magnon eigenstates of the anisotropic ferromagnet. Ultimately, the mismatch is necessarily compensated by the lattice [82]. As this term contributes directly to the spin current flowing out of the lead to which a spin bias is applied, it offers a way to probe the ellipticity of magnons through local spin current measurements.

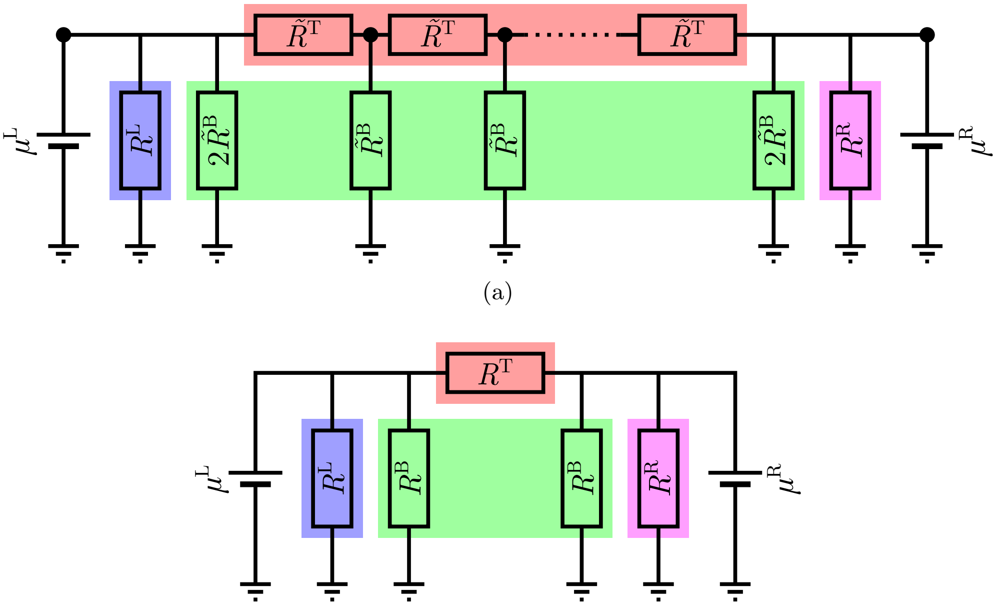
$\tilde{R}^{\mathrm{T}}$
$\tilde{R}^{\mathrm{T}}$
$\tilde{R}^{\mathrm{T}}$
μ^{L}
R^{L}
$2\tilde{R}^{\mathrm{B}}$
$\tilde{R}^{\mathrm{B}}$
$\tilde{R}^{\mathrm{B}}$
$2\tilde{R}^{\mathrm{B}}$
R^{R}
μ^{R}
R^{T}
μ^{L}
R^{L}
R^{B}
R^{B}
R^{R}
μ^{R}

(a)

(b)

Figure 5.2: Resistor network diagrams of our model system. (a): In the full diagram, each black dot represents a spin, each resistor $\tilde{R}^{\mathrm{T}}$ represents an inter-spin coupling, and each resistor $\tilde{R}^{\mathrm{B}}$ represents a coupling to the field(s) responsible for Gilbert-like damping. The spin currents through the resistors $R^{\mathrm{L/R}}$ are given by the lead-local terms $-j^{\mathrm{L/R}}$. (b): By repeated application of the $\Delta - Y$ transform [98], one may collapse the internal couplings (red and green blocks), thereby reducing the N-spin resistor network to a five-resistor form. In this reduced diagram, the current through R^{T} (from right to left) is given by $j^{\mathrm{R}\to\mathrm{L}}$ and the currents through the left (right) resistors R^{B} are represented by the bulk terms $-j^{\mathrm{B}\to\mathrm{L(R)}}$. The lead-local resistors remain unchanged.

Taking the resistor network analogy further, the reduced model of Fig. 5.2b provides us with a new set observables more generic than the spin currents themselves, namely the spin resistances R^{T}, $R^{\mathrm{L/R}}$ and R^{B}. Setting $\mu^{\mathrm{R}} = 0$ and formally expanding the left-lead spin current terms in μ^{L}, we obtain

$$j_{\mathrm{s}}^{\mathrm{R}\to\mathrm{L}} = j_{\mathrm{s}0}^{\mathrm{R}\to\mathrm{L}}(T^{\mathrm{L}}, T^{\mathrm{R}}) - \frac{1}{R^{\mathrm{T}}}\mu^{\mathrm{L}}, \tag{5.39a}$$

$$j_{\mathrm{s}}^{\mathrm{B}\to\mathrm{L}} = j_{\mathrm{s}0}^{\mathrm{B}\to\mathrm{L}}(T^{\mathrm{L}}, T^{\mathrm{B}}) - \frac{1}{R^{\mathrm{B}}}\mu^{\mathrm{L}}, \tag{5.39b}$$

$$j_{\mathrm{s}}^{\mathrm{L}} = -\frac{1}{R^{\mathrm{L}}}\mu^{\mathrm{L}}. \tag{5.39c}$$

Here $j_{\mathrm{s}0}^{\mathrm{R}\to\mathrm{L}}(T^{\mathrm{L}}, T^{\mathrm{R}})$ and $= j_{\mathrm{s}0}^{\mathrm{B}\to\mathrm{L}}(T^{\mathrm{L}}, T^{\mathrm{B}})$ are spin Seebeck effect [76, 99] terms that vanish when $T^{\mathrm{L}} = T^{\mathrm{R}}$ and $T^{\mathrm{L}} = T^{\mathrm{B}}$, respectively.

5.3 Numerical implementation and results

The framework outlined in the previous section is implemented numerically for system sizes of order $N = 20$. At low or moderate damping, the functions in our setup are sharply peaked in the frequency domain; frequency integrals are evaluated with an adaptive trapezoidal algorithm to avoid missing such peaks. As the setup requires matrices of size $2N \times 2N$ and the computation of observables includes one matrix inversion and multiple dense matrix multiplications per frequency sample, the numerical implementation scales poorly with system size. However, as the qualitative differences between systems of size $N = 40$ and $N = 20$ turn out to be minimal, we believe the latter to be a fair compromise between manageable computation time and sufficient capture of large-system behavior.

Our use of simplistic linear damping leads to a logarithmic divergence if the frequency integrals in the expressions for ρ or ρ^{SC} are taken from $-\infty$ to ∞. We regularize the integrals by restricting the integration interval to $[-\varepsilon_{\max}, \varepsilon_{\max}]$, where

$$\varepsilon_{\max} = \lim_{N\to\infty} \varepsilon_N. \tag{5.40}$$

We seek to investigate qualitative changes in the behavior of our system as the anisotropy K is increased, while mitigating the effects of changes to the energetics of the ferromagnet's eigenstates. To realize this, we shall keep the elliptical magnon gap ε_1, given by Eq. (5.12), fixed. Furthermore, we keep the exchange-like constant J fixed, and adjust the field-like parameter $\Delta = 2J\cos\left(\frac{\pi}{N+1}\right) + \sqrt{\varepsilon_1^2 + K^2}$ accordingly. Finally, we shall measure all energy scales relative to J, which is numerically realized by setting $J = 1$.

5.3.1 Spin conductances

We compute the spin conductances

$$G^{\mathrm{T}} \equiv \frac{1}{R^{\mathrm{T}}}, \tag{5.41a}$$

$$G^{\mathrm{B}} \equiv \frac{1}{R^{\mathrm{B}}}, \tag{5.41b}$$

and

$$G^{\mathrm{L}} \equiv \frac{1}{R^{\mathrm{L}}} \tag{5.41c}$$

by fitting the components of $j^{\mathrm{L}}_{\mathrm{s,tot}}$ to Eqs. (5.39) for small values of μ^{L}, setting $T^{\mathrm{L}} = T^{\mathrm{R}} = T^{\mathrm{B}} = T$ and $\mu^{\mathrm{R}} = 0$. We consider a system with parameters $N = 20$, $\alpha = 0.001$, $\varepsilon_1 = 0.025J$ and $\eta^{\mathrm{L}} = \eta^{\mathrm{R}} = 8$. (Here, the values for $\eta^{\mathrm{L/R}}$ are chosen in line with Zheng *et al.* [77], while our choices for α and ε_1 are fairly arbitrary within the low-damping and low-gap regimes, respectively.) Note that because we have set $\hbar = 1$, the conductances are dimensionless.

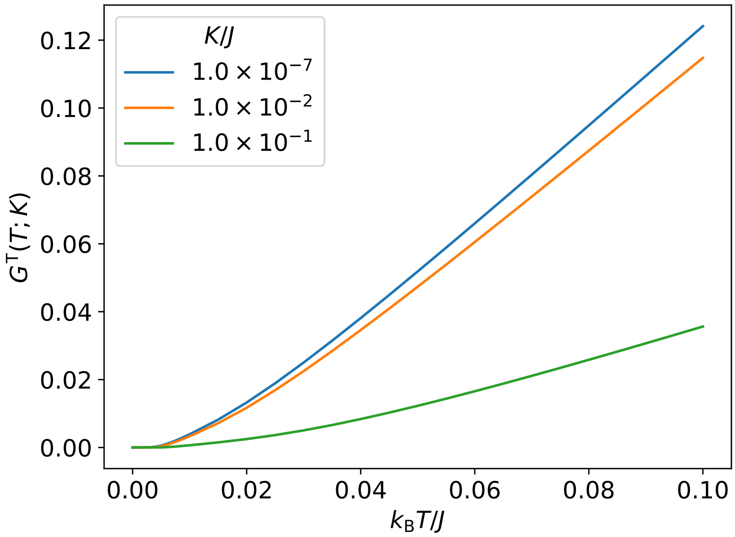

Figure 5.3: Tunneling conductance versus temperature at magnon gap $\varepsilon_1/J = 0.025$, for different values of the anisotropy K.

Figure 5.3 shows the tunneling conductance G^{T} vs. temperature $k_{\mathrm{B}}T$ at various values of K. In all cases, the tunneling conductance vanishes at $T = 0$ (to numerical accuracy; the highly nonlinear behavior at low temperature limits the fitting accuracy) and slowly transitions to being linear with temperature. The effect of anisotropy is to suppress the conductance, although this effect is small until $K/J = \mathcal{O}(0.1)$, i.e. very large anisotropy (e.g. for yttrium-iron garnet, a comparison of literature values [18, 100–103] yields $K/J = \mathcal{O}(10^{-3}$—$10^{-2})$, although the range is highly variable between different materials [14]). Physically, this may be understood by the fact that the leads are not commensurate to the elliptical spin waves, which causes an increase in reflection at the interface.

The bulk conductance G^{B}, shown in Fig. 5.4, similarly vanishes at $T = 0$ and is suppressed by anisotropy. Unlike the tunneling conductance, where the transition to a linear regime is smeared out at higher anisotropies, the bulk conductance transitions more abruptly, at $k_{\mathrm{B}}T/J \sim 0.005$. The suppression with anisotropy is mild: at $k_{\mathrm{B}}T/J = 0.1$, increasing the anisotropy from $K/J = 1 \times 10^{-7}$ to $K/J = 1 \times 10^{-1}$ suppresses the bulk conductance by roughly 8%. Our formalism does not elucidate the physical mechanism underlying this suppression, however, given its small magnitude, we believe it to be a natural consequence of the anisotropy-dependence of the dispersion, rather than being the result of any nontrivial effect.

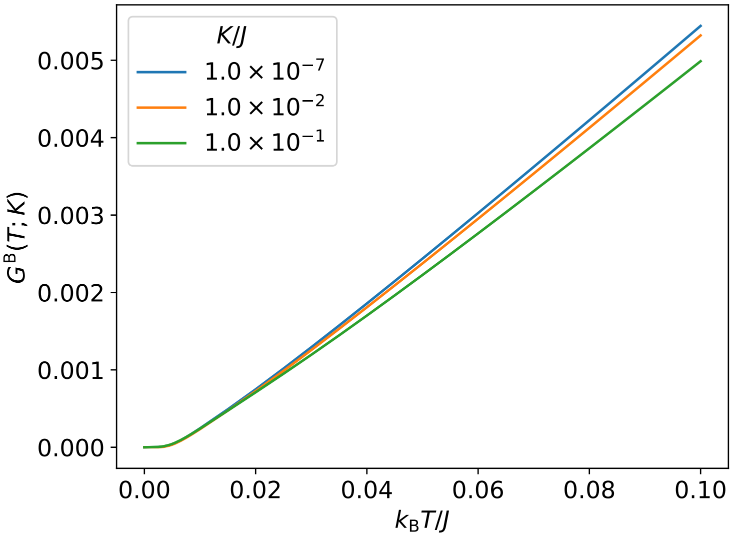

Figure 5.4: Bulk conductance versus temperature at magnon gap $\varepsilon_1/J = 0.025$, for different values of the anisotropy K.

The relatively abrupt transition to a linear regime is a direct consequence of the low-μ^{L} behavior of the difference of statistical matrices in the bulk spin current integrand (5.38b):

$$\begin{aligned}\coth\left(\frac{\omega}{2k_{\mathrm{B}}T}\right) \mp \coth\left(\frac{\pm\omega-\mu^{\mathrm{L}}}{2k_{\mathrm{B}}T}\right)& \\ \approx \pm\frac{\mu^{\mathrm{L}}}{k_{\mathrm{B}}T-k_{\mathrm{B}}T\cosh\left(\frac{\omega}{k_{\mathrm{B}}T}\right)}&. \end{aligned} \tag{5.42}$$

Given that the most significant contribution to G^{B} arises from a narrow region of $\iota^{\mathrm{B}\to\mathrm{L}}$ centred around $\omega=\varepsilon_1$ (as one would expect), we may judiciously substitute $\omega=\varepsilon_1=0.025J$ in this expression. Dividing by μ^{L}, we then obtain a function that exhibits a kink near $k_{\mathrm{B}}T/J=0.005$, similar to the bulk conductance. We may thus conclude, qualitatively, that the kink is explained by the requirement for the temperature to overcome the finite gap.

In Fig. 5.5, it can be seen that the lead-local conductance G^{L} nearly vanishes at low anisotropy (as expected) and reaches a magnitude roughly comparable to the bulk conductance at the fairly high anisotropy value $K/J=1\times10^{-2}$.

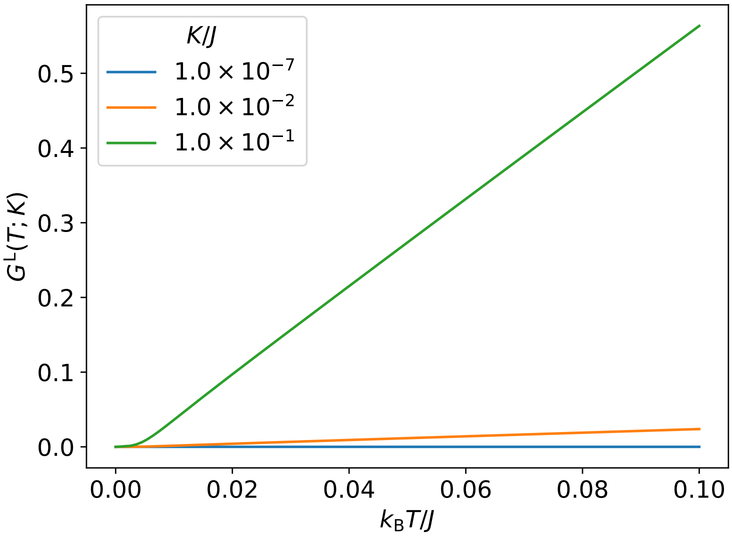

Figure 5.5: Lead-local conductance versus temperature at magnon gap $\varepsilon_1/J=0.025$, for different values of the anisotropy K.

However, G^{L} is vastly enhanced at the very high anisotropy value $K/J = \mathcal{O}(0.1)$, becoming several times larger than the tunneling conductance, indicating most spin is lost to the lattice at the left-lead interface. This bears similarity to the appearance of evanescent spin waves in anisotropic systems [104], however, rigorously showing the relation between these effects requires reconstructing the classical wave picture from our formalism, which is beyond the scope of this work. Like the bulk conductance, the transition to a linear regime in the lead-local conductance is relatively abrupt for the $K/J = 1 \times 10^{-1}$ curve.

Although the tunneling and bulk conductances are suppressed by increasing anisotropy, the corresponding increase in the lead-local conductance is greater than the decrease in the sum of tunneling and bulk conductances. In other words, the conductance of the parallel combination of the three spin resistors R^{T}, R^{B} and R^{L} *increases* with increasing anisotropy, while the individual conductances of R^{T} and R^{B} decrease. Thus, although our model does not provide an obvious way to separate the bulk and lead-local contributions, it suggests the presence of anisotropy causes the local spin conductance to increase, while the nonlocal conductance decreases, thereby potentially providing an experimental way to probe the anisotropy of a ferromagnetic insulator using spin current measurements.

5.3.2 Correlation functions and squeezing

To gain insight into the distribution of spin and the profile of spin nonconservation in the ferromagnet, we compute the density matrix at low and high anisotropy. Figure 5.6a shows the spin density matrix $\left\langle b_i^\dagger(t) b_j(t) \right\rangle$ in a low-damping ($\alpha = 1 \times 10^{-3}$), low anisotropy ($K/J = 1 \times 10^{-7}$) system where only the left lead is attached ($\eta^{\mathrm{L}} = 8$, $\eta^{\mathrm{R}} = 0$) and no biasing is applied ($\mu^{\mathrm{L}} = \mu^{\mathrm{R}} = 0$). The temperature is taken to be homogeneous at $k_{\mathrm{B}} T^{\mathrm{L}} = k_{\mathrm{B}} T^{\mathrm{R}} = k_{\mathrm{B}} T^{\mathrm{B}} = 0.1J$. The gap is set to $\varepsilon_1 = 0.025J$, which is a reasonable value for e.g. yttrium-iron garnet [18, 105].

In Fig. 5.6, the horizontal axes correspond to the site indices i and j. The spin density is slightly elevated at the attached lead, but primarily accumulates deep within the bulk, taking the shape of the crest of a standing wave whose wavelength is twice the sample size. Here it is immediately apparent that the Holstein-Primakoff magnons are significantly delocalized, as the correlations $\left\langle b_i^\dagger(t) b_j(t) \right\rangle$ decrease only slowly as $|i - j|$ grows.

At low anisotropy, the leads and bulk try to drive the system towards the same set of states, so the anomalous correlations $\left\langle b_i^\dagger(t) b_j^\dagger(t) \right\rangle$, shown in Fig. 5.6b, vanish everywhere up to numerical accuracy. The spin density plots remain virtually unchanged with increasing anisotropy up until about $K/J = \mathcal{O}(10^{-3})$.

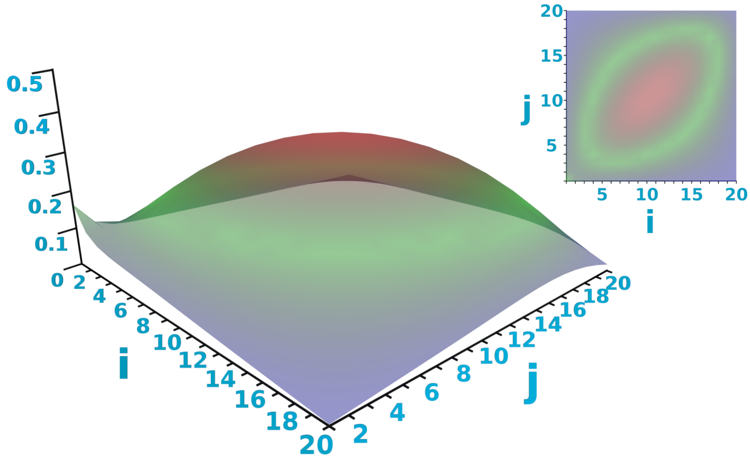

(a)

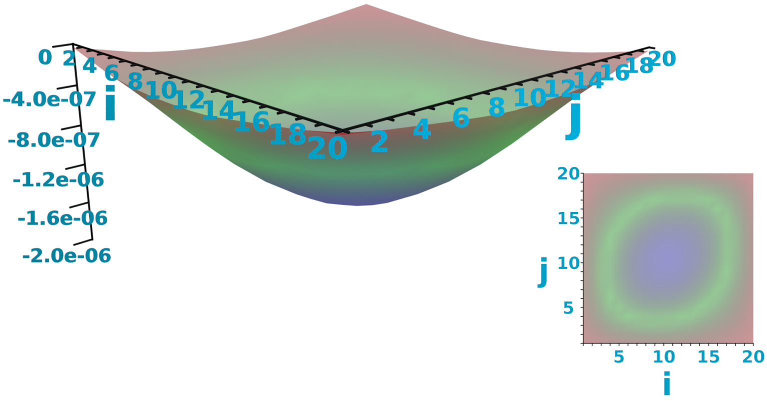

(b)

Figure 5.6: Normal and anomalous spin densities for a system of size $N = 20$ with only the left lead attached ($\eta^{\mathrm{L}} = 8$, $\eta^{\mathrm{R}} = 0$), low Gilbert-like damping $\alpha = 1 \times 10^{-3}$, temperature $T/J = 0.1$, gap $\varepsilon_1/J = 0.025$, and anisotropy $K/J = 1 \times 10^{-7}$. The horizontal axes represent the site indices i and j. Insets: heatmaps of the corresponding 3D plots. (a): normal density $\langle b_i^\dagger(t) b_j(t) \rangle$. (b): anomalous density $\langle b_i^\dagger(t) b_j^\dagger(t) \rangle$.

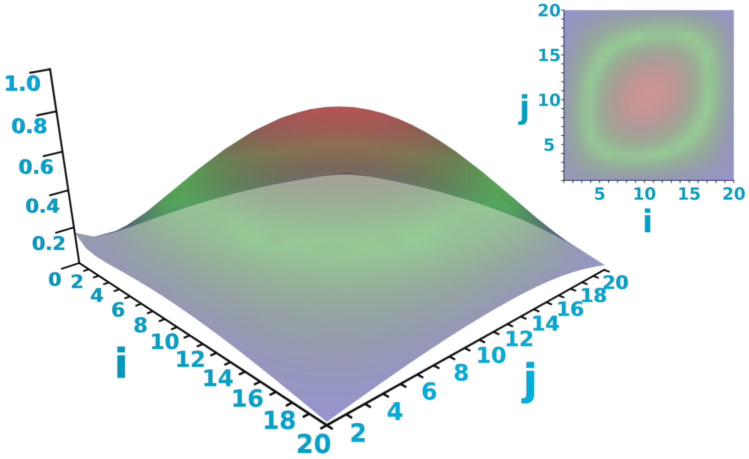

(a)

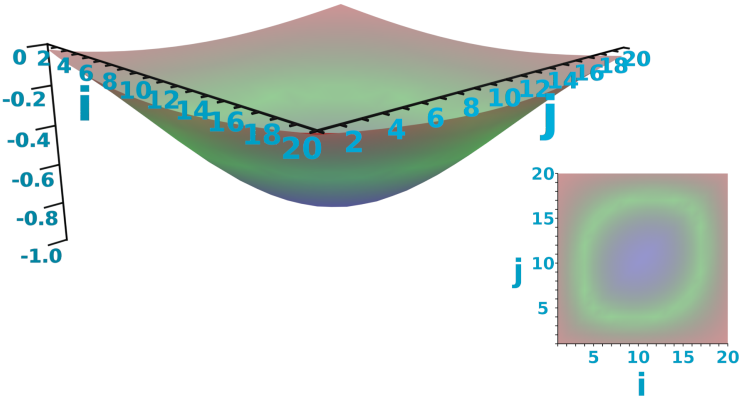

(b)

Figure 5.7: Normal and anomalous spin densities for a system with high anisotropy, $K/J = 5 \times 10^{-2}$. All other parameters are equal to those in Fig. 5.6. (a): normal density $\langle b_i^\dagger(t) b_j(t) \rangle$. (b): anomalous density $\langle b_i^\dagger(t) b_j^\dagger(t) \rangle$.

At much greater anisotropy—$K/J = 5 \times 10^{-2}$ shown in Fig 5.7—the amplitude of the spin density at the center of the sample increases significantly (Fig 5.7a), but the qualitative appearance of the profile remains broadly the same. However, as shown in Fig. 5.7b, the anomalous correlations now take a large negative value, highlighting that the Holstein-Primakoff magnons are no longer good basis states in the ferromagnetic bulk.

In Figs. 5.8 and 5.9 we plot the equivalent matrices in the basis of elliptical magnons: the horizontal axes now represent the quantum number, and the diagonals of the plots are ordered by increasing energy. In this basis, the ordinary block $\langle \psi_m^\dagger \psi_n \rangle$ of the correlation function $\langle \Psi_m^\dagger \Psi_n \rangle$ is almost exactly diagonal at low anisotropy ($K/J = 1 \times 10^{-7}$ shown in Fig. 5.8a). As we keep the gap ε_1 fixed, our chosen parameters lead to excitation of the lowest few modes only, regardless of anisotropy, with the overwhelming majority of quasiparticles being in the ground state (as indicated by the large spike at $m = n = 1$). In Fig. 5.8b, it can be seen that the anomalous block $\langle \psi_m^\dagger \psi_n^\dagger \rangle$ nearly vanishes, as expected (the same is true for $\langle \psi_m \psi_n \rangle$).

Figure 5.9a) shows that the qualitative behavior of the ordinary correlations $\langle \psi_m^\dagger \psi_n \rangle$ does not change significantly even at the high anisotropy value $K/J = 5 \times 10^{-2}$. However, the anomalous block $\langle \psi_m^\dagger \psi_n^\dagger \rangle$, shown in Fig. 5.9b now exhibits a small but noticeable deviation from zero, and becomes asymmetric. This asymmetry ultimately stems from the fact that $\langle b_i^\dagger b_j \rangle \neq \langle b_i b_j^\dagger \rangle$. The bosonic relations are nevertheless preserved because the full matrix $\langle \Psi_m^\dagger \Psi_n \rangle$ is symmetric.

As explained previously, we may use the density matrix to directly compute uncertainty of the spin operators, which we expect to become squeezed at high anisotropy. In Fig. 5.10, we plot the uncertainty amplitudes $\Delta \bar{S}_i^x$ and $\Delta \bar{S}_i^y$ for $K/J = 1 \times 10^{-7}$ and $K/J = 1 \times 10^{-1}$, with weak left-lead coupling $\eta^{\mathrm{L}} = 0.1$ and no right lead attached. In the case of zero bias ($\mu^{\mathrm{L}} = 0$, Fig. 5.10a), it can be seen that high anisotropy causes the magnons to become squeezed throughout the sample. At site 1, where the left lead is attached, both $\Delta \bar{S}^x$ and $\Delta \bar{S}^y$ are squeezed, in an apparent violation of the uncertainty principle. However, this may be explained by the fact that we only consider the lowest-order self-energy contribution of the lead coupling: this ignores higher-order electronic contributions to the total wavefunction at the interface, and it stands to reason—although it remains to be verified—that the uncertainty principle is not violated if higher-order contributions are taken into account.

Taking only sites $i > 1$ into account, we find that squeezing commences at site 20 (the 'far side' of the chain, where no lead is attached) for $K/J \approx 3 \times 10^{-2}$. Squeezing increases with increasing anisotropy, with the effect being

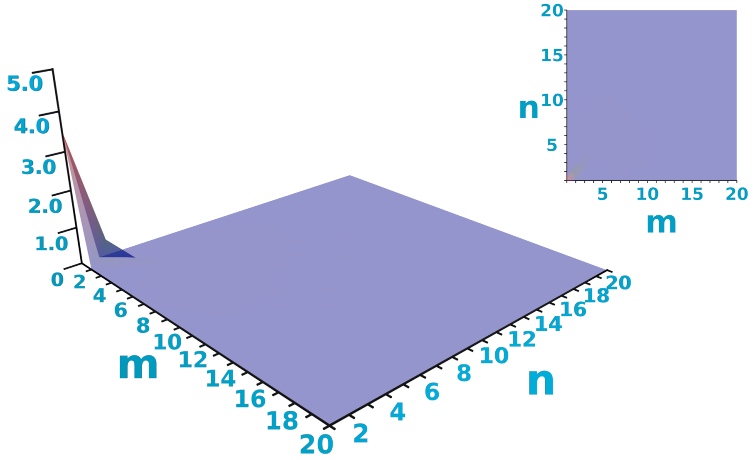

(a)

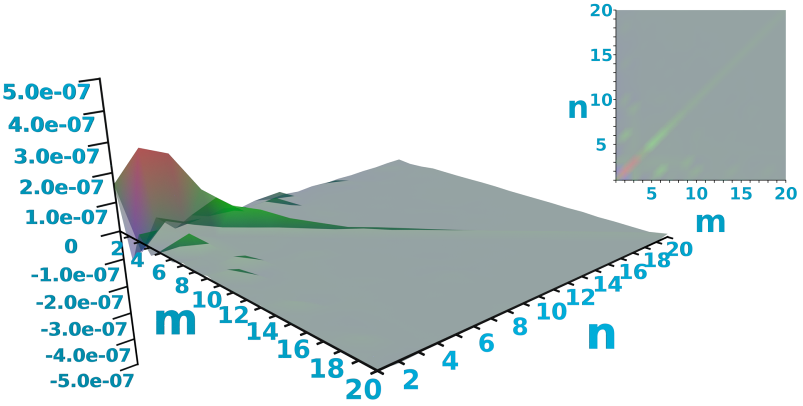

(b)

Figure 5.8: Normal and anomalous elliptical magnon densities for a system with low anisotropy, $K/J = 1 \times 10^{-7}$. All other parameters are equal to those in Fig. 5.6. The horizontal axes represent the quantum numbers m and n. (a): normal density $\langle \psi_m^\dagger(t)\psi_n(t) \rangle$. (b): anomalous density $\langle \psi_m^\dagger(t)\psi_n^\dagger(t) \rangle$. The minor (light green) fluctuations are near the scale of numerical error (10^{-8}) and may be unphysical.

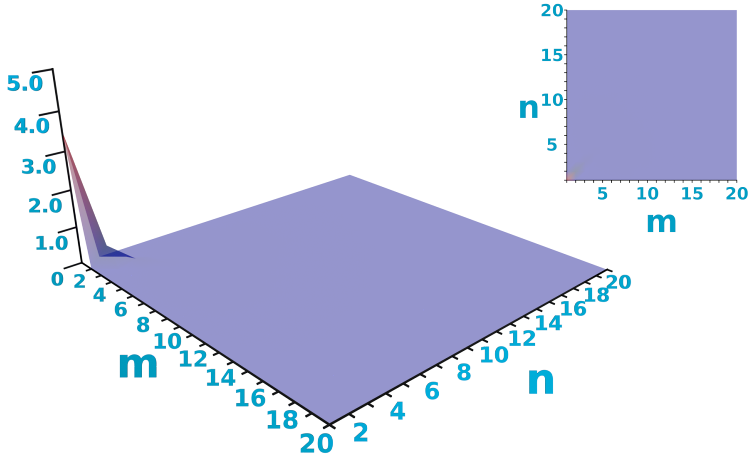

(a)

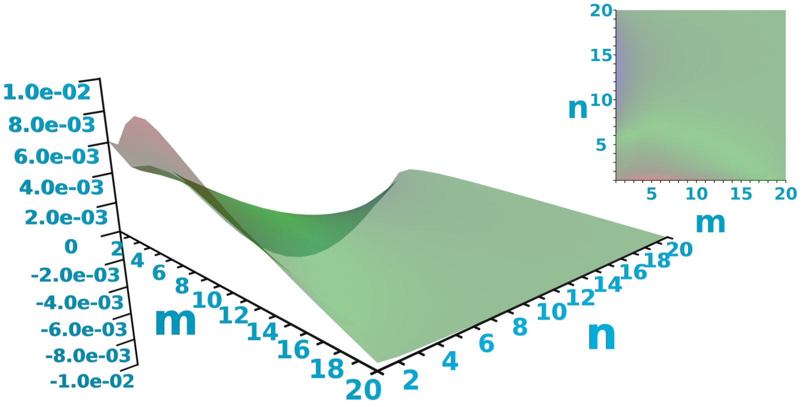

(b)

Figure 5.9: Normal and anomalous elliptical magnon densities for a system with high anisotropy, $K/J = 5 \times 10^{-2}$. All other parameters are equal to those in Fig. 5.6. (a): normal density $\langle \psi_m^\dagger(t)\psi_n(t) \rangle$. (b): anomalous density $\langle \psi_m^\dagger(t)\psi_n^\dagger(t) \rangle$.

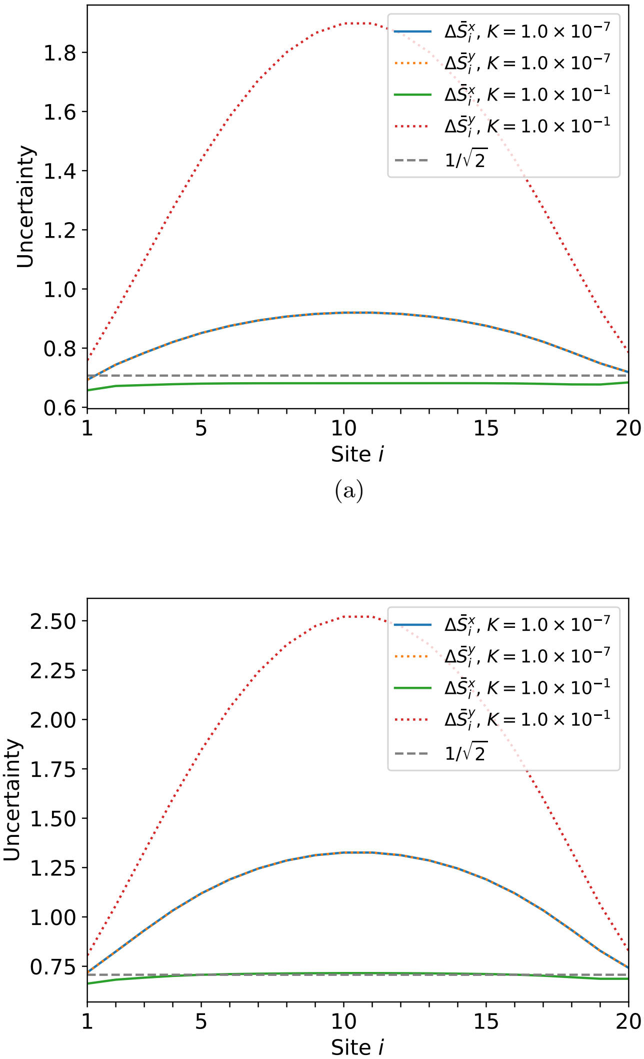

(a)

(b)

Figure 5.10: Uncertainty in the spin operators S^x (solid lines) and S^y (dotted lines), for a system of size $N = 20$ with only the left lead attached ($\eta^{\mathrm{L}} = 0.1$, $\eta^{\mathrm{R}} = 0$), low Gilbert-like damping $\alpha = 1\times10^{-3}$, temperature $k_{\mathrm{B}}T/J = 0.1$, gap $\varepsilon_1/J = 0.025$, and different anisotropies. When the spin uncertainty drops below $\frac{1}{\sqrt{2}}$ (dashed line), the state is squeezed. At very high anisotropy, the magnons become squeezed throughout the system. Note that the $\Delta\bar{S}^x$ and $\Delta\bar{S}^y$ curves lie on top of each other at $K/J = 1\times10^{-7}$, indicating the magnons are coherent at low anisotropy. (a): without applied bias ($\mu^{\mathrm{L}} = 0$). (b): with bias at left lead ($\mu^{\mathrm{L}}/J = 0.1$).

strongest at the center of the sample, where the overall spin density is the highest. By applying a spin bias at the attached lead ($\mu^{\mathrm{L}}/J = 0.1$ shown in Fig. 5.10b), squeezing is diminished throughout the sample, and the overall uncertainty markedly increases. A local bias may thus be used to effect a global change in the uncertainty.

5.4 Conclusions and outlook

We have developed and numerically implemented a NEGF formalism to describe the transport of elliptically polarized magnons in finite-sized ferromagnetic insulators terminated by metallic leads. The presence of anisotropy in a ferromagnetic insulator can give rise to a novel parasitic local spin resistance, and additionally acts to suppress the spin conductance measured between the metallic leads. However, our model predicts that these effects are mild in ferromagnets with weak anisotropy, and become significant only when the ferromagnet exhibits strong anisotropy.

We have shown that the NEGF formalism allows theoretical access to the anomalous correlation functions $\left\langle b_i b_j \right\rangle$ and $\left\langle b_i^\dagger b_j^\dagger \right\rangle$, which may obtain a large amplitude in the presence of anisotropy, and provide a measure for the degree of nonconservation of spin and ellipticity of magnons. Likewise, the correlation functions $\left\langle \psi_m \psi_n \right\rangle$ and $\left\langle \psi_m^\dagger \psi_n^\dagger \right\rangle$ in the basis of eigenstates of the free anisotropic ferromagnetic insulator obtain a nonzero value in the presence of coupling to metallic leads which inject a well-defined amount of spin, provided the anisotropy is large and the lead coupling is sufficiently strong. Moreover, strong anisotropy produces squeezing of $\Delta \bar{S}^x$, which may be observable in the form of reduced shot noise [86] and find applications in quantum information science.

Although we have focussed on ferromagnets, where anisotropy tends to be significantly weaker than the exchange interaction, it stands to reason that much stronger observable effects may be realized in antiferromagnets, where similar anomalous Hamiltonian terms are introduced by coupling between sublattices, but are now governed by the exchange interaction itself [81].

While we have provided some examples of effects produced by the introduction of anisotropy, our model is simplistic, and omits several features one would expect to find in a realistic system. A possible extension, for example, would be the introduction of disorder, which can take the form of spatial fluctuations in both Δ and K. Moreover, our model considers only weak interactions between magnons and the leads and lattice (i.e. lowest-order self-energy terms), while higher-order contributions may be relevant to physical systems. We have likewise neglected magnon-magnon interactions, while several real systems are known or believed to violate this assumption [106–108].

Finally, the parameter space of our model (with or without extensions) is quite large, and therefore remains mostly unexplored. Hence, it is plausible that more observable effects of the spin-conservation breaking anisotropies can be found, for example through the spin Seebeck effect.

5.5 Appendix: Derivation of the steady-state spin current

We define the total spin current as the negative time-derivative of the total HP magnon number density (as each magnon carries spin 1), i.e.

$$\begin{aligned} j_{\mathrm{s}}^{\mathrm{tot}} &= -\partial_t \operatorname{Tr}\left\langle b^\dagger(t)b(t)\right\rangle \\ &= -\frac{1}{2}\partial_t\left[\operatorname{Tr}\left\{\left\langle b^\dagger(t)b(t)\right\rangle + \left\langle b(t)b^\dagger(t)\right\rangle\right\} - N\right] \\ &= -\frac{1}{2}\partial_t \operatorname{Tr}\left\langle \phi^\dagger(t)\phi(t)\right\rangle = -\operatorname{Re}\operatorname{Tr}\left\langle \phi^\dagger(t)\partial_t\phi(t)\right\rangle . \end{aligned} \tag{5.43}$$

Note that the trace on the first two lines is over the spatial indices alone and therefore has N terms, whereas on the last line, it is over the full matrix and therefore has $2N$ terms. To evaluate Eq. (5.43), we introduce a stochastic field

$$\xi(\omega) = -g(\omega)\phi(\omega) \tag{5.44}$$

obeying

$$\left\langle \xi(\omega)\xi^\dagger(\omega')\right\rangle = \pi\mathrm{i}\delta(\omega-\omega')\Sigma^{\mathrm{K}}(\omega). \tag{5.45}$$

By construction, ξ is the Hubbard-Stratonovich field that decouples the quantum-quantum term of the Schwinger-Keldysh action for the continuum-limit field theory. A more detailed derivation is given e.g. by Kamenev [109].

Inserting Eq. (5.22) into Eq. (5.44) and taking the Fourier transform, we find the evolution equation

$$-\mathrm{i}\partial_t\phi(t) = \sigma_3 h\phi(t) + \sigma_3\int \mathrm{d}t'\Sigma(t-t')\phi(t') - \sigma_3\xi(t), \tag{5.46}$$

which we may plug into Eq. (5.43) to obtain

$$\begin{aligned} j_{\mathrm{s}}^{\mathrm{tot}} = -\operatorname{Im}\operatorname{Tr}\Bigg\{ & \left\langle \phi^{\dagger}(t)\sigma_3 h\phi(t)\right\rangle \\ & + \left\langle \phi^{\dagger}(t)\sigma_3 \int \mathrm{d}t'\Sigma(t-t')\phi(t')\right\rangle \\ & - \left\langle \phi^{\dagger}(t)\sigma_3\xi(t)\right\rangle \Bigg\}. \end{aligned} \tag{5.47}$$

Here the first term is the Hamiltonian evolution of the system, and the second and third terms represent driving by external factors: the second term concerns the interaction with the lead electrons and with the field(s) responsible for Gilbert-like damping, and the third term contains the effect of quantum noise.

In the steady state, the total spin current vanishes by definition, and thus the first term necessarily cancels against the driving terms. In an experiment where the system is held out of equilibrium by external driving, the net external source/sink current are then given by the sum of the last two terms of Eq. (5.47). However, these terms, as given, sum over all of the spin currents within the system, including unobservable contributions that occur deep within the bulk and never exit the ferromagnet, whereas the actually observable spin currents are those which flow out of the leads. This quantity is obtained when one replaces Σ with $\Sigma^{\mathrm{L/R}}$ and ξ with $\xi^{\mathrm{L/R}}$ in Eq. (5.47). Here we define $\xi^{\mathrm{L/R}}$ to be the stochastic field obeying

$$\left\langle \xi^{\mathrm{L/R}}(\omega)\xi^{\dagger}(\omega')\right\rangle = 2\pi\mathrm{i}\delta(\omega-\omega')\Sigma^{\mathrm{L/R}}(\omega)F^{\mathrm{L/R}}(\omega), \tag{5.48}$$

where $2\Sigma^{\mathrm{L/R}}(\omega)F^{\mathrm{L/R}}(\omega)$ is the left/right lead term of the Keldysh self energy.

Thus, focussing now on the spin current flowing out of the left lead (in the following derivation, one may obtain equivalent expressions for the right lead by swapping L and R), we find

$$\begin{aligned} j_{\mathrm{s}}^{\mathrm{L,tot}} = -\operatorname{Im}\operatorname{Tr}\Bigg\{ & \left\langle \phi^{\dagger}(t)\sigma_3 \int \mathrm{d}t'\Sigma^{\mathrm{L}}(t-t')\phi(t')\right\rangle \\ & - \left\langle \phi^{\dagger}(t)\sigma_3\xi^{\mathrm{L}}(t)\right\rangle \Bigg\}. \end{aligned} \tag{5.49}$$

Next, by Fourier transforming and using Eq. (5.44) to write ϕ in terms of ξ, we obtain

$$\begin{aligned} j_\mathrm{s}^{\mathrm{L,tot}} = -\operatorname{Im}\operatorname{Tr}\int \frac{\mathrm{d}\omega}{2\pi}\frac{\mathrm{d}\omega'}{2\pi}\mathrm{e}^{\mathrm{i}t(\omega'-\omega)} &\times \left\{ \left\langle \xi^\dagger(\omega) g^\dagger(\omega)\sigma_3\Sigma^\mathrm{L}(\omega')g(\omega')\xi(\omega')\right\rangle \right. \\ &\left. + \left\langle \xi^\dagger(\omega)g^\dagger(\omega)\sigma_3\xi^\mathrm{L}(\omega')\right\rangle \right\}. \end{aligned} \tag{5.50}$$

Reordering terms using the properties of the trace and making use of Eqs. (5.45), (5.48) and (5.27), this gives

$$\begin{aligned} j_\mathrm{s}^{\mathrm{L,tot}} = -\operatorname{Re}\operatorname{Tr}\int \frac{\mathrm{d}\omega}{2\pi}\, g^\dagger(\omega)\sigma_3\Sigma^\mathrm{L}(\omega)g(\omega) &\times \left\{ \Sigma^\mathrm{L}(\omega)F^\mathrm{L}(\omega) + \Sigma^\mathrm{R}(\omega)F^\mathrm{R}(\omega) \right. \\ &\left. + \Sigma^\mathrm{B}(\omega)\mathcal{T}^{-1}F^\mathrm{B}(\omega)\mathcal{T} + g^{-1}(\omega)F^\mathrm{L}(\omega) \right\}. \end{aligned} \tag{5.51}$$

Inserting the Dyson equation for $g^{-1}(\omega)$, we find

$$\begin{aligned} j_\mathrm{s}^{\mathrm{L,tot}} = -\operatorname{Re}\operatorname{Tr}\int \frac{\mathrm{d}\omega}{2\pi} &\left\{ \iota^{\mathrm{R}\to\mathrm{L}}(\omega) + \iota^{\mathrm{B}\to\mathrm{L}}(\omega) \right. \\ &\left. + g^\dagger(\omega)\sigma_3\Sigma^\mathrm{L}(\omega)g(\omega)\left[\omega\sigma_3 - h\right]F^\mathrm{L}(\omega) \right\}, \end{aligned} \tag{5.52}$$

where $\iota^{\mathrm{R}\to\mathrm{L}}(\omega)$ and $\iota^{\mathrm{B}\to\mathrm{L}}$ are given by Eqs. (5.38a) and (5.38b), respectively. By using that $\operatorname{Re}\operatorname{Tr} M = \frac{1}{2}\operatorname{Tr}(M + M^\dagger)$ for an arbitrary square matrix M, the term involving $\omega\sigma_3$ can easily be shown to vanish. In a similar vein, we find

$$\begin{aligned} &-\operatorname{Re}\operatorname{Tr}\left\{ g^\dagger(\omega)\sigma_3\Sigma^\mathrm{L}(\omega)g(\omega)hF^\mathrm{L}(\omega)\right\} \\ &\qquad = \frac{1}{2}\operatorname{Tr}\left\{ g^\dagger(\omega)\sigma_3\Sigma^\mathrm{L}(\omega)g(\omega)\left[F^\mathrm{L}(\omega), h\right]\right\}. \end{aligned} \tag{5.53}$$

In the absence of a spin accumulation, $F^\mathrm{L}(\omega)$ becomes a scalar function multiplying the identity matrix, causing the commutator to vanish. Therefore, we may add the term

$$0 = \operatorname{Tr} g^\dagger(\omega)\sigma_3\Sigma^\mathrm{L}(\omega)g(\omega)h\, F^\mathrm{L}(\omega)\big|_{\mu^\mathrm{L}=0}, \tag{5.54}$$

thereby recovering Eq. 5.38c). Finally, in the limit $K \to 0$, the Hamiltonian h becomes block-diagonal, so that the commutator in Eq. (5.53) causes $\iota^{\mathrm{L}}(\omega)$ to vanish in absence of anisotropy.

6 NONLOCAL SPIN TRANSPORT IN ONE-DIMENSIONAL ANTIFERROMAGNETIC INSULATORS

6.1 Introduction

The field of spintronics concerns itself with the study of spin as an information carrier, and typically involves the use of one or more magnetically ordered materials. While magnetic ordering can be roughly subdivided into two classes—ferromagnetic and antiferromagnetic—the materials under consideration in mainstream spintronics have, until very recently, almost exclusively been ferromagnets (FMs). As antiferromagnets (AFMs) lack a ground-state magnetization, manipulating the antiferromagnetic order parameter (the Néel vector) poses considerable challenges, and it has long been thought that AFMs did not present any practical applications [17, 110]. More recently, however, it has been shown that the Néel vector may be manipulated electrically, which, combined with AFMs' robustness against magnetic fields and terahertz dynamics, has rekindled research into antiferromagnetic spintronics.

As is the case in FMs, a perturbation of the antiferromagnetic order parameter produces spin waves or magnons. However, in contrast to FMs, where a single band is sufficient to describe magnons at the quadratic order, the simplest description of an AFM consists of two sublattices with opposing spin orientations, which leads to a two-band spin wave description. Moreover, the two antiferromagnetic magnon bands intrinsically exhibit pair production, which gives rise to anomalous correlation functions and broken spin conservation (in the sense that the pair has a well-defined spin, but its components can interact and decay individually).

In this manuscript, we extend a Green's function formalism developed earlier by our group for isotropic and anisotropic FMs [2, 77] to antiferromagnetic insulators. Although we have showed previously [2] that anomalous correlation functions are present in strongly anisotropic FMs, their magnitude only becomes significant at stronger anisotropies than are commonly seen in physical materials. However, in antiferromagnetic magnon systems, pair-producing terms contain a component that is directly proportional to the exchange con-

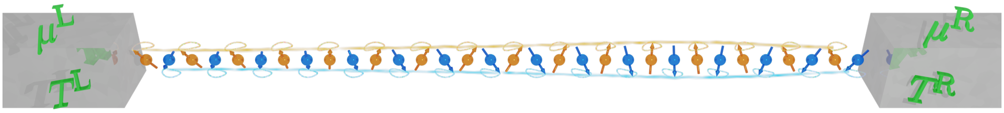

Figure 6.1: Cartoon depiction of spin waves in a 1D antiferromagnetic spin chain attached to metallic leads. The presence of two spin species produces two magnon bands (amber and blue swirls). The metallic leads are modelled as having a spin accumulation μ^X and temperature T^X, where $X = \text{L}$ for the left lead and $X = \text{R}$ for the right lead.

stant, leading us to hypothesise that the corresponding 'anomalous' effects may be significantly stronger in AFMs. Furthermore, the two-sublattice nature of AFMs broadens the parameter space, for example by allowing external leads to couple to the sublattices with different strength.

6.2 Methods and results

In this section, we outline the system we wish to study, and the methods we use to do so.

6.2.1 System and Hamiltonian

We consider a one-dimensional (1D) discrete antiferromagnetic Heisenberg spin chain (simplified depiction shown in Figure 6.1), consisting of two sublattices labelled A and B. In the ground state, sites of the A-sublattice have spin projection $+S$ on the z-axis, while B-sites have spin projection $-S$. The chain consists of N unit cells, each of which contains one spin belonging to the A sublattice and one belonging to the B sublattice. The chain therefore has $2N$ spins in total, and we assume its leftmost (rightmost) site belongs to the A-sublattice (B-sublattice). The Hamiltonian of this system is

$$\begin{aligned} H = J\sum_{i=1}^{N} \hat{\boldsymbol{S}}_i^A \cdot \hat{\boldsymbol{S}}_i^B + J\sum_{i=1}^{N-1} \hat{\boldsymbol{S}}_i^B \cdot \hat{\boldsymbol{S}}_{i+1}^A - h_{\text{mag}} S \sum_{i=1}^{N} \left[\hat{S}_i^{Az} + \hat{S}_i^{Bz}\right] \\ - \frac{K}{2}\sum_{i=1}^{N} \left[(S_i^{Az})^2 + (S_i^{Bz})^2\right]. \end{aligned} \tag{6.1}$$

Here, $J > 0$ is the exchange constant, $h_{\text{mag}} S$ is an externally applied magnetic field (judiciously scaled with S), and $K > 0$ is an easy-z-axis anisotropy constant. $\hat{\boldsymbol{S}}_i^A$ ($\hat{\boldsymbol{S}}_i^B$) is the vectorial spin operator acting on the A-type (B-type) site of the i'th unit cell. We choose K to be sufficiently large to ensure all spins are collinear with the z-axis in the ground state, i.e. to prevent the system from entering the spin-flop phase [111, 112].

We apply the second-order spin-S antiferromagnetic Holstein-Primakoff transformation [26, 28] to Eq. (6.1):

$$\hat{S}_i^{Ax} = \sqrt{\frac{S}{2}}\left(\hat{a}_i + \hat{a}_i^\dagger\right), \tag{6.2a}$$

$$\hat{S}_i^{Ay} = -\mathrm{i}\sqrt{\frac{S}{2}}\left(\hat{a}_i - \hat{a}_i^\dagger\right), \tag{6.2b}$$

$$\hat{S}_i^{Az} = S - \hat{a}_i^\dagger \hat{a}_i, \tag{6.2c}$$

and

$$\hat{S}_i^{Bx} = \sqrt{\frac{S}{2}}\left(\hat{b}_i + \hat{b}_i^\dagger\right), \tag{6.2d}$$

$$\hat{S}_i^{By} = \mathrm{i}\sqrt{\frac{S}{2}}\left(\hat{b}_i - \hat{b}_i^\dagger\right), \tag{6.2e}$$

$$\hat{S}_i^{Bz} = -S + \hat{b}_i^\dagger \hat{b}_i. \tag{6.2f}$$

Here $\hat{a}_i^\dagger$ ($\hat{a}_i$) and $\hat{b}_i^\dagger$ ($\hat{b}_i$) are the creation (annihilation) operators of A-band and B-band magnons, respectively, localized at unit cell i. These operators obey the bosonic commutation relations

$$[\hat{a}_i, \hat{a}_j^\dagger] = [\hat{b}_i, \hat{b}_j^\dagger] = \delta_{ij}, \tag{6.3a}$$

$$[\hat{a}_i, \hat{a}_j] = [\hat{b}_i, \hat{b}_j] = [\hat{a}_i^\dagger, \hat{a}_j^\dagger] = [\hat{b}_i^\dagger \hat{b}_j^\dagger] = 0, \tag{6.3b}$$

with operators of different bands commuting:

$$[\hat{a}_i, \hat{b}_j] = [\hat{a}_i^\dagger, \hat{b}_j^\dagger] = [\hat{a}_i, \hat{b}_i^\dagger] = [\hat{a}_i^\dagger, \hat{b}_j] = 0. \tag{6.3c}$$

Up to quadratic terms in the bosonic operators, the resulting Hamiltonian reads

$$\begin{aligned} H = JS\Bigg\{ &\sum_{i=1}^{N}\left[\hat{a}_i\hat{b}_i + \hat{a}_i^\dagger\hat{b}_i^\dagger + \left(2 + \frac{h_{\mathrm{mag}}}{J} + \frac{K}{J}\right)\hat{a}_i^\dagger\hat{a}_i + \left(2 - \frac{h_{\mathrm{mag}}}{J} + \frac{K}{J}\right)\hat{b}_i^\dagger\hat{b}_i\right] \\ &+ \sum_{i=1}^{N-1}\left[\hat{a}_{i+1}\hat{b}_i + \hat{a}_{i+1}^\dagger\hat{b}_i^\dagger\right] - \hat{a}_1^\dagger\hat{a}_1 - \hat{b}_N^\dagger\hat{b}_N\Bigg\}, \end{aligned} \tag{6.4}$$

where we have ignored unimportant global energy shifts.

Eq. (6.4) is further reduced by defining the vector operator

$$\hat{\Phi} = \left(\hat{a}_1, \hat{a}_2, \ldots, \hat{a}_N, \hat{b}_1^\dagger, \hat{b}_2^\dagger, \ldots, \hat{b}_N^\dagger\right)^{\mathrm{T}}, \tag{6.5}$$

which has $2N$ components in total. We then obtain

$$H = \hat{\Phi}^\dagger h \hat{\Phi}, \tag{6.6}$$

where

$$h \equiv \begin{pmatrix} h^{AA} & h^{AB} \\ h^{BA} & h^{BB} \end{pmatrix}. \tag{6.7}$$

The four $N \times N$ submatrices have the following components:

$$h_{ij}^{AA} = JS\left(2 + \frac{h_{\mathrm{mag}}}{J} + \frac{K}{J} - \delta_{i,1}\right)\delta_{ij}, \tag{6.8a}$$

$$h_{ij}^{AB} = JS\left(\delta_{ij} + \delta_{i,j+1}\right), \tag{6.8b}$$

$$h_{ij}^{BA} = h_{ji}^{AB}, \tag{6.8c}$$

$$h_{ij}^{BB} = JS\left(2 - \frac{h_{\mathrm{mag}}}{J} + \frac{K}{J} - \delta_{i,N}\right)\delta_{ij}. \tag{6.8d}$$

The $2N \times 2N$ Hamiltonian matrix h is diagonalized by a para-unitary transformation [30], i.e. a matrix $\mathcal{T}$ obeying

$$\sigma_3 \mathcal{T}^\dagger = \mathcal{T}^{-1}\sigma_3, \tag{6.9}$$

where $\sigma_3 = \mathrm{diag}(\mathbb{I}_N, -\mathbb{I}_N)$ is the $2N \times 2N$ analog of the third Pauli matrix, with $\mathbb{I}_N$ the $N \times N$ identity matrix. Unlike the anisotropic ferromagnet [2], no simple closed expressions for the paravalues or paravector components exist for an antiferromagnetic spin chain of arbitrary length; we therefore opt to perform the diagonalization numerically. We normalize all energies to the exchange scale by setting $J = 1$, and fix the magnon gap (lowest paravalue) ε_1 to a constant by using the Alefeld-Potra-Shi algorithm (TOMS Algorithm 748) [113] to vary h_{mag}.

Diagonalization of the Hamiltonian yields the transformed operators

$$\hat{\Psi} \equiv \left(\hat{\alpha}_1, \quad \ldots, \quad \hat{\alpha}_N, \quad \hat{\beta}_1^\dagger, \quad \ldots, \quad \hat{\beta}_N^\dagger\right)^{\mathcal{T}} \tag{6.10}$$

given by

$$\hat{\Psi} = \mathcal{T}\hat{\Phi}. \tag{6.11}$$

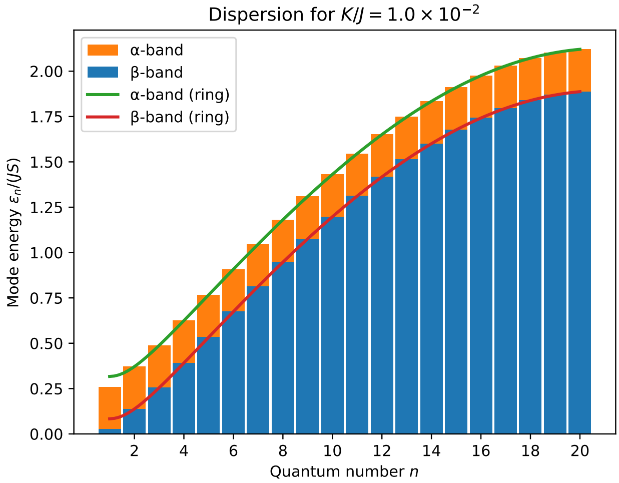

Figure 6.2: Example of the discrete band structure (bar plots) at intermediate anisotropy $K/J = 1 \times 10^{-2}$. The line plots are analytical results for a chain with periodic boundary conditions; no numerical fitting is applied.

The operators $\hat{\alpha}_n^\dagger$ and $\hat{\beta}_n^\dagger$ produce eigenstates of the free antiferromagnetic Hamiltonian, which are superpositions of the spin-± 1 HP states and therefore do not have a well-defined spin. As a result, spin transport through an AFM is necessarily spin-nonconserving. The quantum number n is defined to correspond to increasing energy within a given band, i.e. $\hat{\alpha}_{n+1}^\dagger$ ($\hat{\beta}_{n+1}^\dagger$) creates a mode with higher energy than $\hat{\alpha}_n^\dagger$ ($\hat{\beta}_n^\dagger$). For positive values of h_{mag} and K, the energy level ε_n^β of the β-band is always lower than the corresponding α-band level ε_n^α. An example of the band structure can be seen in Figure 6.2. By comparison, closing the spin chain into a ring (and thereby imposing periodic boundary conditions) by adding the term $J\hat{\boldsymbol{S}}_N^B \cdot \hat{\boldsymbol{S}}_1^A$ to Eq. (6.1), the diagonalization may be performed analytically, yielding the dispersion relations (up to common energy shift, which we have dropped to conform to the para-unitary results)

$$\varepsilon_n^{\alpha,\mathrm{ring}} = S\sqrt{(2J+K)^2 - 4J^2\cos\left(\frac{\pi(n-1)}{2N}\right)} + h_{\mathrm{mag}}S; \tag{6.12a}$$

$$\varepsilon_n^{\beta,\mathrm{ring}} = S\sqrt{(2J+K)^2 - 4J^2\cos\left(\frac{\pi(n-1)}{2N}\right)} - h_{\mathrm{mag}}S. \tag{6.12b}$$

These dispersion relations have been included in Figure 6.2 for reference; it can be seen that only the lowest energy level of each band shows significant deviation from the analytical continuum limit. Eqs. (6.12) further impose the condition

$$|h_{\text{mag}}| < \sqrt{K(4J+K)}\ : \tag{6.13}$$

if this is violated, $\varepsilon_0^{\beta,\text{ring}}$ (for $h_{\text{mag}} > 0$) or $\varepsilon_0^{\alpha,\text{ring}}$ (for $h_{\text{mag}} < 0$) becomes negative, creating an instability that will push the system into the spin-flop phase.

6.2.2 Green's function formalism

To study spin transport in our system, we develop a discrete, real-space non-equilibrium Green's function formalism. We focus on steady-state behavior, so that the time dependence of all functions $\mathfrak{f}(t,t')$ obeys

$$\mathfrak{f}(t,t') = \mathfrak{f}(t-t'). \tag{6.14}$$

We may then Fourier transform to the frequency domain, and obtain the retarded Green's function $g(\omega)$—which contains the spectral properties of the magnons—from the Dyson equation:

$$g(\omega) = [\omega\sigma_3 - h - \Sigma(\omega)]^{-1}. \tag{6.15}$$

Here, $\Sigma(\omega)$ is the retarded self-energy arising due to the magnons' interaction with electrons, phonons, etc. Following our previous work [2], we may directly write down the self-energy contributions from coupling to external leads at the left and right ends of the spin chain (corresponding to unit cells 1 and N, respectively). We further allow each lead to have different coupling strengths to spins from either sublattice, making for a total of four retarded self-energy components originating from the leads, which have the form

$$\Sigma_{\sigma\tau}^{X,\gamma}(\omega) = -\mathrm{i}\eta^{X,\gamma}(\omega - \mu^X\sigma_3)\delta_{\sigma,\sigma^{X,\gamma}}\delta_{\sigma\tau}, \tag{6.16}$$

where X indexes the lead ($X = \mathrm{L}$ for the left lead or $X = \mathrm{R}$ for the right lead) and $\gamma \in \{A, B\}$ indexes the sublattice. $\eta^{X,\gamma}$ is a real scalar coupling constant, and μ^X is the spin accumulation at lead X. σ and τ are component indices of the full $2N \times 2N$ matrix. The two Kronecker deltas specify that only the diagonal matrix component corresponding to the lead site in question is nonzero; see Table 6.1. We define the full lead self-energy of lead X as

$$\Sigma^X = \sum_\gamma \Sigma^{X,\gamma}. \tag{6.17}$$

X	γ	$\sigma^{X,\gamma}$
L	A	1
L	B	$N+1$
R	A	N
R	B	$2N$

Table 6.1: Matrix index $\sigma^{X,\gamma}$ in the full $2N \times 2N$ space for lead X and sublattice γ, such that the only nonzero matrix element of the lead self-energy $\Sigma^{X,\gamma}_{\sigma\rho}(\omega)$ is $(\sigma^{X,\gamma}, \sigma^{X,\gamma})$.

The leads serve to directly inject spin by coupling to the HP magnon operators $\hat{a}_i$ and $\hat{b}_i$, which are superpositions of the diagonalized operators $\hat{\alpha}_n$ and $\hat{\beta}_n$. In contrast, we additionally consider a bulk damping self-energy component that acts to thermalize the system towards the eigenstates of the free AFM:

$$\Sigma^{\mathrm{B}}(\omega) = -\mathrm{i}\alpha\omega\mathcal{T}^{\dagger}\mathcal{T}, \tag{6.18}$$

where α is the (non-negative, real) Gilbert-like damping constant.

In principle, we allow the left lead, antiferromagnetic bulk and right lead to have different temperatures, respectively T^{L}, T^{B} and T^{R}. Assuming each subsystem forms a sufficiently large bath to be unaffected by coupling to the magnon distribution, we may use the fluctuation-dissipation theorem to compute the Keldysh self-energy components from their retarded counterparts:

$$\Sigma^{\mathrm{K},X}(\omega) = 2\Sigma^{X}(\omega)F^{X}(\omega); \tag{6.19}$$

$$\Sigma^{\mathrm{K},\mathrm{B}}(\omega) = 2\Sigma^{\mathrm{B}}(\omega)\mathcal{T}^{-1}F^{X}(\omega)\mathcal{T}. \tag{6.20}$$

Here, we define the statistical matrices

$$F^{X}(\omega) = \mathrm{diag}\left\{\coth\left(\frac{\omega-\mu^{X}}{2k_{\mathrm{B}}T^{X}}\right), -\coth\left(\frac{-\omega-\mu^{X}}{2k_{\mathrm{B}}T^{x}}\right)\right\}, \tag{6.21}$$

where $X \in \{\mathrm{L},\mathrm{R},\mathrm{B}\}$, $k_{\mathrm{B}}T^{X}$ is the thermal energy of component X, and we assume the absence of a magnon chemical potential, i.e. $\mu^{\mathrm{B}} = 0$.

Using the total Keldysh self-energy Σ^{K}—which is the sum of the contributions given by Eqs. (6.19) and (6.20)—we compute the lesser Green's function

$$g^{<}(\omega) = g(\omega)\Sigma^{\mathrm{K}}(\omega)g^{\dagger}(\omega) - g(\omega) + g^{\dagger}(\omega), \tag{6.22}$$

which describes the quasiparticle density and off-diagonal correlations at finite temperature.

6.2.3 Spin conductance

One of the more useful mesoscopic parameters to understand and control in the context of magnonic information processing is the spin conductance of the magnetic material in use. Setting the right-lead spin accumulation μ^{R} to zero, we define the (effective, nonlinear) total spin conductance of the left lead as

$$G^{\mathrm{L,tot}} = -\frac{\partial j_{\mathrm{s}}^{\mathrm{L,tot}}}{\partial \mu^{\mathrm{L}}}. \tag{6.23}$$

Here, $j_{\mathrm{s}}^{\mathrm{L,tot}}$ is the total spin current flowing out of the left lead, in response to a spin accumulation μ^{L} at the same lead.

Following Sterk *et al.* [2], $j_{\mathrm{s}}^{\mathrm{L,tot}}$ comprises three contributions: a tunneling contribution $j_{\mathrm{s}}^{\mathrm{L,T}}$ that describes the spin current sourced from the right lead, a bulk contribution $j_{\mathrm{s}}^{\mathrm{L,B}}$ describing spin lost to the lattice from the chain itself, and a lead-local contribution $j_{\mathrm{s}}^{\mathrm{L}}$ that may be viewed as spin 'rejected' by the interface between the lead and the chain, and ultimately dumped into the lattice. The expressions for the three contributions are identical to those found in the ferromagnetic case (see previous chapter):

$$j_{\mathrm{s}}^{\mathrm{L,T}} = -\operatorname{Re}\operatorname{Tr}\int \frac{\mathrm{d}\omega}{2\pi} g^{\dagger}(\omega)\sigma_3\Sigma^{\mathrm{L}}(\omega)g(\omega)\Sigma^{\mathrm{R}}(\omega)\left[F^{\mathrm{R}}(\omega) - F^{\mathrm{L}}(\omega)\right], \tag{6.24a}$$

$$j_{\mathrm{s}}^{\mathrm{L,B}} = -\operatorname{Re}\operatorname{Tr}\int \frac{\mathrm{d}\omega}{2\pi} g^{\dagger}(\omega)\sigma_3\Sigma^{\mathrm{L}}(\omega)g(\omega)\Sigma^{\mathrm{B}}(\omega)\left[\mathcal{T}^{-1}F^{\mathrm{B}}(\omega)\mathcal{T} - F^{\mathrm{L}}(\omega)\right], \tag{6.24b}$$

$$j_{\mathrm{s}}^{\mathrm{L}} = -\operatorname{Re}\operatorname{Tr}\int \frac{\mathrm{d}\omega}{2\pi} g^{\dagger}(\omega)\sigma_3\Sigma^{\mathrm{L}}(\omega)g(\omega)h\left[F^{\mathrm{L}}(\omega)\big|_{\mu^{\mathrm{L}}=0} - F^{\mathrm{L}}(\omega)\right]. \tag{6.24c}$$

Figures 6.3, 6.4 and 6.5 show typical nonlinear bulk, lead-local and tunneling conductances, respectively. In these plots, coupled sites have coupling constant $\eta^{X,\gamma} = 1$, while decoupled sites have $\eta^{X,\gamma} = 0$. $N = 20$ unit cells are used, the Gilbert-like damping $\alpha = 0.01$, anisotropy $K/J = 0.01$, and the magnon gap is kept constant at $\varepsilon_1^{\alpha}/J = 0.025$. All component systems are kept at the same temperature; $T^{\mathrm{L}} = T^{\mathrm{R}} = T^{\mathrm{B}} = T$. The three spin conductance contributions exhibit a strong quantitative and qualitative dependence on the configuration of the attached leads, notably becoming negative in some configurations. As one would expect, the bulk and lead-local conductances of the left lead exhibit only a weak dependence on the right lead, and we have therefore opted to only show configurations with both right-lead sites coupled in Figures 6.3 and 6.4. When the left lead is coupled only to the B-site), the bulk conductance is negative while the lead-local conductance obtains a small positive value. Conversely, when it is the A-site that is coupled, the bulk conductance is positive while the lead-local becomes negative. When both sites of the left lead are attached, both the bulk and lead-local conductances are positive, with the lead-local conductance over two orders of magnitude larger compared to the single-site cases.

The configuration of the right lead is of much greater importance to the tunneling conductance. Qualitatively, decoupling the A-site of either lead produces a negative tunneling conductance at low biases. A very notable exception is the case where the A-site of *both* leads is decoupled: here, the tunneling conductance is positive at $\mu^{\mathrm{L}} = 0$ and decreases linearly at increasing bias.

While individual conductance contributions may become negative depending on the lead configuration, their sum (shown in Figure 6.6) remains positive. The magnitude of the conductances generally increases with temperature, provided the thermal energy is significantly greater than the applied spin bias.

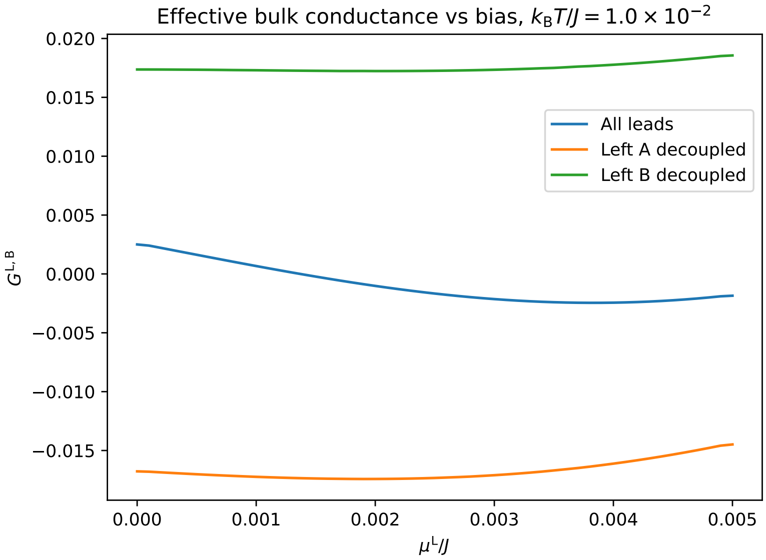

Figure 6.3: Effective nonlinear bulk spin conductance $G^{\mathrm{L,B}}$ at the left lead.

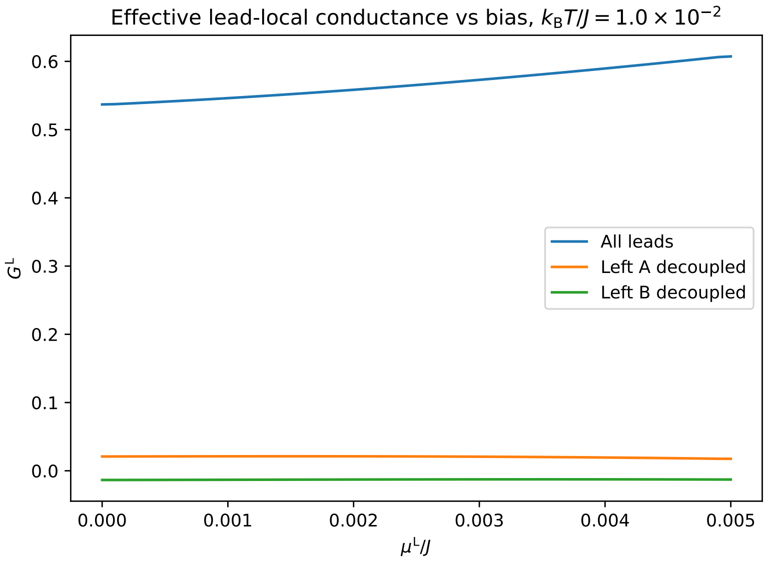

Figure 6.4: Effective nonlinear lead-local spin conductance G^{L} at the left lead.

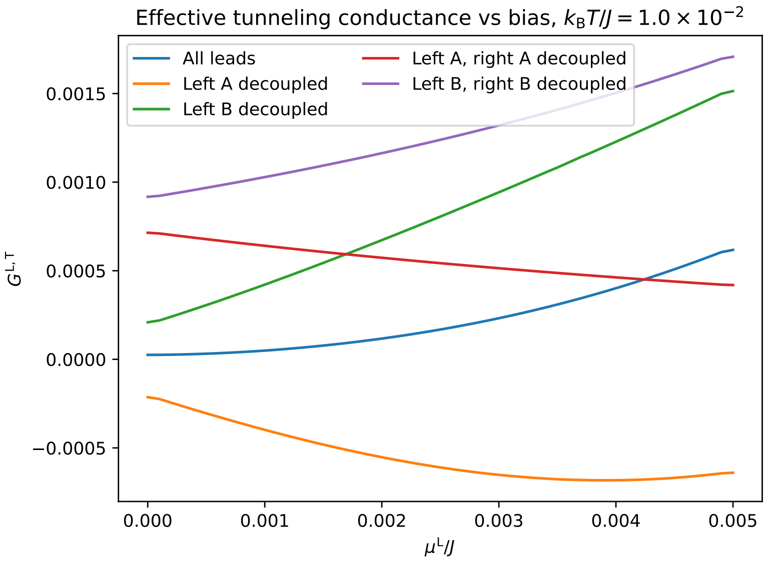

Figure 6.5: Effective nonlinear tunneling spin conductance $G^{\mathrm{L,T}}$ at the left lead.

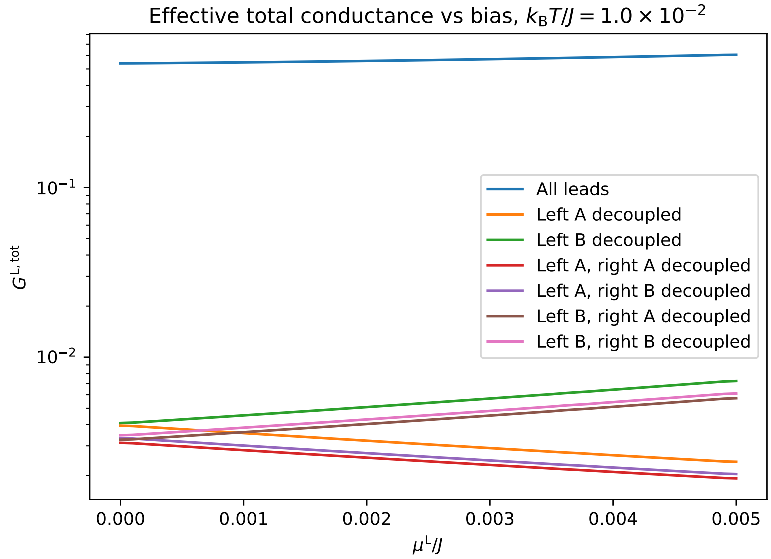

Figure 6.6: Total effective nonlinear spin conductance $G^{L,B}$ at the left lead. Note the logarithmic vertical axis. Configurations with only the right A or right B site decoupled produce curves that are identical to the all-leads configuration to within one part in 10000, and have been omitted because they are indistinguishable at this scale.

6.2.4 Correlation functions

NEGF formalism additionally allows us to gain insight into the spatial spin distribution of each sublattice. The steady-state magnon number of unit cell i (at arbitrary time) is encoded on the diagonal of the lesser Green's function:

$$\left\langle \hat{a}_i^\dagger \hat{a}_i \right\rangle = \int \frac{\mathrm{d}\omega}{2\pi} \mathrm{i} g_{ii}^<(\omega); \tag{6.25}$$

$$\left\langle \hat{b}_i^\dagger \hat{b}_i \right\rangle = \int \frac{\mathrm{d}\omega}{2\pi} \mathrm{i} g_{i+N,i+N}^<(\omega), \tag{6.26}$$

where the indices on $g^<(\omega)$ refer to entries of the full $2N \times 2N$ matrix. Similarly, off-diagonal elements of the upper left (lower right) blocks of $\mathrm{i}g^<(\omega)$ are magnon number correlations of the A (B) sublattice in different unit cells, whereas elements of the off-diagonal blocks of $\mathrm{i}g^<(\omega)$ are anomalous correlations of the forms $\left\langle \hat{a}_i^\dagger \hat{b}_j^\dagger \right\rangle$ and $\left\langle \hat{b}_i \hat{a}_j \right\rangle$.

The correlation functions $\left\langle \hat{a}_i^\dagger \hat{a}_j \right\rangle$, $\left\langle \hat{b}_i^\dagger \hat{b}_j \right\rangle = \left\langle \hat{b}_i \hat{b}_j^\dagger \right\rangle - \delta_{ij}$ and $\left\langle \hat{a}_i^\dagger \hat{b}_j^\dagger \right\rangle$ are shown

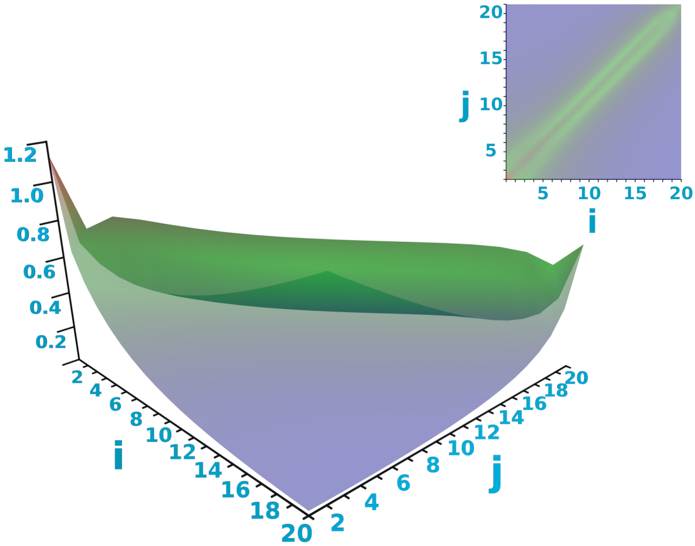

Figure 6.7: A-sublattice correlation matrix $\left\langle \hat{a}_i^\dagger \hat{a}_j \right\rangle$ at temperature $k_\mathrm{B}T/J = 0.01$, Gilbert-like damping $\alpha = 0.01$, lead couplings $\eta^{\mathrm{L},A} = \eta^{\mathrm{L},B} = \eta^{\mathrm{R},A} = \eta^{\mathrm{R},B} = 1$, anisotropy $K/J = 0.01$ and magnon gap $\varepsilon_1^\alpha = 0.025$. Inset: top-down view (heat map).

in Figures 6.7, 6.8 and 6.9, respectively, with lead coupling $\eta^{\mathrm{L},A} = \eta^{\mathrm{L},B} = \eta^{\mathrm{R},A} = \eta^{\mathrm{R},B} = 1$ and bias $\mu^\mathrm{L} = \mu^\mathrm{B} = 0$. Contrary to the 'standing wave' distribution seen in ferromagnets [2], magnons of both sublattices have a more even distribution throughout the sample, albeit with a distinct asymmetry caused by boundary conditions of the chain, i.e. the last two terms of Eq. (6.4). Despite the absence of bias, a pronounced overdensity of A-magnons and underdensity of B-magnons is present at the leads, their magnitude growing monotonically with the lead couplings $\eta^{X,\gamma}$. From a technical point of view, our NEGF framework does not impose bounds on these over- and underdensities, making it necessary to verify that the quasiparticle densities $\left\langle \hat{a}_1^\dagger \hat{a}_1 \right\rangle$, $\left\langle \hat{a}_N^\dagger \hat{a}_N \right\rangle$, $\left\langle \hat{b}_1^\dagger \hat{b}_1 \right\rangle$ and $\left\langle \hat{b}_N^\dagger \hat{b}_N \right\rangle$ stay within physically reasonable range of $[0, S]$, as required by the truncated HP transformation.

The anomalous correlation matrices closely reflect the anomalous blocks of the Hamiltonian, having maximal amplitudes both on its diagonal (corresponding to A-to-B coupling within a single unit cell) and one position displaced from the diagonal (reflecting the inter-unit-cell B-to-A coupling).

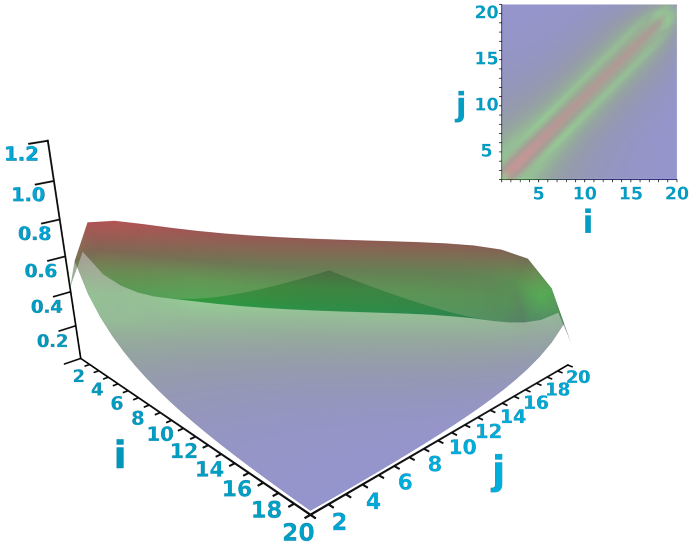

Figure 6.8: B-sublattice correlation matrix $\left\langle \hat{b}_i^\dagger \hat{b}_j \right\rangle$. For parameters, see Figure 6.7.

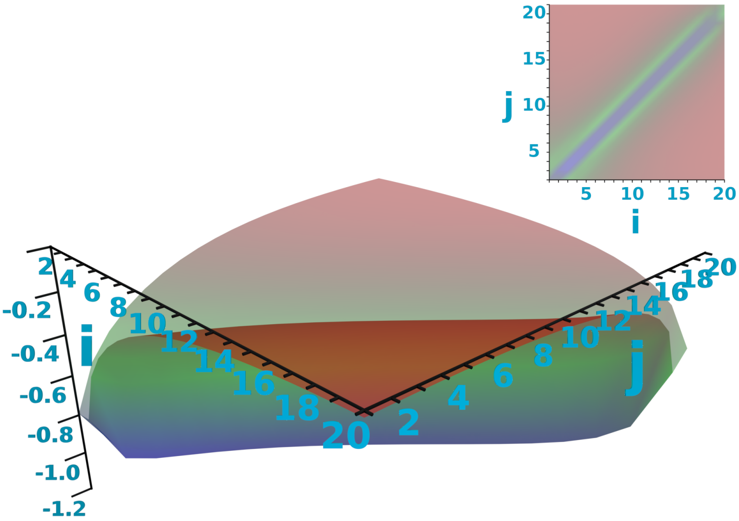

Figure 6.9: Inter-sublattice pair correlation matrix $\left\langle \hat{a}_i^\dagger \hat{b}_j^\dagger \right\rangle$. For parameters, see Figure 6.7.

6.3 Discussion, conclusions and outlook

Our results indicate that one-dimensional antiferromagnetic spin chains have the potential to act as pure spin conductors in a fashion similar to ferromagnetic insulators. Whereas ferromagnetic magnons exhibit particle-hole coupling in the presence of strong anisotropy, antiferromagnetic spin wave theory inherently yields two magnon species that are coupled at the exchange scale. In magnetic materials, the exchange energy is typically much greater than the combined anisotropy, and as a result, effects of the 'anomalous' coupling are amplified in AFMs.

Despite the mathematical similarity between AFMs and strongly anisotropic FMs, some key phenomenological differences exist. Most importantly, the spin conductance depends strongly on the configuration of the attached external leads. While the total spin conductance is always positive, individual contributions may become negative depending on the lead coupling strengths of each sublattice, as well as the applied spin bias and temperature. The exact conditions leading to negative conductance contributions appear to be highly nontrivial; for example, at $k_{\mathrm{B}}T/J = 0.01$, the tunneling conductance is negative at low bias when the A-site of either lead is decoupled, but not when *both* A-sites are decoupled. When all lead sites are attached, the bulk conductance is positive at low bias, experiences a negative local minimum, and then starts to rise again as the bias approaches the thermal energy scale. A solid *physical* explanation for this behavior has thus far eluded us.

Whereas the bulk and lead-local spin conductivities do not appear to be accessible in physical systems, nonlocal transport experiments essentially measure the tunneling conductivity directly. Our work indicates that if an uneven coupling between the leads and the individual sublattices can be engineered, such that one lead couples more strongly to the B-sublattice than to the A-sublattice, the nonlocal signal may flip its sign with respect to an evenly coupled configuration, or one in which the coupling to the A-sublattice is strongest.

It is known that antiferromagnets exhibit sublattice entanglement [114, 115], and one may therefore envision that antiferromagnetic magnonics can lead to applications in quantum information processing. The sublattice entanglement of the two magnon species may be quantified through, for example, entanglement entropy [116, 117] or concurrence [117–119]. In general, such parameters involve the computation of the reduced density matrix, obtained by tracing out the degrees of freedom of one of the sublattices. While bosonic density matrices are in principle infinite-dimensional objects, in the special case where multiparticle correlation functions factorize into products of single-particle ones—for example, the ground state of an isolated system,—the reduced density matrix of an N-site subsystem is parameterized by N real numbers, and may be obtained by diagonalization of the block of $\mathrm{i}g^<$ corresponding to the subsystem [120–123]. For that scenario, Peschel [122] provides simple expressions for the reduced density matrices of an arbitrary bipartition, and the resulting entanglement entropy. Unfortunately, as their derivation derivation relies on the applicability of Wick's theorem, these expressions break down for our system at finite temperature and/or in the presence of Gilbert-like damping or lead coupling.

Nevertheless, we believe it is possible to rederive the appropriate expressions by applying Wick's theorem on the Keldysh contour. If such expressions can be found—a feat which we humbly defer to future work—the sublattice entanglement entropy should be directly accessible using the framework outlined in this manuscript—a computation which we believe would be of significant value to the fields of quantum information science and quantum magnonics.

7 SUMMARY AND OUTLOOK

As it becomes more and more difficult to miniaturize electronic circuits, the information industry is faced with an existential crisis: soon, it will no longer be possible to significantly expand the computational power of tried-and-trusted electronic technology. It should come as no surprise that both science and industry are frantically searching for a way to avert this impending catastrophe, and (perhaps more surprisingly) are willing to entertain the notion of abandoning conventional electronics altogether if a more future-proof alternative can be found. One field of research that has this potential is spintronics: the use of intrinsic angular momentum—better known as spin—of electrons to store information.

One of the key promises of spintronics is the ability to transport digital information without the need to shuttle around electrons, thereby avoiding the adverse phenomenon of Joule heating. To this end, one may simply perturb the magnetic order of a magnetic material. Doing so generates a spin wave or *magnon*, in which spin is passed between neighboring electrons while their position remains unchanged.

In the subfield of magnonics—the study of magnons—the use of electrically insulating magnetic materials is currently being studied extensively. Novel effects are regularly predicted by theoreticians, while experimentalists continue to design new ways to verify these predictions in the laboratory. Conversely, experimentalists frequently discover discrepancies between their measurements and accepted theory, leaving the theoreticians scrambling to explain said measurements.

The path that ultimately led to Chapter 4 of this thesis is something of a hybrid. In 2015, Avci *et al.* [42] discovered an unexpected magnetoresistance signature in an experiment involving a ferromagnetic conductor in contact with a heavy metal (HM). Although the effect seemed similar to spin Hall magnetoresistance (SMR), the magnitude of the contribution changed when the direction of the current through the sample was reversed—a feature not seen in ordinary SMR—and thus, it was dubbed *unidirectional* spin Hall magnetoresistance (USMR).

Following this discovery, Zhang and Vignale [46] found a possible explanation: electronic spin accumulation caused by spin-dependent electron mobility would produce a magnetoresistance with the same asymmetry. At the same time, it has been established both experimentally and theoretically that such an electronic spin accumulation could likewise couple to a distribution of magnons in a ferromagnetic *insulator* (FI). Thus, we hypothesised that USMR may likewise be found in FI|HM bilayer systems.

In Chapter 4, we develop that hypothesis into a concrete set of predictions. A magnonic contribution USMR can exist, but may be significantly smaller in magnitude than the electronic contribution found by Avci *et al.* [42]. Importantly, in FI|HM bilayers, there is a fairly narrow range of HM layer thicknesses at which a significant USMR is produced; if the layer is too thick or too thin, the USMR drops off rapidly. We further show that USMR benefits from high temperatures, a high spin-Hall angle in the HM, and low anisotropy in the FI. Conversely, it is suppressed by a large magnon diffusion length.

Despite our prediction that any magnonic USMR present in platinum|yttrium iron garnet (Pt|YIG) bilayers would most likely be extremely small, Liu *et al.* [124] have observed USMR in exactly this system. Contrary to the predictions of our model, the signal increases with *decreasing* YIG thickness. This suggests that while our model has its merits—such as the experimentally supported prediction that magnonic USMR vanishes at low temperatures—it is perhaps overly simplistic. Extensions such as nonuniform equilibrium magnetization, coupled heat and spin transport, or forgoing the linearization of the interfacial spin current may yield more realistic results.

Whereas magnetoresistive effects such as USMR are by definition in the domain of hybrid spintronic/electronic systems, in Chapter 5, we explore a purely spintronic effect: the ballistic transport of elliptically polarized magnons through a ferromagnetic insulator. Here, we assume a strongly anisotropic one-dimensional FI is contacted on both sides by a metallic lead, each of which has a given spin accumulation. The leads inject well-defined packets of spin in the form of circular magnons, which are superpositions of the elliptical magnon states native to the anisotropic FI, thus breaking the conservation of spin.

To study the transport properties of an elliptical-magnon channel, we develop a discrete, real-space non-equilibrium Green's function (NEGF) formalism, incorporating the lead coupling and bulk damping directly at the self-energy level. While the leads couple to the circular magnon operators, we assume the bulk damping instead acts on the elliptical magnon number. Expressed in the basis of elliptical operators, this bulk damping is mathematically identical to the standard form of Gilbert damping, however, as it does not act on the classical magnetization in a trivial way, we refer to it as 'Gilbert-like damping'.

When a weak spin accumulation is applied to one of the leads, the system acts as a spin resistor network, with a ‘tunneling’ resistor between neighboring sites, and ‘bulk’ resistors that siphon spin to ‘ground’ (i.e. the crystal lattice). Although the individual spin resistances are not trivially accessible, the network may be simplified using the $\Delta - Y$ transform [98], leading to system-scale effective resistances. To avoid divergent behavior, we instead compute the corresponding conductances, and find three terms: a ‘tunneling’ term describing the conductance between the left and right leads, a ‘bulk’ term describing the effective ‘pull-down’ conductance to ground, and a novel term corresponding to a parasitic conductance connecting the sites at which the leads are attached to ground.

All three conductances increase monotonically with temperature, and are asymptotically linear. The lead-local term vanishes when anisotropy is absent, but becomes the dominant term at high anisotropy, indicating most spin injected at the leads is lost immediately. Although the tunneling conductance smoothly settles into the linear-in-temperature regime, the bulk and lead-local conductance exhibit a fairly sharp kink, which is directly related to the magnon gap: at low temperatures, not enough thermal energy is present to excite a significant number of magnons.

The ellipticity of magnons further leads to squeezing: the quantum uncertainty of the spin operator itself becomes elliptical. In particular, while the Robertson uncertainty principle [96] dictates that in the circular case, the spin uncertainty along any axis must be greater than $\frac{1}{\sqrt{2}}$, squeezing allows the uncertainty along the semiminor axis of the ellipse to be smaller than this, as long as long as the product of the uncertainty along any two orthogonal axis is greater than $\frac{1}{2}$. This feature may find applications in quantum information science, in particular in reducing shot noise. Although magnon squeezing becomes significant in a strongly anisotropic ferromagnet, our results show that it may globally be decreased by applying a local spin accumulation at one of the leads.

Modifying the NEGF framework to treat antiferromagnets is mathematically simple, and even yields identical expressions for the spin conductances found in elliptical ferromagnets. However, the two-sublattice nature of antiferromagnetic spin chains and the exchange-scale coupling between the resulting magnon bands leads to significantly different phenomenology. For example, magnons distribute more evenly through an antiferromagnetic spin chain than through a ferromagnetic one. Furthermore, by imposing different coupling strengths between the leads and the A and B sublattices, substantial changes in the spin conductances can be realized.

The work on discrete non-equilibrium Green’s function formalism for magnonics presented in this thesis provides many avenues that currently remain unexplored. Incorporating magnon-magnon interactions may be of particular interest, as our results show that significant magnon densities may be reached even at fairly low temperatures. Inclusion of inhomogeneity in parameters such as magnetic field, Gilbert-like damping or anisotropy may improve the realism of the modelled systems, and would be simple to implement. Another subject worthy of study using this formalism is the interaction between magnons and domain walls. In all of these cases, extension to two or three dimensions may significantly affect the resulting scattering processes.

In the long-term future, a thorough understanding of the behavior of magnons—including transport, but also their interaction with e.g. spin textures such as skyrmions—may lead to pure-spintronic devices featuring low dissipation and extremely high operating frequencies. This, in turn, may revitalize advancement of computer hardware after the expected breakdown of Moore's law.

8 SAMENVATTING EN VOORUITBLIK

Naarmate het moeilijker en moeilijker wordt om elektronische circuits te verkleinen, wacht de informatieindustrie een existentiële crisis: binnenkort zal het onmogelijk worden om de rekenkracht van computers significant te vergroten door middel van bekende en vertrouwde elektronische technologie. Het mag dan ook geen verrassing zijn dat zowel de wetenschap als de industrie met milde paniek op zoek zijn naar manieren om deze dreigende catastrofe af te wenden, en daarbij (wellicht verrassender) zelfs met het idee durven spelen om de conventionele elektronica geheel af te danken, mits er een toekomstbestendiger alternatief gevonden kan worden. Eén onderzoeksgebied dat hier wellicht aan voldoet is de spintronica: het gebruik van intrinsiek impulsmoment—beter bekend als spin—van elektronen om informatie op te slaan.

Eén van de meest veelbelovende eigenschappen van spintronica is de mogelijkheid om digitale informatie te verplaatsen zonder daarbij elektronen heen en weer te sturen, waardoor het ongewenste fenomeen van Ohmse verwarming vermeden wordt. Om dit te bereiken, hoeft men slechts de magnetische orde van een magnetisch materiaal in beroering te brengen. Dit veroorzaakt een spingolf of *magnon*, waarbij spin tussen aanliggende elektronen wordt doorgegeven, zonder dat hun positie verandert.

In het deelgebied van magnonica—het onderzoeken van magnonen—wordt het gebruik van elektrisch isolerende magnetische materialen momenteel uitvoerig onderzocht. Met regelmaat worden nieuwe effecten voorspeld door de theoretici, terwijl de experimentatoren telkens nieuwe manieren zoeken om deze voorspellingen in het laboratorium te bevestigen. Anderzijds stuiten experimentalisten ook regelmatig op tegenstrijdigheden tussen hun metingen en de gevestigde theorie, waardoor theoretici weer op zoek moeten naar verklaringen voor die metingen.

De weg uiteindelijk naar Hoofdstuk 4 van deze scriptie heeft geleid is een mengelmoes van deze routes. In 2015 ontdekten Avci *et al.* [42] kenmerken van een onverwachte magnetoweerstand in een experiment waarin een ferromagnetische geleider in contact stond met een zwaar metaal (ZM). Hoewel het effect leek op spin-Hallmagnetoresistentie (SMR), veranderde de grootte van de bijdrage als de richting van de stroom door het testobject omgekeerd werd—iets dat niet bij gewone SMR voorkomt—en dus werd het *unidirectionele* spin-Hall magnetoweerstand (USMR) genoemd.

Na deze ontdekking kwamen Zhang and Vignale [46] met een mogelijke verklaring: opeenhoping van elektronische spin door spinafhankelijke elektronmobiliteit zou een magnetoresistentie met dezelfde asymmetrie produceren. Tegelijkertijd was ook zowel experimenteel als theoretisch vastgesteld dat een dergelijke elektronische spinopeenhoping kan koppelen aan een magnondistributie in een ferromagnetische *isolator* (FI). Hierdoor kwamen wij met de hypothese dat men wellicht ook USMR zou kunnen vinden in tweelaagse FI|ZM-systemen.

In Hoofdstuk 4 werken we die hypothese uit tot een verzameling concrete voorspellingen. Een magnonische bijdrage aan USMR kan bestaan, maar is mogelijk veel kleiner dan de elektronische bijdrage van Avci *et al.* [42]. Voornamelijk moet in FI|ZM-bilagen de dikte van de ZM-laag binnen een vrij klein bereik liggen om significante USMR te produceren; als de laag te dik of te dun is, neemt de USMR snel af. Verder laten we zien dat hoge temperature, grote spin-Hallhoek in de ZM-laag, en lage anisotropie in de FI-laag een positieve invloed op de USMR hebben. Daarentegen is een grote magnondiffusielengte juist een verkleinende factor.

Ondanks onze voorspelling dat magnonische USMR in platina|yttrium-ijzergranaat (Pt|YIG) bilagen waarschijnlijk extreem klein is, hebben Liu *et al.* [124] precies in dit systeem USMR waargenomen. In tegenstelling tot de voorspellingen van ons model, blijkt het signaal sterker te worden bij *lagere* YIG-diktes. Hoewel ons model zeker nut heeft—bijvoorbeeld in de experimenteel ondersteunde voorspelling dat magnonische USMR bij lage temperaturen verdwijnt—suggereert dit dat het wellicht te eenvoudig is. Uitbreidingen zoals niet-uniforme magnetisatie in evenwicht, gekoppeld warmte- en spintransport, of het niet lineariseren van de spinstroom door de interface tussen lagen kunnen wellicht realistischere resultaten leveren.

Waar magnetoresistentie-effecten zoals USMR per definitie in het domein van hybride spintronisch/elektronische systemen liggen, richten we ons in Hoofdstuk 5 op een puur spintronisch effect: het ballistische transport van elliptisch gepolariseerde magnonen door een ferromagnetische isolator. Hierbij gaan we uit van een sterk anisotrope, eendimensionale FI, die aan beide kanten met een metalen contact verbonden is, waarbij de contacten beiden hun eigen spinaccumulatie hebben. Door deze contacten worden goedgedefinieerde pakketjes spin geïnjecteerd, in de vorm van circulaire magnonen. Deze bestaan uit superposities van de elliptische magnontoestanden in de anisotrope FI, waardoor spinbehoud gebroken wordt.

Om de transporteigenschappen van een kanaal voor elliptische magnonen te bestuderen, ontwikkelen we een discreet non-equilibrium Greense functieformalisme (NEGF formalisme) in reële ruimte, waarbij we de koppeling aan de contacten en demping in de bulk direct op het niveau van zelfenergie meenemen. Hoewel de contacten koppelen aan de circulaire magnonoperatoren, nemen we aan dat de bulkdemping op het elliptische magnongetal werkt. Als men deze bulkdemping uitdrukt in de basis van elliptische operatoren, is de vorm wiskundig identiek aan de standaardvorm van Gilbertdemping, maar omdat deze niet op een triviale manier uitwerking heeft op de klassieke magnetisatie, kiezen we voor de term 'Gilbert-achtige demping'.

Wanneer op één van de contacten een kleine spinaccumulatie geplaatst wordt, gedraagt het systeem zich als een netwerk van spinweerstanden, met een 'tunnelingweerstand' tussen aanliggende spinposities, en 'bulkweerstanden' die spin naar de 'aarde' afvoeren (d.w.z. het kristalrooster). Hoewel de individuele spinweerstanden niet op een triviale manier te beschrijven zijn, kan het netwerk vereenvoudigd worden door middel van de $\Delta - Y$transformatie [98], waaruit effectieve weerstanden op systeemschaal volgen. Om divergent gedrag te voorkomen, berekenen i.p.v. weerstanden de spingeleidingen, en vinden daarbij drie termen: een 'tunnelingterm' die de geleiding tussen de linker- en rechtercontacten beschrijft, een 'bulkterm' die de 'pull-downgeleiding' naar de aarde beschrijft, en en nieuwe term die overeenkomt met een parasitische geleiding die de spinposities van de contacten met de aarde verbindt.

Alle drie geleidingen zijn strikt stijgend met temperatuur, en zijn asymptotisch lineair. De contact-lokale term verdwijnt als anisotropie afwezig is, maar wordt dominant bij hoge anisotropie, wat aangeeft dat de meeste spin die door een contact geïnjecteerd wordt, meteen verdwijnt. Hoewel de tunnelinggeleiding geleidelijk naar het lineaire regime in temperatuur overgaat, tonen de bulk- en contact-lokale geleidingen een vrij scherpe knik, die direct voortvloeit uit de magnonkloof: bij lage temperaturen is er niet genoeg thermische energie aanwezig om een significant aantal magnonen aan te slaan.

Verder veroorzaakt de ellipticiteit van magnonen 'squeezing': de kwantumonzekerheid van de spinoperator zelf wordt elliptisch. Daar het onzekerheidsprincipe van Robertson [96] stelt dat de onzekerheid langs elke as in het *circulaire* geval groter moet zijn dan $\frac{1}{\sqrt{2}}$, maakt squeezing het mogelijk om langs de korte as van de ellips een kleinere onzekerheid te hebben, zolang het product van de onzekerheid langs elke twee orthogonale assen maar groter is dan $\frac{1}{2}$. Dit fenomeen heeft mogelijk toepassingen in de kwantuminformatiekunde, met name in het verminderen van hagelruis. Hoewel magnonsqueezing significant wordt in sterk anisotrope ferromagneten, laten onze resultaten zien dat het mogelijk is om de squeezing globaal te verminderen door op één van de contacten lokaal een spinaccumulatie aan te brengen.

Wiskundig gezien is het eenvoudig om het NEGF-framework aan te passen voor antiferromagneten; dit geeft zelfs identieke uitdrukkingen voor de spingeleidingen. Daarentegen zorgen de twee subroosters van antiferrmagnetische spinketens, alsook de koppeling tussen de resulterende magnonbanden op de schaal van de uitwisselingsenergie, voor beduidend andere fenomenologie. Zo verspreiden magnonen zich veel regelmatiger over een antiferromagnetische keten dan een ferromagnetische. Verder kan men door verschillende koppelingssterktes tussen de externe draden en de A- en B-subroosters op te leggen, grote verschillen in de spingeleidingen teweegbrengen.

In het raamwerk voor discreet non-equilibrium Greense functieformalisme dat in deze scriptie voorgelegd wordt, zijn nog veel onverkende paden aanwezig. Daarbij kan het met name interessant zijn om magnon-magnoninteracties mee te nemen, gezien onze resultaten aantonen dat zelfs bij vrij lage temperaturen al grote magnondichtheden bereikt kunnen worden. Het toevoegen van inhomogeniteiten in paramteres zoals het magneetveld, de Gilbert-achtige demping of de anisotropie kunnen het model wellicht realistischer maken, en zijn niet moeilijk om te implementeren. Een ander onderwerp dat het bestuderen met dit formalisme waard is, is de interactie tussen magnonen en domeinmuren. In al deze gevallen kan een uitbreiding naar twee of drie dimensies grote gevolgen hebben voor de resulterende verstrooiingsprocessen.

Op lange termijn kan een grondig begrip van magnonen—zowel magnontransport en bijvoorbeeld de interactie tussen magnonen en spintexturen zoals skyrmionen—leiden tot de ontwikkeling van puur-spintronische apparaten met lage dissipatie en extreem hoge klokfrequenties. Op zijn beurt zou dit de vooruitgang van computerhardware nieuw leven in kunnen blazen na de verwachte val van de Wet van Moore.

ACKNOWLEDGEMENTS

First and foremost I wish to thank my mother, who passed away on 23 January 2021, mere days from her 68th birthday. Without her by my side I would not have made it this far, and it is with her memory by my side that I know I can go on. Mum, thank you for everything, and with this thesis, I fulfil my promise.

I want to thank Rembert for being an amazing supervisor, and for giving me the opportunity to take the wonderful journey that my PhD has been. Rembert, you always had my back and gave me all the guidance I needed; it was a great pleasure working with you, and with the others in your group. Most of all, thank you for helping me through this difficult final year, for being someone I could always confide in, for being a friend and mentor instead of a boss.

Andreas, Huaiyang and Akash, thank you for the great collaborations. Scott and Jiansen, thank you for helping me along when I was still very green behind the gills. And of course, Scott, Jiansen, Andreas, Etienne, Camilo, Dion, Ruben, Huaiyang, Tim, Joren, Pieter, Valentina, Ivan, Lukasz, and all the Master and Bachelor students: thanks for all the fun group meetings, and for being great coworkers!

Kaveh, if it hadn't been for my bachelor project with you and Jan, I might never have heard of spintronics, so thank you for putting me on this path, and also for helping me with my CV, and of course for the fun project.

And finally, thanks to all the wonderful friends I made back at Leiden University: Anne, Bas, Dieuwertje, Fré, Hiddo, Irene, Isabel, Koen, Marlize, Marten, Matthijs, Remko and Thomas. As I write this, I've known you for almost a decade, and what a decade it has been! From carrying each other through gruelling homework sessions, to amazing summer holidays and hilarious game nights, there's never been a lack of fun. It's safe to say you were what kept me going when I was about to crack under the pressure, and you are the ones who picked me up when the world shattered beneath my feet.

CURRICULUM VITÆ

Peter Sterk is geboren op 26 februari 1990 te Goes. Op 6 juli 2012 heeft hij het Voorbereidend Wetenschappelijk Onderwijs afgerond door middel van Staatsexamen. Vervolgens begon hij aan de Universiteit Leiden met de opleiding Natuurkunde, waarbij hij de Bachelor afsloot met de scriptie getiteld MAGNETISATION CHARACTERISTICS OF NONCOLLINEAR FERROMAGNETIC BILAYERS, na onderzoek te hebben gedaan in de groep van prof. dr. Jan Aarts. In de Master specialiseerde hij zich in de richting Theoretical Physics en verkoos hij een breed vakkenpakket, waarin gecondenseerde materie, kosmologie en hoge-energiefysica allen vertegenwoordigd waren. In het collegejaar 2016-2017 voegde hij zich bij de groep van prof. dr. Koenraad Schalm, en gebruikte hij numerieke methoden om onderzoek te doen naar de vorming van geladen zwarte gaten in anti-De Sitterruimte. Op 31 augustus 2017 rondde hij deze Masteropleiding af met de scriptie FORMATION OF BLACK BRANES WITH $U(1)$ SCALAR HAIR. Hierna werd hij aangenomen tot promovendus onder de begeleiding van prof. dr. Rembert Duine aan de Universiteit Utrecht, en schakelde daarbij terug naar het onderwerp Spintronica, waarmee hij tijdens zijn Bacheloronderzoek kennis had gemaakt. Daarvan is dit proefschrift het gevolg.

BIBLIOGRAPHY

[1] W. P. Sterk, D. Peerlings, and R. A. Duine. Magnon contribution to unidirectional spin hall magnetoresistance in ferromagnetic-insulator/heavy-metal bilayers. *Phys. Rev. B*, 99:064438, Feb 2019. doi:10.1103/PhysRevB.99.064438.

[2] W. P. Sterk, H. Y. Yuan, Andreas Rückriegel, Babak Zare Rameshti, and R. A. Duine. Green's function formalism for nonlocal elliptical magnon transport. *Phys. Rev. B*, 104:174404, Nov 2021. doi:10.1103/PhysRevB.104.174404.

[3] H. Y. Yuan, W. P. Sterk, Akashdeep Kamra, and Rembert A. Duine. Pure dephasing of magnonic quantum states. *Phys. Rev. B*, 106:L100403, Sep 2022. doi:10.1103/PhysRevB.106.L100403.

[4] H. Y. Yuan, W. P. Sterk, Akashdeep Kamra, and Rembert A. Duine. Master equation approach to magnon relaxation and dephasing. *arXiv e-prints*, art. arXiv:2209.02961, September 2022. doi:10.48550/arXiv.2209.02961.

[5] Julius Edgar Lilienfeld. Method and apparatus for controlling electric currents, January 28 1930. US Patent 1,745,175.

[6] J. Bardeen and W. H. Brattain. The Transistor, A Semi-Conductor Triode. *Physical Review*, 74(2):230–231, July 1948. doi:10.1103/PhysRev.74.230.

[7] Cornelis Disco. *Getting new technologies together : studies in making sociotechnical order*. Walter de Gruyter, Berlin New York, 1998. ISBN 978-3-11-015630-0.

[8] David C Brock, editor. *Understanding Moore's Law: Four Decades of Innovation*. Chemical Heritage Foundation, Philadelphia, PA, May 2006. ISBN 0941901416.

[9] Atsufumi Hirohata, Keisuke Yamada, Yoshinobu Nakatani, Ioan-Lucian Prejbeanu, Bernard Diény, Philipp Pirro, and Burkard Hillebrands. Review on spintronics: Principles and device applications. *Journal of Magnetism and Magnetic Materials*, 509:166711, September 2020. doi:10.1016/j.jmmm.2020.166711.

[10] L. Bruno Chandrasekar, K. Gnanasekar, and M. Karunakaran. Spintronics – a mini review. *Superlattices and Microstructures*, 136:106322, 2019. ISSN 0749-6036. doi:10.1016/j.spmi.2019.106322.

[11] Can Onur Avci. Picosecond switching in a ferromagnet. *Nature Electronics*, 3(11):660–661, 2020. doi:10.1038/s41928-020-00502-8.

[12] Kaushalya Jhuria, Julius Hohlfeld, Akshay Pattabi, Elodie Martin, Aldo Ygnacio Arriola Córdova, Xinping Shi, Roberto Lo Conte, Sébastien Petit-Watelot, Juan Carlos Rojas-Sanchez, Grégory Malinowski, *et al.* Spin–orbit torque switching of a ferromagnet with picosecond electrical pulses. *Nature Electronics*, 3(11):680–686, 2020. doi:10.1038/s41928-020-00488-3.

[13] Atsushi Ono and Sumio Ishihara. Ultrafast reorientation of the Néel vector in antiferromagnetic Dirac semimetals. *npj Computational Mathematics*, 7:171, January 2021. doi:10.1038/s41524-021-00641-2.

[14] J. M. D. Coey. *Magnetism and magnetic materials.* Cambridge University Press, Cambridge New York, 2009. ISBN 978-0-511-67743-4.

[15] S. V. Vonsovskiĭ. *Ferromagnetic resonance the phenomenon of resonant absorption of a high-frequency magnetic field in ferromagnetic substances.* Pergamon Press, Oxford,New York, 1966. ISBN 9781483151489.

[16] L. J. Cornelissen, J. Liu, R. A. Duine, J. Ben Youssef, and B. J. van Wees. Long-distance transport of magnon spin information in a magnetic insulator at room temperature. *Nature Physics*, 11(12):1022–1026, December 2015. doi:10.1038/nphys3465.

[17] Matthias B. Jungfleisch, Wei Zhang, and Axel Hoffmann. Perspectives of antiferromagnetic spintronics. *Physics Letters A*, 382(13):865–871, April 2018. doi:10.1016/j.physleta.2018.01.008.

[18] Vladimir Cherepanov, Igor Kolokolov, and Victor L'vov. The saga of YIG: Spectra, thermodynamics, interaction and relaxation of magnons in a complex magnet. *Physics Reports*, 229(3):81–144, July 1993. doi:10.1016/0370-1573(93)90107-O.

[19] Gesche Nahrwold, Jan M. Scholtyssek, Sandra Motl-Ziegler, Ole Albrecht, Ulrich Merkt, and Guido Meier. Structural, magnetic, and transport properties of Permalloy for spintronic experiments. *Journal of Applied Physics*, 108(1):013907-013907-6, July 2010. doi:10.1063/1.3431384.

[20] Min Zhang and Chaoyong Deng. Magnetic, optical and electrical properties of permalloy films by dc magnetron sputtering. *Journal of Materials Science: Materials in Electronics*, 32:1–12, 02 2021. doi:10.1007/s10854-020-05234-1.

[21] Guo-Xing Miao and Arunava Gupta. *Growth and Properties of Epitaxial Chromium Dioxide (CrO2) Thin Films and Heterostructures*, pages 511–536. Springer US, Boston, MA, 2009. ISBN 978-0-387-85600-1. doi:10.1007/978-0-387-85600-1_17.

[22] Nguyen D. Dung, Yuuki Ota, Kiyohiro Sugiyama, Tatsuma D. Matsuda, Yoshinori Haga, Koichi Kindo, Masayuki Hagiwara, Tetsuya Takeuchi, Rikio Settai, and Yoshichika Ōnuki. Magnetic Properties of Single Crystalline RCu_2Si_2 (R: Rare Earth). *Journal of the Physical Society of Japan*, 78(2):024712, February 2009. doi:10.1143/JPSJ.78.024712.

[23] Neil W. Ashcroft and N. David Mermin. *Solid state physics.* Holt, Rinehart and Winston, New York, 1976. ISBN 978-0030839931.

[24] Wolfgang Nolting and Anupuru Ramakanth. *Quantum Theory of Magnetism.* 2009. ISBN 978-3-540-85416-6. doi:10.1007/978-3-540-85416-6.

[25] N. D. Mermin and H. Wagner. Absence of Ferromagnetism or Antiferromagnetism in One- or Two-Dimensional Isotropic Heisenberg Models. *Physical Review Letters*, 17(22):1133–1136, November 1966. doi:10.1103/PhysRevLett.17.1133.

[26] T. Holstein and H. Primakoff. Field Dependence of the Intrinsic Domain Magnetization of a Ferromagnet. *Physical Review*, 58:1098–1113, December 1940. doi:10.1103/PhysRev.58.1098.

[27] Aleksandr Il'ich Akhiezer, Viktor Grigor'evich Bar'yakhtar, and Sergei Vladimirovich Peletminskii. Spin waves. 1968.

[28] J. Stein. Flow equations and extended Bogoliubov transformation for the Heisenberg antiferromagnet near the classical limit. *European Physical Journal B*, 5(2):193–201, September 1998. doi:10.1007/s100510050434.

[29] The Nobel Committee for Physics. Scientific background on the Nobel Prize in Physics 2021. Royal Swedish Academy of Sciences, October 2021. URL `https://www.nobelprize.org/prizes/physics/2021/summary/`.

[30] J. H. P. Colpa. Diagonalization of the quadratic boson hamiltonian. *Physica A Statistical Mechanics and its Applications*, 93:327–353, September 1978. doi:10.1016/0378-4371(78)90160-7.

[31] Henrik Bruus and Karsten Flensberg. *Many-body quantum theory in condensed matter physics: an introduction.* Oxford University Press, 2004. ISBN 978-0198566335.

[32] Jairo Sinova, Sergio O. Valenzuela, J. Wunderlich, C. H. Back, and T. Jungwirth. Spin Hall effects. *Reviews of Modern Physics*, 87(4):1213–1260, October 2015. doi:10.1103/RevModPhys.87.1213.

[33] N. F. Mott. The Scattering of Fast Electrons by Atomic Nuclei. *Proceedings of the Royal Society of London Series A*, 124(794):425–442, June 1929. doi:10.1098/rspa.1929.0127.

[34] T. J. Gay and F. B. Dunning. Mott electron polarimetry. *Review of Scientific Instruments*, 63(2):1635–1651, February 1992. doi:10.1063/1.1143371.

[35] Michel I. Dyakonov. *Spin Physics in Semiconductors*, volume 157. Springer, 2008. ISBN 978-3-540-78820-1. doi:10.1007/978-3-540-78820-1.

[36] Motoi Kimata, Hua Chen, Kouta Kondou, Satoshi Sugimoto, Prasanta K. Muduli, Muhammad Ikhlas, Yasutomo Omori, Takahiro Tomita, Allan. H. MacDonald, Satoru Nakatsuji, and Yoshichika Otani. Magnetic and magnetic inverse spin Hall effects in a non-collinear antiferromagnet. *Nature*, 565(7741):627–630, January 2019. doi:10.1038/s41586-018-0853-0.

[37] T. Nan, C. X. Quintela, J. Irwin, G. Gurung, D. F. Shao, J. Gibbons, N. Campbell, K. Song, S. Y. Choi, L. Guo, R. D. Johnson, P. Manuel, R. V. Chopdekar, I. Hallsteinsen, T. Tybell, P. J. Ryan, J. W. Kim, Y. Choi, P. G. Radaelli, D. C. Ralph, E. Y. Tsymbal, M. S. Rzchowski, and C. B. Eom. Controlling spin current polarization through non-collinear antiferromagnetism. *Nature Communications*, 11:4671, September 2020. doi:10.1038/s41467-020-17999-4.

[38] Xianzhe Chen, Shuyuan Shi, Guoyi Shi, Xiaolong Fan, Cheng Song, Xiaofeng Zhou, Hua Bai, Liyang Liao, Yongjian Zhou, Hanwen Zhang, Ang

Li, Yanhui Chen, Xiaodong Han, Shan Jiang, Zengwei Zhu, Huaqiang Wu, Xiangrong Wang, Desheng Xue, Hyunsoo Yang, and Feng Pan. Observation of the antiferromagnetic spin Hall effect. *Nature Materials*, 20(6): 800–804, January 2021. doi:10.1038/s41563-021-00946-z.

[39] T. McGuire and R. Potter. Anisotropic magnetoresistance in ferromagnetic 3d alloys. *IEEE Transactions on Magnetics*, 11:1018–1038, July 1975. doi:10.1109/TMAG.1975.1058782.

[40] G. Binasch, P. Grünberg, F. Saurenbach, and W. Zinn. Enhanced magnetoresistance in layered magnetic structures with antiferromagnetic interlayer exchange. *Physical Review B*, 39:4828–4830, March 1989. doi:10.1103/PhysRevB.39.4828.

[41] Y.-T. Chen, S. Takahashi, H. Nakayama, M. Althammer, S. T. B. Goennenwein, E. Saitoh, and G. E. W. Bauer. Theory of spin Hall magnetoresistance. *Physical Review B*, 87(14):144411, April 2013. doi:10.1103/PhysRevB.87.144411.

[42] C. O. Avci, K. Garello, A. Ghosh, M. Gabureac, S. F. Alvarado, and P. Gambardella. Unidirectional spin Hall magnetoresistance in ferromagnet/normal metal bilayers. *Nature Physics*, 11:570–575, July 2015. doi:10.1038/nphys3356.

[43] K. Yasuda, A. Tsukazaki, R. Yoshimi, K. S. Takahashi, M. Kawasaki, and Y. Tokura. Large Unidirectional Magnetoresistance in a Magnetic Topological Insulator. *Physical Review Letters*, 117(12):127202, September 2016. doi:10.1103/PhysRevLett.117.127202.

[44] Y. Yin, D.-S. Han, M. C. H. de Jong, R. Lavrijsen, R. A. Duine, H. J. M. Swagten, and B. Koopmans. Thickness dependence of unidirectional spin-Hall magnetoresistance in metallic bilayers. *Applied Physics Letters*, 111 (23):232405, December 2017. doi:10.1063/1.5003725.

[45] C. O. Avci, M. Mann, A. J. Tan, P. Gambardella, and G. S. D. Beach. A multi-state memory device based on the unidirectional spin Hall magnetoresistance. *Applied Physics Letters*, 110(20):203506, May 2017. doi:10.1063/1.4983784.

[46] S. S.-L. Zhang and G. Vignale. Theory of unidirectional spin Hall magnetoresistance in heavy-metal/ferromagnetic-metal bilayers. *Physical Review B*, 94(14):140411, October 2016. doi:10.1103/PhysRevB.94.140411.

[47] K. J. Kim, T. Moriyama, T. Koyama, D. Chiba, S. W. Lee, S. J. Lee, K. J. Lee, H. W. Lee, and T. Ono. Current-induced asymmetric magnetoresistance due to energy transfer via quantum spin-flip process. *ArXiv e-prints*, March 2016.

[48] C. O. Avci, J. Mendil, G. S. D. Beach, and P. Gambardella. Origins of the Unidirectional Spin Hall Magnetoresistance in Metallic Bilayers. *Physical Review Letters*, 121(8):087207, August 2018. doi:10.1103/PhysRevLett.121.087207.

[49] E. M. Chudnovsky. Theory of Spin Hall Effect: Extension of the Drude Model. *Physical Review Letters*, 99(20):206601, November 2007. doi:10.1103/PhysRevLett.99.206601.

[50] W. Zhang, W. Han, X. Jiang, S.-H. Yang, and S. S. P. Parkin. Role of transparency of platinum-ferromagnet interfaces in determining the intrinsic magnitude of the spin Hall effect. *Nature Physics*, 11:496–502, June 2015. doi:10.1038/nphys3304.

[51] S. A. Bender and Y. Tserkovnyak. Interfacial spin and heat transfer between metals and magnetic insulators. *Physical Review B*, 91(14):140402, April 2015. doi:10.1103/PhysRevB.91.140402.

[52] Y. Tserkovnyak, A. Brataas, and G. E. Bauer. Enhanced Gilbert Damping in Thin Ferromagnetic Films. *Physical Review Letters*, 88(11):117601, March 2002. doi:10.1103/PhysRevLett.88.117601.

[53] Scott A. Bender, Rembert A. Duine, and Yaroslav Tserkovnyak. Electronic Pumping of Quasiequilibrium Bose-Einstein-Condensed Magnons. *Physical Review Letters*, 108(24):246601, June 2012. doi:10.1103/PhysRevLett.108.246601.

[54] S. Takahashi, E. Saitoh, and S. Maekawa. Spin current through a normal-metal/insulating-ferromagnet junction. In *Journal of Physics Conference Series*, volume 200 of *Journal of Physics Conference Series*, page 062030. IOP Publishing, January 2010. doi:10.1088/1742-6596/200/6/062030.

[55] S. S.-L. Zhang and S. Zhang. Spin convertance at magnetic interfaces. *Physical Review B*, 86(21):214424, December 2012. doi:10.1103/PhysRevB.86.214424.

[56] C. Tang, M. Aldosary, Z. Jiang, H. Chang, B. Madon, K. Chan, M. Wu, J. E. Garay, and J. Shi. Exquisite growth control and magnetic properties

of yttrium iron garnet thin films. *Applied Physics Letters*, 108(10):102403, March 2016. doi:10.1063/1.4943210.

[57] L. J. Cornelissen, K. J. H. Peters, G. E. W. Bauer, R. A. Duine, and B. J. van Wees. Magnon spin transport driven by the magnon chemical potential in a magnetic insulator. *Physical Review B*, 94(1):014412, July 2016. doi:10.1103/PhysRevB.94.014412.

[58] S. S.-L. Zhang and S. Zhang. Magnon Mediated Electric Current Drag Across a Ferromagnetic Insulator Layer. *Physical Review Letters*, 109(9): 096603, August 2012. doi:10.1103/PhysRevLett.109.096603.

[59] C. O. Avci, K. Garello, J. Mendil, A. Ghosh, N. Blasakis, M. Gabureac, M. Trassin, M. Fiebig, and P. Gambardella. Magnetoresistance of heavy and light metal/ferromagnet bilayers. *Applied Physics Letters*, 107(19): 192405, November 2015. doi:10.1063/1.4935497.

[60] M. Schreier, A. Kamra, M. Weiler, J. Xiao, G. E. W. Bauer, R. Gross, and S. T. B. Goennenwein. Magnon, phonon, and electron temperature profiles and the spin Seebeck effect in magnetic insulator/normal metal hybrid structures. *Physical Review B*, 88(9):094410, September 2013. doi:10.1103/PhysRevB.88.094410.

[61] M. G. Pini, P. Politi, and R. L. Stamps. Anisotropy effects on the magnetic excitations of a ferromagnetic monolayer below and above the Curie temperature. *Physical Review B*, 72(1):014454, July 2005. doi:10.1103/PhysRevB.72.014454.

[62] H. Skarsvåg, C. Holmqvist, and A. Brataas. Spin Superfluidity and Long-Range Transport in Thin-Film Ferromagnets. *Physical Review Letters*, 115(23):237201, December 2015. doi:10.1103/PhysRevLett.115.237201.

[63] J. F. Dillon. Ferrimagnetic Resonance in Yttrium Iron Garnet. *Physical Review*, 105:759–760, January 1957. doi:10.1103/PhysRev.105.759.

[64] G. P. Rodrigue, H. Meyer, and R. V. Jones. Resonance Measurements in Magnetic Garnets. *Journal of Applied Physics*, 31:S376–S382, May 1960. doi:10.1063/1.1984756.

[65] ASM Handbook Committee. *ASM handbook*, volume 2. ASM International, Materials Park, Ohio, October 1990. ISBN 978-0871703781. URL `https://www.asminternational.org/search/-/journal_content/56/10192/06182G/PUBLICATION`.

[66] Yue Zhang, Weisheng Zhao, Jacques-Olivier Klein, Wang Kang, Damien Querlioz, Youguang Zhang, Dafiné Ravelosona, and Claude Chappert. Spintronics for low-power computing. In *2014 Design, Automation & Test in Europe Conference & Exhibition (DATE)*, pages 1–6. IEEE, 2014.

[67] D. Pinna, F. Abreu Araujo, J. V. Kim, V. Cros, D. Querlioz, P. Bessiere, J. Droulez, and J. Grollier. Skyrmion Gas Manipulation for Probabilistic Computing. *Physical Review Applied*, 9(6):064018, June 2018. doi:10.1103/PhysRevApplied.9.064018.

[68] Kyung Mee Song, Jae-Seung Jeong, Biao Pan, Xichao Zhang, Jing Xia, Sunkyung Cha, Tae-Eon Park, Kwangsu Kim, Simone Finizio, Jörg Raabe, *et al.* Skyrmion-based artificial synapses for neuromorphic computing. *Nature Electronics*, 3(3):148–155, 2020. doi:10.1038/s41928-020-0385-0.

[69] Stuart S. P. Parkin, Masamitsu Hayashi, and Luc Thomas. Magnetic Domain-Wall Racetrack Memory. *Science*, 320(5873):190, April 2008. doi:10.1126/science.1145799.

[70] Saül Vélez, Jakob Schaab, Martin S. Wörnle, Marvin Müller, Elzbieta Gradauskaite, Pol Welter, Cameron Gutgsell, Corneliu Nistor, Christian L. Degen, Morgan Trassin, Manfred Fiebig, and Pietro Gambardella. High-speed domain wall racetracks in a magnetic insulator. *Nature Communications*, 10:4750, October 2019. doi:10.1038/s41467-019-12676-7.

[71] V. V. Kruglyak, S. O. Demokritov, and D. Grundler. Magnonics. *Journal of Physics D Applied Physics*, 43(26):264001, July 2010. doi:10.1088/0022-3727/43/26/264001.

[72] Yabin Fan, P. Quarterman, Joseph Finley, Jiahao Han, Pengxiang Zhang, Justin T. Hou, Mark D. Stiles, Alexander J. Grutter, and Luqiao Liu. Manipulation of coupling and magnon transport in magnetic metal-insulator hybrid structures. *Phys. Rev. Applied*, 13(6):061002, Jun 2020. doi:10.1103/PhysRevApplied.13.061002.

[73] H. Wu, L. Huang, C. Fang, B. S. Yang, C. H. Wan, G. Q. Yu, J. F. Feng, H. X. Wei, and X. F. Han. Magnon Valve Effect between Two Magnetic Insulators. *Physical Review Letters*, 120(9):097205, March 2018. doi:10.1103/PhysRevLett.120.097205.

[74] CY Guo, CH Wan, WQ He, MK Zhao, ZR Yan, YW Xing, X Wang, P Tang, YZ Liu, S Zhang, *et al.* A nonlocal spin hall magnetoresistance

in a platinum layer deposited on a magnon junction. *Nature Electronics*, pages 1–5, 2020. doi:10.1038/s41928-020-0425-9.

[75] N. Prasai, B. A. Trump, G. G. Marcus, A. Akopyan, S. X. Huang, T. M. McQueen, and J. L. Cohn. Ballistic magnon heat conduction and possible Poiseuille flow in the helimagnetic insulator Cu_2OSeO_3. *Physical Review B*, 95(22):224407, June 2017. doi:10.1103/PhysRevB.95.224407.

[76] Koichi Oyanagi, Takashi Kikkawa, and Eiji Saitoh. Magnetic field dependence of the nonlocal spin Seebeck effect in Pt/YIG/Pt systems at low temperatures. *AIP Advances*, 10(1):015031, January 2020. doi:10.1063/1.5135944.

[77] J. Zheng, S. Bender, J. Armaitis, R. E. Troncoso, and R. A. Duine. Green's function formalism for spin transport in metal-insulator-metal heterostructures. *Physical Review B*, 96(17):174422, November 2017. doi:10.1103/PhysRevB.96.174422.

[78] Kouki Nakata, Pascal Simon, and Daniel Loss. Spin currents and magnon dynamics in insulating magnets. *Journal of Physics D: Applied Physics*, 50(11):114004, feb 2017. doi:10.1088/1361-6463/aa5b09.

[79] Camilo Ulloa, A. Tomadin, J. Shan, M. Polini, B. J. van Wees, and R. A. Duine. Nonlocal Spin Transport as a Probe of Viscous Magnon Fluids. *Physical Review Letters*, 123(11):117203, September 2019. doi:10.1103/PhysRevLett.123.117203.

[80] W. Heisenberg. Zur Theorie des Ferromagnetismus. *Zeitschrift fur Physik*, 49(9-10):619–636, September 1928. doi:10.1007/BF01328601.

[81] Akashdeep Kamra, Wolfgang Belzig, and Arne Brataas. Magnon-squeezing as a niche of quantum magnonics. *Applied Physics Letters*, 117(9):090501, August 2020. doi:10.1063/5.0021099.

[82] Jiansen Zheng, Andreas Rückriegel, Scott A. Bender, and Rembert A. Duine. Ellipticity and dissipation effects in magnon spin valves. *Physical Review B*, 101(9):094402, March 2020. doi:10.1103/PhysRevB.101.094402.

[83] Camilo Ulloa and R. A. Duine. Magnon Spin Hall Magnetoresistance of a Gapped Quantum Paramagnet. *Physical Review Letters*, 120(17):177202, April 2018. doi:10.1103/PhysRevLett.120.177202.

[84] Leonid V Keldysh *et al.* Diagram technique for nonequilibrium processes. *Sov. Phys. JETP*, 20(4):1018–1026, 1965.

[85] Jørgen Rammer. *Quantum field theory of non-equilibrium states.* Cambridge Univ. Press, Cambridge, 2007. ISBN 978-0521188005.

[86] A. Kamra and W. Belzig. Super-Poissonian Shot Noise of Squeezed-Magnon Mediated Spin Transport. *Physical Review Letters*, 116(14): 146601, April 2016. doi:10.1103/PhysRevLett.116.146601.

[87] D. F. Walls. Squeezed states of light. *Nature*, 306:141–146, November 1983. doi:10.1038/306141a0.

[88] Nancy Aggarwal, Torrey J Cullen, Jonathan Cripe, Garrett D Cole, Robert Lanza, Adam Libson, David Follman, Paula Heu, Thomas Corbitt, and Nergis Mavalvala. Room-temperature optomechanical squeezing. *Nature Physics*, 16(7):784–788, 2020. doi:0.1038/s41567-020-0877-x.

[89] R. J. Doornenbal, A. Roldán-Molina, A. S. Nunez, and R. A. Duine. Spin-Wave Amplification and Lasing Driven by Inhomogeneous Spin-Transfer Torques. *Physical Review Letters*, 122(3):037203, January 2019. doi:10.1103/PhysRevLett.122.037203.

[90] A. Rückriegel and R. A. Duine. Hannay angles in magnetic dynamics. *Annals of Physics*, 412:168010, January 2020. doi:10.1016/j.aop.2019.168010.

[91] T. D. Graß, F. E. A. dos Santos, and A. Pelster. Excitation spectra of bosons in optical lattices from the Schwinger-Keldysh calculation. *Physical Review A*, 84(1):013613, July 2011. doi:10.1103/PhysRevA.84.013613.

[92] Supriyo Datta. Nanoscale device modeling: the Green's function method. *Superlattices and Microstructures*, 28(4):253–278, October 2000. doi:10.1006/spmi.2000.0920.

[93] Kathrin Ganzhorn, Stefan Klingler, Tobias Wimmer, Stephan Geprägs, Rudolf Gross, Hans Huebl, and Sebastian T. B. Goennenwein. Magnon-based logic in a multi-terminal YIG/Pt nanostructure. *Applied Physics Letters*, 109(2):022405, July 2016. doi:10.1063/1.4958893.

[94] T. L. Gilbert. A Phenomenological Theory of Damping in Ferromagnetic Materials. *IEEE Transactions on Magnetics*, 40(6):3443–3449, November 2004. doi:10.1109/TMAG.2004.836740.

[95] Hartmut Haug. *Quantum kinetics in transport and optics of semiconductors.* Springer, Berlin New York, 2008. ISBN 978-3-540-73561-8.

[96] H. P. Robertson. The Uncertainty Principle. *Physical Review*, 34(1):163–164, July 1929. doi:10.1103/PhysRev.34.163.

[97] Massimiliano Ventra. *Electrical transport in nanoscale systems.* Cambridge University Press, Cambridge, UK New York, 2008. ISBN 0521896347.

[98] Arthur Edwin Kennelly. The equivalence of triangles and three-pointed stars in conducting networks. *Electrical world and engineer*, 34(12):413–414, 1899.

[99] Gerrit E. W. Bauer, Eiji Saitoh, and Bart J. van Wees. Spin caloritronics. *Nature Materials*, 11(5):391–399, May 2012. doi:10.1038/nmat3301.

[100] S. A. Sharko, A. I. Serokurova, N. N. Novitskii, V. A. Ketsko, M. N. Smirnova, R. Gieniusz, A. Maziewski, and A. I. Stognij. Ferromagnetic and FMR properties of the YIG/TiO_2/PZT structures obtained by ion-beam sputtering. *Journal of Magnetism and Magnetic Materials*, 514: 167099, November 2020. doi:10.1016/j.jmmm.2020.167099.

[101] Li-Shan Xie, Guang-Xi Jin, Lixin He, Gerrit E. W. Bauer, Joseph Barker, and Ke Xia. First-principles study of exchange interactions of yttrium iron garnet. *Physical Review B*, 95(1):014423, January 2017. doi:10.1103/PhysRevB.95.014423.

[102] D. T. Edmonds and R. G. Petersen. Effective Exchange Constant in Yttrium Iron Garnet. *Physical Review Letters*, 2(12):499–500, June 1959. doi:10.1103/PhysRevLett.2.499.

[103] Andrew J. Princep, Russell A. Ewings, Simon Ward, Sandor Tóth, Carsten Dubs, Dharmalingam Prabhakaran, and Andrew T. Boothroyd. The full magnon spectrum of yttrium iron garnet. *npj Quantum Materials*, 2:63, November 2017. doi:10.1038/s41535-017-0067-y.

[104] V. D. Poimanov, A. N. Kuchko, and V. V. Kruglyak. Scattering of exchange spin waves from a helimagnetic layer sandwiched between two semi-infinite ferromagnetic media. *Physical Review B*, 102(10):104414, September 2020. doi:10.1103/PhysRevB.102.104414.

[105] B. Kaplan and R. Kaplan. Anisotropy effects on the spin wave gap of two dimensional magnets at zero temperature. *Journal of Magnetism and Magnetic Materials*, 356:95–97, April 2014. doi:10.1016/j.jmmm.2013.12.048.

[106] Claudius Gros, Wolfgang Wenzel, Andreas Fledderjohann, P. Lemmens, M. Fischer, G. Güntherodt, M. Weiden, C. Geibel, and F. Steglich. Magnon-magnon interactions in the spin-peierls compound cugeo$_3$. *Phys. Rev. B*, 55(22):15048–15052, Jun 1997. doi:10.1103/PhysRevB.55.15048.

[107] Jilei Chen, Chuanpu Liu, Tao Liu, Yang Xiao, Ke Xia, Gerrit E. W. Bauer, Mingzhong Wu, and Haiming Yu. Strong Interlayer Magnon-Magnon Coupling in Magnetic Metal-Insulator Hybrid Nanostructures. *Physical Review Letters*, 120(21):217202, May 2018. doi:10.1103/PhysRevLett.120.217202.

[108] Yuzan Xiong, Yi Li, Mouhamad Hammami, Rao Bidthanapally, Joseph Sklenar, Xufeng Zhang, Hongwei Qu, Gopalan Srinivasan, John Pearson, Axel Hoffmann, Valentine Novosad, and Wei Zhang. Probing magnon-magnon coupling in exchange coupled $Y_3Fe_5O_{12}$/Permalloy bilayers with magneto-optical effects. *Scientific Reports*, 10:12548, July 2020. doi:10.1038/s41598-020-69364-6.

[109] Alex Kamenev. Keldysh and doi-peliti techniques for out-of-equilibrium systems. In *Strongly Correlated Fermions and Bosons in Low-Dimensional Disordered Systems*, pages 313–340. Springer, 2002. ISBN 978-1402007484.

[110] Louis Neel. Magnetism and Local Molecular Field. *Science*, 174(4013): 985–992, December 1971. doi:10.1126/science.174.4013.985.

[111] Allan Morrish. *The physical principles of magnetism.* IEEE Press, New York, 2001. ISBN 078036029X.

[112] Louis Néel. Propriétés magnétiques de l'état métallique et énergie d'interaction entre atomes magnétiques. *Annales de Physique*, 11(5):232–279, January 1936. doi:10.1051/anphys/193611050232.

[113] G. E. Alefeld, F. A. Potra, and Yixun Shi. Algorithm 748: Enclosing zeros of continuous functions. *ACM Trans. Math. Softw.*, 21(3):327–344, sep 1995. ISSN 0098-3500. doi:10.1145/210089.210111.

[114] D. Wuhrer, N. Rohling, and W. Belzig. Theory of quantum entanglement and structure of the two-mode squeezed antiferromagnetic magnon vacuum. *Physical Review B*, 105(5):054406, February 2022. doi:10.1103/PhysRevB.105.054406.

[115] Yan Chen, Paolo Zanardi, Z. D. Wang, and F. C. Zhang. Sublattice entanglement and quantum phase transitions in antiferromagnetic spin

chains. *New Journal of Physics*, 8(6):97, June 2006. doi:10.1088/1367-2630/8/6/097.

[116] J. I. Latorre and A. Riera. A short review on entanglement in quantum spin systems. *Journal of Physics A Mathematical General*, 42(50):504002, December 2009. doi:10.1088/1751-8113/42/50/504002.

[117] Ryszard Horodecki, Paweł Horodecki, Michał Horodecki, and Karol Horodecki. Quantum entanglement. *Reviews of Modern Physics*, 81(2): 865–942, April 2009. doi:10.1103/RevModPhys.81.865.

[118] Xiuhong Gao, Albeverio Sergio, Kai Chen, Shaoming Fei, and Xianqing Li-Jost. Entanglement of formation and concurrence for mixed states. *Frontiers of Computer Science in China*, 2(2):114–128, 2008. doi:10.1007/s11704-008-0017-8.

[119] William K. Wootters. Entanglement of Formation of an Arbitrary State of Two Qubits. *Physical Review Letters*, 80(10):2245–2248, March 1998. doi:10.1103/PhysRevLett.80.2245.

[120] Ingo Peschel. LETTER TO THE EDITOR: Calculation of reduced density matrices from correlation functions. *Journal of Physics A Mathematical General*, 36(14):L205–L208, April 2003. doi:10.1088/0305-4470/36/14/101.

[121] Ingo Peschel and Viktor Eisler. Reduced density matrices and entanglement entropy in free lattice models. *Journal of Physics A Mathematical General*, 42(50):504003, December 2009. doi:10.1088/1751-8113/42/50/504003.

[122] Ingo Peschel. Special Review: Entanglement in Solvable Many-Particle Models. *Brazilian Journal of Physics*, 42(3-4):267–291, August 2012. doi:10.1007/s13538-012-0074-1.

[123] Temple He, Javier M. Magán, and Stefan Vandoren. Entanglement entropy of periodic sublattices. *Physical Review B*, 95(3):035130, January 2017. doi:10.1103/PhysRevB.95.035130.

[124] G. Liu, Xi-guang Wang, Z. Z. Luan, L. F. Zhou, S. Y. Xia, B. Yang, Y. Z. Tian, Guang-hua Guo, J. Du, and D. Wu. Magnonic unidirectional spin hall magnetoresistance in a heavy-metal–ferromagnetic-insulator bilayer. *Phys. Rev. Lett.*, 127:207206, Nov 2021. doi:10.1103/PhysRevLett.127.207206.